

ABSTRACT

Title of Dissertation: OCCUPANT-ORIENTED INDOOR ENVIRONMENTAL CONTROLS IN PUBLIC SPACES

Lingzhe Wang, Doctor of Philosophy, 2023

Dissertation directed by: Jelena Srebric, Professor
Department of Mechanical Engineering

The indoor environment has significant impacts on the health and comfort of building occupants. In addition, occupant behavior can affect building energy consumption. It is essential to consider actual occupant needs when controlling indoor environmental systems. To provide a healthy, comfortable, and energy-efficient indoor environment, the present dissertation presents a comprehensive research framework for occupant-oriented indoor environmental controls by conducting (i) air quality characterization in occupant breathing zone, (ii) data-driven thermal comfort identification, and (iii) simultaneous air quality, thermal comfort, and building energy controls.

For air quality characterization in occupant breathing zone, the present dissertation characterized aerosol plumes associated with the risk of airborne virus transmission to investigate the occupant requirements for air quality controls. The study considered both the aerosol plume source strength and convective transport capability by conducting experiments with 18 human subjects. The source strength was characterized by the source aerosol emission rate, and the convective transport capability was characterized by the plume influence distance. The

performances of multiple mitigation strategies were tested. The findings show that controlling the air quality in the breathing zone is crucial for protecting occupants from getting infected by airborne infectious microorganisms.

For data-driven thermal comfort identification, the present dissertation developed data-driven models to predict actual occupant thermal comfort based on physiological variables. By incorporating multiple HRV indices along with wrist temperatures, the performance of the models was significantly improved, achieving more than four times the accuracy compared to models based solely on wrist temperatures. This highlights the crucial role of HRV as physiological variables in accurately predicting thermal comfort. With the F1 score, the performance evaluation index of the developed machine learning thermal comfort model, exceeded the value of 0.90, this investigation provides a reliable thermal comfort prediction method, which could be used in actual building occupant-oriented controls.

For simultaneous air quality, thermal comfort, and building energy controls, this dissertation developed a wearable micro air cleaner and deployed the extremum seeking control. The wearable micro air cleaner achieved 60% - 70% protective efficiency for both nasal and mouth breathing. Importantly, unlike current mitigation methods such as masks, this device allows users to be thermal comfortable when the indoor air temperature is above 25 °C. Additionally, this dissertation implemented the extremum seeking control to balance the trade-offs between individual thermal comfort preferences and building energy consumption in real-time. This control method successfully achieved energy savings of up to 22% compared to a constant temperature setpoint of 24 °C. The developed framework for simultaneous air quality, thermal comfort, and building energy controls holds great potential in providing building occupants with a healthy, comfortable, and energy-efficient indoor environment.

OCCUPANT-ORIENTED INDOOR ENVIRONMENTAL CONTROLS IN
PUBLIC SPACES

by

Lingzhe Wang

Dissertation submitted to the Faculty of the Graduate School of the
University of Maryland, College Park, in partial fulfillment
of the requirements for the degree of
Doctor of Philosophy
2023

Advisory Committee:

Professor Jelena Srebric (Chair/Advisor)

Professor Hosam Fathy

Associate Professor Jin-Oh Hahn

Professor Bao Yang

Professor Donald Milton (Dean's Representative)

© Copyright by
Lingzhe Wang
2023

Dedication

To my beloved parents.

Acknowledgements

I would like to express my deepest gratitude to Dr. Jelena Srebric, my advisor, for her invaluable guidance and unwavering support throughout this journey. She was always available to answer my questions and provide feedback, which helped me finish research projects that produce this dissertation.

I am also grateful to my dissertation committee members, Dr. Hosam Fathy, Dr. Jin-Oh Hahn, Dr. Bao Yang, and Dr. Donald Milton for their valuable insights on my dissertation. Their constructive suggestions helped me grow both as a student and as a researcher.

I would like to thank all my colleagues in Department of Mechanical Engineering, who were always willing to help and collaborate. Their perspectives were instrumental in shaping my research and helping me overcome challenges.

I would also like to express my gratitude to my family and friends, who provided me with assistance and encouragement throughout my academic journey. Their love kept me motivated, even during the most challenging times.

Table of Contents

Dedication.....	ii
Acknowledgements.....	iii
Table of Contents.....	iv
List of Tables.....	v
List of Figures.....	vi
1. Introduction.....	1
1.1 Background.....	1
1.2 Literature review.....	2
1.2.1 Air quality characterization.....	2
1.2.2 Thermal comfort identification.....	4
1.2.3 Indoor environmental controls.....	5
2. Research objectives and outline.....	8
2.1 Research gaps, objectives and tasks.....	8
2.2 Dissertation outline.....	11
3. Air quality characterization in occupant breathing zone.....	15
3.1 Introduction.....	15
3.2 Methodology.....	17
3.3 Results.....	31
3.4 Discussion.....	45
3.5 Summary.....	50
4. Data-driven thermal comfort identification.....	52
4.1 Introduction.....	52
4.2 Methodology.....	58
4.3 Results.....	73
4.4 Discussion.....	84
4.5 Summary.....	86
5. Simultaneous air quality, thermal comfort, and building energy controls.....	88
5.1 Introduction.....	88
5.2 Methodology.....	94
5.3 Results.....	107
5.4 Discussion.....	131
5.5 Summary.....	132
6. Discussion.....	135
6.1 Implications of the dissertation findings.....	135
6.2 Future work.....	137
7. Conclusions and contributions.....	139
7.1 Conclusions.....	139
7.2 Contributions.....	141
7.3 Summary of publications.....	143
Bibliography.....	146

List of Tables

Table 1 Human subject information	19
Table 2 Effective flow area of musical performances	24
Table 3 Specifications of experiment equipment.....	28
Table 4 Source characterization data of aerosol plumes from musical performances	35
Table 5 Convective capability characterization data of aerosol plumes from musical performances.....	36
Table 6 Comprehensive characterization of aerosol plumes from musical performances.....	41
Table 7 Source Aerosol concentration (particle/L) reduction by mitigation methods	44
Table 8 Horizontal jet length (mm) reduction by mitigation methods	44
Table 10 Information of human subjects.	59
Table 11 Technical specification of the sensors.	60
Table 12 Value range of the physiological variables and thermal comfort/sensation indices.	69
Table 13 Feature group description.	70
Table 14 Optimal hyperparameters of machine learning models	71
Table 15 Values of performance indices of the linear SVM models.....	78
Table 16 Values of performance indices of the KNN models.....	79
Table 17 Values of performance indices of the RF models.....	80
Table 18 Values of performance indices of the SVM with RBF kernel models.	80
Table 19 Information of human subjects.	97
Table 20 Technical specification of the sensors.	98
Table 21 Assumptions for thermal comfort model.....	103
Table 22 Protective efficiencies with different location for air diffuser.....	108
Table 23 Protective efficiencies with varied airflow rates for air supply.	109
Table 24 p-values and Cohen's d values of each variable at different indoor air temperatures.....	113
Table 25 Feature group descriptions.....	115
Table 26 Test F1 scores of machine learning models with different feature groups	116
Table 27 Training and test scores of KNN models.....	117
Table 28 Training and test scores of RF models.....	119
Table 29 Training and test scores of SVM_RBF models	121

List of Figures

Figure 1 Overview of the dissertation workflow	12
Figure 2 Description of terminologies in source strength and convective transport capability characterization of aerosol plumes from musical performances (a. Instrument, b. Singing).	17
Figure 3 Mitigation Methods. a. Cloth mask. b. Surgical mask. c. N95 mask. d. Bell cover. e. MERV-13 filter.	18
Figure 4 Environmental chamber setup	21
Figure 5 Source aerosol measurements with funnels for singing (left) and instrument (right)	23
Figure 6 Description of BOS experiment setup	26
Figure 7 Description of PIV experiment setup	28
Figure 8 Source strength characterization of aerosol plumes from musical performances. a. Source velocity. b. Source airflow rate. c. Source aerosol concentration including high shedder. d. Source aerosol emission rate including high shedder. (note: “source” refers to the time-averaged data collected at singer mouth or instrument outlet)	33
Figure 9 Source strength characterization of aerosol plumes from performance categories (singing, brass instrument and woodwind instrument). a. Source velocity. b. Source airflow rate. c. Source aerosol concentration. d. Source aerosol emission rate (note: “source” refers to the time-averaged data collected at singer mouths or instrument outlets).	34
Figure 10 Size distribution of aerosol from musical performances	34
Figure 11 a. Jets of the aerosol plumes from brass instruments. b. Jets of the aerosol plumes from woodwind instruments. c. Jets of the aerosol plumes from singing and flute. Note that the velocity scale is different in each panel.	38
Figure 12 Convective transport capability characterization of aerosol plumes. a. Horizontal jet lengths (musical performance). b. Horizontal jet lengths (performance categories). c. Plume influence distances (musical performance). d. Plume influence distances (performance categories).....	39
Figure 13 Comprehensive characterization of aerosol plumes	40
Figure 14 Qualitative comparison of measured average aerosol concentration in different jets of aerosol plumes. (Note: The values of the concentrations can be found in Table 4).....	41
Figure 15 Source Aerosol concentration and horizontal jet length reduction by mitigation methods (singing and clarinet). a. Real-time source aerosol concentration of aerosol plumes from singing (with/without mitigation methods). b. Real-time source aerosol concentration of aerosol plumes from clarinet (with/without mitigation methods). c. horizontal jet length comparison of singing (with/without mitigation methods). d. horizontal jet length comparison of clarinet (with/without mitigation methods).....	43
Figure 16 Research scheme of this study.....	58
Figure 17 Human subject wearing the bracelet sensor.	61

Figure 18 Feature importance analysis of (A) thermal sensation (B) thermal comfort	70
Figure 19 Statistical analysis results for thermal sensation. (A) Mean and 95% confidence interval of thermal sensation. (B) Comparison of the thermal sensation distribution before and after PCD requesting.	74
Figure 20 Statistical analysis results for thermal comfort. (A) Mean and 95% confidence interval of thermal comfort. (B) Comparison of the thermal comfort distribution before and after PCD requesting.	75
Figure 21 Statistical analysis results for wrist temperature. (A) Mean and 95% confidence interval of the wrist temperature. (B) Comparison of the wrist temperature distribution before and after PCD requesting.	76
Figure 22 Statistical analysis results for SDNN and LF/HF. (A) Mean and 95% confidence interval of the SDNN. (B) Comparison of the SDNN distribution before and after the PCD requesting. (C) Mean and 95% confidence interval of the LF/HF. (D) Comparison of the LF/HF distribution before and after the PCD requesting.	77
Figure 23 Average performance indices of different feature groups	82
Figure 24 Average performance indices of different machine learning methods with M5	83
Figure 25 User wearing the wearable micro air cleaner	95
Figure 26 Experimental setup of the protective performance evaluation	96
Figure 27 Thermal Comfort Response of Occupants with Different Metabolic Rate	105
Figure 28 Extremum seeking control system.....	106
Figure 29 Diffuser locations, (left) Diffuser above the eyes, (right) Diffuser in front of the face.....	107
Figure 30 Thermal sensation and comfort responses at different indoor air temperatures. (A) Overall thermal sensation. (B) Overall thermal comfort. (C) Local thermal sensation. (D) Local thermal comfort.....	111
Figure 31 Physiological responses at different indoor air temperatures. (A) Face temperature. (B) Heart rate. (C) SDNN. (D) LF/HF.....	112
Figure 32 Feature importance of the overall and local thermal sensation and comfort	114
Figure 33 Test F1 scores of feature groups.....	117
Figure 34 Pareto Front of Two-objective Optimization (PPD of Occupant 1 Vs. PPD of Occupant 2).....	124
Figure 35 Pareto Front of Three-objective Optimization (PPD of Occupant 1 vs. PPD of Occupant 2 vs. Energy consumption).....	125
Figure 36 Energy Consumption and Temperature for Energy Usage Optimization	126
Figure 37 Thermal Comfort and Temperature for Single-Occupant Thermal Comfort Optimization	127
Figure 38 Thermal Comfort and Temperature for Two-objective Extremum Seeking Control	128
Figure 39 Thermal Comfort, Energy Consumption, and Temperature for Three-objective Extremum Seeking Control.....	129
Figure 40 Thermal Comfort, Energy Consumption and Temperature for Staggered Three-objective Extremum Seeking Control	130

List of Abbreviations

ANN	Artificial Neural Network
ASHRAE	American Society of Heating, Refrigerating and Air-Conditioning Engineers
AUC	Area Under Curve of the Receiver Operating Characteristic
BMI	Body Mass Index
CV _{R-R}	Coefficient of Variation in R-R Intervals
DT	Decision Tree
FFT	Fast Fourier Transform
HF	High Frequency
HRV	Heart Rate Variability
HVAC	Heating, Ventilation, and Air-conditioning
iA	Instantaneous Amplitude
IRB	Institutional Review Board
KNN	K Nearest Neighbor
LF	Low Frequency
NB	Naïve Bayes
PCD	Personal Conditioning Device
PMV	Predicted Mean Vote
pNNx	Percentage of R-R Interval that Differ by x Milliseconds
PNS	Parasympathetic Nervous System
PPD	Predicted Percentage of Dissatisfied
PPG	Photoplethysmography
RBF	Radial Basis Function
RF	Random Forest
RMSSD	Root Mean Square of Successive Differences between Adjacent R-R intervals
ROC	Receiver Operating Characteristic
SDNN	Standard Deviation of Intervals between Normal Heartbeats
SDSD	Standard Deviation of Successive Differences between Adjacent R-R intervals
SNS	Sympathetic Nervous System
SVM	Support Vector Machine
SVM_L	Linear Support Vector Machine
SVM_RB	Support Vector Machine with Radial Basis Function Kernel
F	Support Vector Machine with Radial Basis Function Kernel
TC	Thermal Comfort
TS	Thermal Sensation
ULF	Ultra-Low Frequency
VLF	Very-Low Frequency

1. Introduction

This chapter presents the background and the literature review.

1.1 Background

The importance of occupants in the indoor environment can be seen in several ways. First, occupants can influence the quality of indoor air by generating airborne disease virus or other pollutants through respiration. The large-scale airborne infectious microorganism transmission in recent COVID-19 pandemic highlights the importance of the air quality for occupant health [1]. Other activities, such as cooking, showering, etc., can also contribute to the buildup of moisture and humidity, which may lead to mold growth and other indoor air quality issues [2], [3]. Second, occupants have different thermal comfort preferences in the indoor environment. Their perception of indoor temperature can affect their productivity and well-being. Even though a state-of-the-art building system is expected to satisfy the thermal comfort of 80% building occupants based on the ASHRAE standard, the average satisfaction rate is still much lower than expectation [4]. It is essential to meet the diverse needs of occupants, such as utilizing effective methods to provide adequate thermal comfort to different individual occupant [5], [6]. Third, buildings account for a significant fraction of global electrical energy consumption [7]. The total energy consumption of building is expected to grow at least 40% by 2040 [8]. Occupant behavior can significantly affect the energy consumption of the building, as they are the ones who use energy for heating, cooling, lighting, and other activities. It is important to control the indoor

environment and building systems based on occupant requirements and behaviors to reduce energy consumption and carbon emissions [9], [10].

1.2 Literature review

The present dissertation conducts the literature review from three perspectives, including air quality characterization, thermal comfort identification, as well as indoor environmental controls. The literature review presented in this chapter aims to find research gaps and develop research objectives.

1.2.1 Air quality characterization

In recent times, the COVID-19 pandemic has had a significant impact on indoor environments and the activities conducted within them. Indoor activities, such as musical performances, serve as illustrative examples with the outbreak of the virus linked to choir performances reported in various countries, including the U.S. [11], Netherlands [12] Germany [13], France [14], Japan [15], and South Korea [16]. One notable instance occurred in Skagit Valley, Washington, where a choir rehearsal took place on March 10, 2020. Following the rehearsal, which lasted 2.5 hours and involved 61 participants, a total of 32 confirmed and 20 probable secondary COVID-19 cases were identified, resulting in three hospitalizations and two deaths [11]. The outbreak in Skagit Valley, Washington [11] was attributed to aerosol transmission, which has been identified as a primary route for the spread of COVID-19 by esteemed organizations such as the World Health Organization (WHO) and the U.S. Centers for Disease Control and Prevention (CDC). This is particularly significant in the context of choir rehearsals, as singing is known to generate a greater number of aerosols compared to

regular speech [17], [18] When individuals engage in indoor activities involving speaking or singing, exhaled gas plumes containing aerosols are released into the surrounding air [19]. These gas plumes disperse and mix with the ambient air due to continuous air movement within the indoor space. Consequently, aerosols carrying viral particles are continuously transported throughout the environment. Direct exposure to the exhaled gas plume from an individual who is an airborne carrier of a disease virus poses a high risk of infection due to the elevated concentration of viral particles in close proximity.

Traditional centralized HVAC systems have disadvantages in preventing airborne infectious microorganism transmissions. In buildings with centralized ventilation, there is a possibility of cross-contamination between different areas [20]. If one area becomes contaminated with infectious airborne pathogens, the centralized system can spread the contaminants to other parts of the building through the ventilation ducts, potentially leading to a wider outbreak. To develop effective air quality control method to prevent airborne infectious microorganism transmission in indoor activities, it is critical to know the extent of the aerosol plume generated by the occupant. The extent is determined by its interactions with thermal plumes around the human body and indoor ventilation flow [21],[22],[23]. Prior studies have characterized the aerosol plumes from speech [24], [25], and from musical performances by focusing on the source strength, such as the aerosol concentration [17], [18], [26]–[30] and the air velocity [29], [31], [32], or the convective transport capability, such as the transport distance [29], [32]–[34].

1.2.2 Thermal comfort identification

One of the primary functions of buildings is to provide the acceptable indoor thermal environment to the occupants [35]. The occupant thermal comfort is particularly important for building controls because the HVAC systems, which are working continuously to make the occupants achieve the thermal satisfaction, consume about 50% of building energy use in developed countries [36].

Thermal comfort models help researchers and engineers to better analyze and design the building environment. A noteworthy example of the thermal comfort models, is Fanger's Predicted Mean Vote/Predicted Percentage of Dissatisfied (PMV/PPD) model [37], which is based on the heat balance over the whole-body surface. This PMV/PPD model is currently widely used building operation and design, as well as standards, such as ASHRAE-55 [38]. Nevertheless, the limitations of this model have been well-documented [39]. The possible discrepancy between PMV and the occupant Actual Mean Vote (AMV) can be noticed [40]. Also, possible bias in the relationship between PMV and PPD may exist [39]. Furthermore, any seasonal psychological adaptation on thermal comfort is ignored and a fixed year-round set temperature point for all occupants is prescribed by PMV/PPD models [41]. To compensate the disadvantages of this model, thermal adaptive model has been introduced for an efficient thermal comfort provision. Contrary to the former, the adaptive model accounts for occupant's thermal adaptation [42] and recognizes the influence of outdoor climate on thermal comfort based on field studies [43]. Because a broad range of thermal comfort zones are preferred, adaptive models' thermal ranges are not as limited as that of the PMV/PPD models. However, these traditional physical-based

thermal comfort models have limitations, such as the lack of personalization, lack of dynamic interactions, and limited feedback loop. Recently, personal thermal comfort models [44] were developed using data-driven methods [45] to provide more flexible and reliable thermal comfort prediction for individual occupant in the indoor environment.

1.2.3 Indoor environmental controls

For the air quality controls, mixing and displacement room air distribution are the main principles of centralized ventilation that are applied today in buildings. However, the clean air supplied far from the occupants is more or less polluted by the time it is inhaled [46], which makes the centralized ventilation to be not enough for occupants' protection in indoor environment. Face masks or respirators could be effective and essential equipment to protect healthcare workers and members of the general public who may be exposed to the virus [47], however, user discomfort while wearing cloth masks is thought to engender behaviors that limit the effectiveness of cloth masks as source control (e.g., adjusting or removing one's mask temporarily while in public) [48]. Personalized ventilation (PV) in comparison with centralized ventilation and masks has two important advantages: first, its potential to improve the inhaled air quality and second, each occupant is delegated the authority to optimize and control temperature, flow rate (local air velocity) and direction of the locally supplied personalized air according to his/her own preference, and thus to improve his/her comfort conditions [46]. The PV has been applied to provide clean air to an individual's inhalation by many means, such as being incorporated in seat headrests [49] and headsets [50]. In practice, personalized airflow is usually blown toward the face from

a nozzle at tens of centimeters away from the face. To properly ventilate the breathing zone and protect respiratory health, the PV effectiveness depends on its complex interactions with the breathing flow, the convective flow around the human body, and the room ventilation flow [51], [52]. Personalized airflow needs a sufficient high momentum (speed) to penetrate the convective flow around the face, as well as sufficient large flow rate to compensate for its dispersion into the room space by mixing with the surrounding air. The distance between the PV nozzle and the face is a key factor to determine flow rate and speed of the personalized airflow. To reduce the mixing of personalized air and surrounding air, it is necessary to supply the breathing zone with the potential core of a PV jet in a sustained manner [53].

Buildings account for a significant fraction of global electrical energy consumption [54]. The total energy consumption of building is expected to grow at least 40% by 2040 [8]. On the other hand, the conventional building is designed to maintain homogeneous indoor ambient condition, especially for a comfortable thermal and visual environment [54]. The American Society of Heating, Refrigerating and Air-Conditioning Engineers (ASHRAE) defines the thermal comfort as an important aspect in representing human satisfaction [38]. Thermal comfort is the state of mind that indicates a person's perceived equilibrium with their environment. The overall comfort level of a building's occupants has a direct impact on their energy consumption patterns. However, even though a state-of-the-art building system is expected to satisfy 80% of the building occupants based on the ASHRAE standard, the average satisfaction rate is still much lower than expectation [4].

To address the conflict between thermal comfort demand and energy consumption, research on occupant-centric controls (OCC) have increased significantly over the past decade [55]. The OCC is a control strategy for the indoor environment, which specifically focuses on decreasing building energy consumption while meeting the current needs of building occupants. It acquires various data from the occupant and indoor environment, and sends the optimal control signals to actuators according to occupants' requirements [56]. Most OCC algorithms for HVAC were incorporated in either conventional reactive controllers [57], and model predictive controls [58]. Reinforcement learning becomes a popular data-driven occupant-centric control method in recent years [59].

2. Research objectives and outline

2.1 *Research gaps, objectives and tasks*

According to the literature review, we found the following research gaps:

1. Need for air quality characterizations in occupant breathing zone:

Centralized ventilation cannot effectively prevent the airborne infectious microorganism transmission. With a centralized ventilation system, if the airborne infectious microorganisms are present in the indoor environment, recirculating contaminated air can spread the pathogens to different zones, potentially increasing the risk of transmission. In addition, centralized ventilation systems provide the same ventilation settings for the entire building, irrespective of the specific needs of different occupants or areas. This can be problematic in situations where some individuals or spaces require higher ventilation rates or specific air quality conditions for infection control purposes. Therefore, the aerosol plumes associated with the risk of airborne virus transmission need to be characterized. In the meantime, the objectives of the novel indoor air quality control method are needed to be defined.

2. Need for data-driven thermal comfort identification:

Even though studies have developed various of thermal comfort models, the models still have limitations in prediction accuracy and actual operation. Some models require very specific input variables (e.g., the PMV model needs the metabolic rate, mean radiance temperature etc.). These variables are costly and almost impossible for real-time monitor by the sensors in the real world. Additionally, the inherency of the human thermal physiological regulation is

not fully considered. Although some data-driven models are developed based on the physiological parameters, mostly only using skin temperature. A reliable data-driven method to identify occupant thermal comfort preference for indoor environmental controls is needed.

3. Need for novel air quality, thermal comfort, and building energy controls:

For air quality control, The current wearable N95 respirators and surgical masks rely on users' lungs to push the air against the filtering surfaces, which is uncomfortable and insufficient during prolonged use. Even though the concept of the personalized ventilation has been presented, typical personalized ventilation provides the localized air supply to the occupant at a fixed location. Slight variations in positioning, orientation, and height of the person may impact the efficacy of the fixed personalized ventilation. If individuals need to move or walk around, such as healthcare and laboratory workers, as well as those working in high-density and congregated workplace settings like correctional facilities and manufacturing facilities, solely relying on fixed personal ventilation may not provide sufficient protection. Most occupant-centric control (OCC) algorithms for HVAC were incorporated in either conventional reactive controllers or model predictive controls. However, the conventional controllers cannot handle the uncertainties well. Additionally, the insufficient accuracy of the models is the main weakness of the model-based controller. Some data-driven control methods, such as the reinforcement learning, are not applicable in actual building control scenarios due to the requirement of a large amount of data. A novel occupant-oriented control

method which simultaneously considers the air quality, thermal comfort, and building energy is required.

According to these research gaps, novel devices and methods are needed for occupant-oriented air quality and thermal comfort controls, therefore the present dissertation brings up three research questions to address occupant needs for indoor environmental control in public spaces:

1. How do localized airborne infectious microorganism sources from occupants change the mitigation strategies for air quality controls in indoor environment?

2. What is the reliable method to identify occupant thermal comfort in indoor environment?

3. How to effectively control the indoor environment to simultaneously meet the requirements of air quality and thermal comfort, while at the same time reducing the building energy consumption.

To answer these research questions, the present dissertation proposes the following research objectives.

Objective 1: Air quality characterization in occupant breathing zone.

Task 1.1 Characterize the aerosol plumes by considering both the source strength and convective transport capability.

Task 1.2 Comprehensively analyze the measured data.

Task 1.3 Find the objectives of the future generation occupant-oriented air quality control.

Objective 2: Data-driven thermal comfort identification.

Task 2.1 Conduct human subject experiments to collect thermal sensation/comfort surveys and physiological data.

Task 2.2 Analyze the data collected in the human subject experiments.

Task 2.3 Develop data-driven thermal comfort models, which could be used in occupant-oriented thermal comfort controls.

Objective 3: Simultaneous air quality, thermal comfort, and building energy controls.

Task 3.1 Develop a novel occupant-oriented air quality control method.

Task 3.2 Develop a novel occupant-oriented thermal comfort control method.

Task 3.3 Develop the control platform which simultaneously considering the air quality, thermal comfort, and energy consumptions.

2.2 Dissertation outline

The research gaps and objectives allow to define the occupant-oriented indoor environmental controls to maintain good air quality in occupant breathing zone, satisfied thermal comfort in indoor environment, and minimal building energy consumption. Figure 1 shows the overview of the dissertation structure.

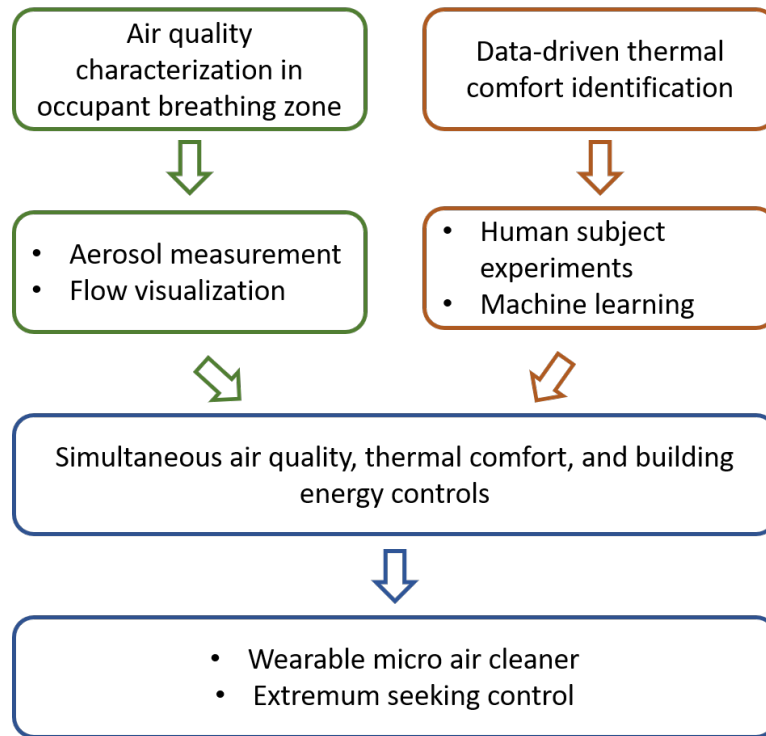


Figure 1 Overview of the dissertation workflow

The research objectives and tasks are aligned with four publications that form the chapters in this dissertation. The remainder of the present dissertation is organized as follows:

Chapter 3 – Air quality characterization in occupant breathing zone. This chapter presents the study conducting aerosol measurements and flow visualizations to characterize the aerosol plumes associated with the risk of airborne virus transmission. The air quality characterization provides the objectives of the novel occupant-oriented air quality control method. The chapter is based on the following publication:

- L. Wang, T. Lin, H. Da Costa, S. Zhu, T. Stockman, A. Kumar, J. Weaver, M. Spede, D. K. Milton, J. Hertzberg, D. Toohey, M. Vance, S. L. Miller, J. Srebric, “Characterization of aerosol plumes from

singing and playing wind instruments associated with the risk of airborne virus transmission,” *Indoor Air*, vol. 32, no. 6, p. e13064, Jun. 2022, doi: 10.1111/INA.13064.

Chapter 4 – Data-driven thermal comfort identification. This chapter presents the study conducting human subject experiments to collect thermal sensation/comfort questionnaires and physiological data. Based on the collected data, machine learning methods are utilized to develop high performance data-driven thermal comfort models. The chapter is based on the following publication:

- L. Wang, D. A. Dalgo, N. Mattise, S. Zhu, and J. Srebric, “Physiological responses and data-driven thermal comfort models with personal conditioning devices (PCD),” *Building and Environment*, p. 110290, Apr. 2023, doi: 10.1016/J.BUILDENV.2023.110290.

Chapter 5 – Simultaneous air quality, thermal comfort, and building energy control. This chapter presents the study develops a novel wearable micro air cleaner as the occupant-oriented air quality control method to promise the air quality in occupant breathing zone. The extremum seeking control is implemented as the occupant-oriented thermal comfort control method to balance individual occupant thermal preferences and building energy consumption. The chapter is based on the following publication:

- L. Wang, S. A. Romo, E. Sanico, H. Da Costa, T. Lin, N. Rabchevsky, M. Kern, S. Zhu, J. Srebric, “A Wearable Micro Air Cleaner for Occupant-oriented Indoor Environmental Controls,” *Building and Environment*, (Under Review).

- L. Wang, T. Hensel, P. Chanpiwat, S. Zhu, and J. Srebric, “Occupant-centric Control of Building Systems based on Real-time Optimization by Extremum Seeking,” in *2022 IEEE International Conference on Environment and Electrical Engineering and 2022 IEEE Industrial and Commercial Power Systems Europe (EEEIC / I&CPS Europe)*, 2022, pp. 1–6. doi: 10.1109/EEEIC/ICPSEurope54979.2022.9854615.

Chapter 6 – Discussion. This chapter discusses the implications of the dissertation findings and future work.

Chapter 7 – Conclusions and contributions. This chapter summaries the conclusions, contributions, and the publications.

3. Air quality characterization in occupant breathing zone

This chapter is reproduced from the following journal paper:

L. Wang, T. Lin, H. Da Costa, S. Zhu, T. Stockman, A. Kumar, J. Weaver, M. Spede, D. K. Milton, J. Hertzberg, D. Toohey, M. Vance, S. L. Miller, J. Srebric, “Characterization of aerosol plumes from singing and playing wind instruments associated with the risk of airborne virus transmission,” *Indoor Air*, vol. 32, no. 6, p. e13064, Jun. 2022, doi: 10.1111/INA.13064.

3.1 Introduction

The Coronavirus Disease 2019 (COVID-19) pandemic has led to a profound impact on music communities, with the total shutdown of music production and public events after a number of the outbreaks related to choir performances were reported in the U.S.[11], Netherlands[12] Germany[13], France[14], Japan[15], and South Korea[16]. For example, on March 10, 2020, in Skagit Valley, Washington, following a 2.5-hour rehearsal with 61 participants including a symptomatic index patient, 32 confirmed and 20 probable secondary COVID-19 cases were identified, including three hospitalizations and two deaths[11]. Aerosol transmission, which has been recognized as a primary route for COVID-19 spread by the World Health Organization (WHO) and the U.S. Center for Disease Control (CDC), was considered to account for the choir rehearsal outbreak in Skagit Valley, Washington[11], due to much more aerosol being produced during singing than talking[17], [18]. During singing, aerosols are released with exhaled gas plumes[19]. With the surrounding air continuously engaged, gas plumes are dispersed until completely mixing with the ambient air. With this process,

aerosols will be continuously transported elsewhere by indoor air currents. Direct exposure to the exhaled gas plume from a SARS-CoV-2 virus carrier at a close distance will cause a high infection risk due to its high viral concentration. This study names the exhaled gas plume to be an "aerosol plume" to emphasize that it contains viral bioaerosols.

To prevent airborne microorganism transmission in musical performances, it is critical to know the extent of the aerosol plume generated by musical performances. The extent is determined by its interactions with thermal plumes around the human body and indoor ventilation flow[21],[22],[23]. Studies have characterized the aerosol plumes from speech[24], [25], and from musical performances by focusing on the source strength, such as the aerosol concentration[17], [18], [26]–[30] and the air velocity[29], [31], [32], or the convective transport capability, such as the transport distance[29], [32]–[34]. However, features were not integrated to provide a comprehensive characterization of aerosol plumes which could help develop effective infection control strategies covering all of the factors contributing to the aerosol transmission. Furthermore, the source strength was mostly characterized by the source aerosol concentration, ignoring the aerosol plume's source airflow rate needed for risk analyses.

This study investigated aerosol plumes from musical performances by considering both the source strength and convective transport capability to form a comprehensive characterization. In addition, the source strength was characterized by the source aerosol emission rate, defined as the source aerosol concentration multiplied by the source airflow rate. The convective transport capability was characterized by the

plume influence distance, defined as the sum of the horizontal jet length and horizontal instrument length. An illustration of definitions of these aerosol plume characteristics is available in Figure 2.

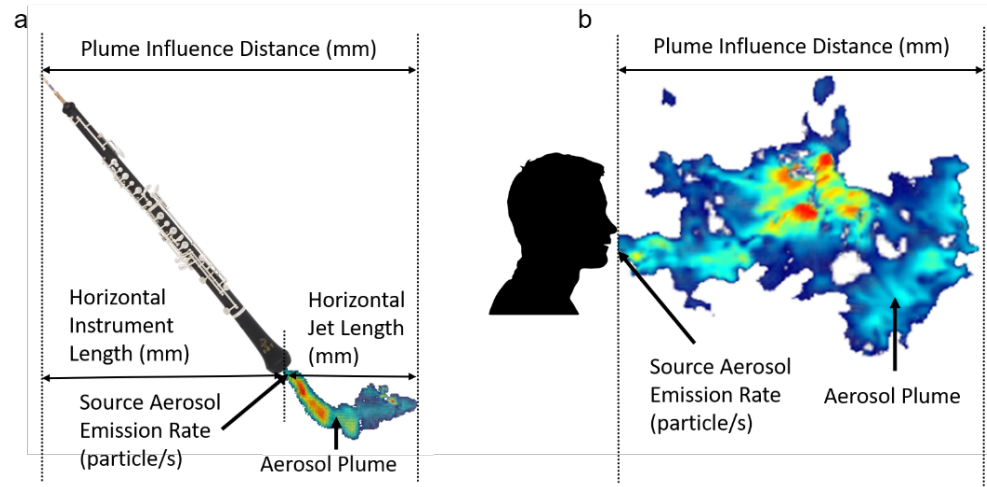


Figure 2 Description of terminologies in source strength and convective transport capability characterization of aerosol plumes from musical performances (a. Instrument, b. Singing).

3.2 Methodology

Human subject experiments with musicians were conducted under an approved Institutional Review Board protocol (IRB 1622465-2). In an environmental chamber, we conducted the source strength characterization by measuring the source aerosol concentration and the source velocity. At the same time, we conducted the convective transport capability characterization by visualizing the aerosol plume. This study also evaluated the performance of mitigation methods, including facial masks and bell covers. Cloth masks, surgical masks, and N95 masks were tested for singing. Bell covers alone and bell covers with MERV-13 filters were tested for playing instruments. The MERV-13 filters were used directly out of the packaging without any exposure to

disinfecting agents such as alcohol. Masks, bell covers and MERV-13 filters used in this study are shown in Figure 3. Experiments took place over roughly five months from November 2020 to March 2021. To protect researchers and participants from COVID-19 infection, following procedures were implemented:

(1) COVID-19 tests and COVID-19 screening surveys were completed by all researchers and participants within three days before the experiment, and only those with a negative test result could participate in the experiment.

(2) Both researchers and participants were required to wear full personal protective equipment (surgical masks and gloves) and keep appropriate social distances (> 6 ft) during experiments.

(3) Before each experiment, the chamber was cleaned by wiping surfaces with alcohol-based disinfectants, mopping the floor with diluted bleach solutions, and running HEPA filter air cleaners to clean the room's air.

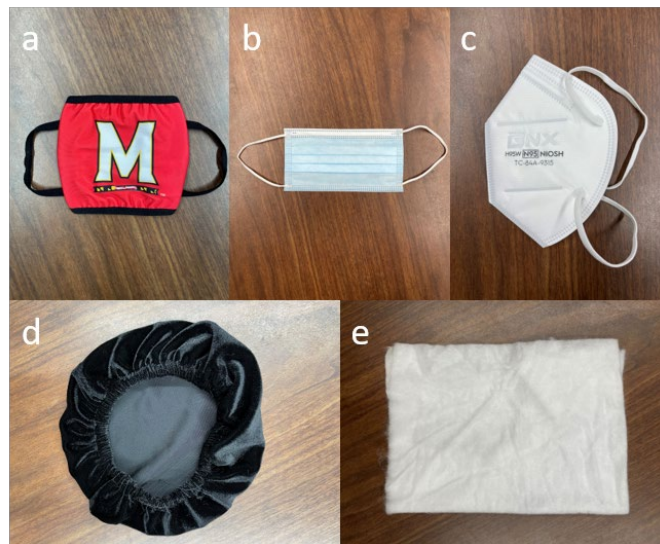


Figure 3 Mitigation Methods. a. Cloth mask. b. Surgical mask. c. N95 mask. d. Bell cover. e. MERV-13 filter.

Human Subjects and Experimental Activities

The musicians in this study were upper-level undergraduate students or graduate students aged between 20-30, from the School of Music, University of Maryland. The experiment included 18 human subjects, representing most of the orchestra's aerosol-producing musicians, such as singing, French horn, trumpet, trombone, flute, clarinet, saxophone and oboe. Detailed information of human subjects can be found in Table 1.

Table 1 Human subject information

	Performance Category	Participant Numbers
Singing	Singing	4
Brass instrument	French Horn	3
	Trumpet	3
	Trombone	1
Woodwind instrument	Flute	3
	Clarinet	1
	Saxophone	2
	Oboe	1
Total		18

The music played by singers and instrument players was consistent for all experiments. Instrument players performed “Holt in E-flat for COVID-19 Study,” which was specifically written for this study[29]. It consisted of a slurred chromatic

scale encompassing each instrument's normal range, and "Holt in Eb," which is a piece of music in the public domain. For singers, the music sample was "Holy, Holy, Holy," with the tempo to be 106 bpm. All musicians were instructed to keep their sound levels at approximately 70-90 dB. A sound level meter was visible to musicians to help control sound levels during experiments. Furthermore, at the experiment onset, each musician was asked to do a warm-up and practice the maintenance of the sound level. During the experiments, each musician was asked to repeat the same piece of music twice in a row without a rest interval. The duration of each musical performance was approximately one minute. Same procedures were conducted for mitigation method tests. Each musical performance was recorded as a time-series dataset, which was used to calculate the time-averaged values. The statistical analysis shown in the figures was conducted on these time-average values.

Environmental Chamber Setup

Experiments were conducted in a climate-controlled chamber, which had a volume of 72 m³ (3.96 m × 4.06 m × 4.47 m). It was well sealed to minimize particle infiltration or exfiltration. The chamber mimicked a typical indoor environment for indoor rehearsal or performance spaces with air temperatures between 22°C ± 2°C, relative humidity levels between 30%-40%, and air velocities between 0.05-0.1 m/s. There was also a small cubic chamber for the particle image velocimetry (PIV) experiment, i.e., PIV chamber, which had dimensions of 1.2 m × 1.2 m × 1.2 m. Figure 4 shows the setup of the environmental chamber.

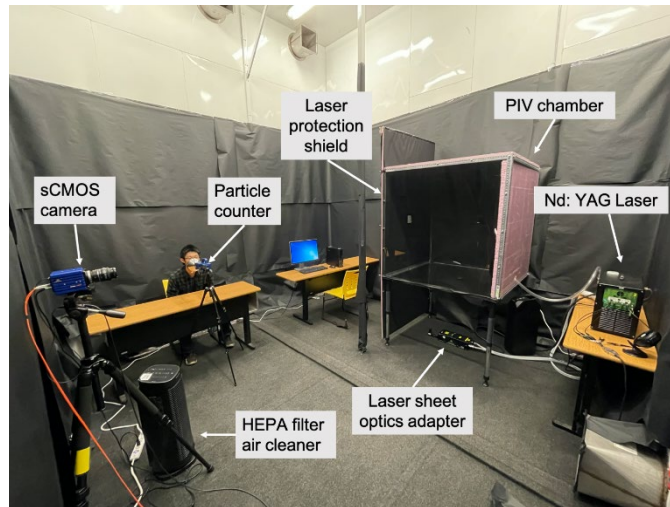


Figure 4 Environmental chamber setup

Experiments to Characterize Source Strength

Two experiments were conducted to investigate the source strength of the aerosol plume from singing and playing wind instruments. One is to measure the source aerosol concentration and size distribution, the other is to measure the source velocity.

In our study, source aerosol concentration measurements deployed the particle counter (TSI 9306, Aerotrak) at the mouth of the singer or the bell of the instrument. The particle counter measures five particle size bins ($0.3 \mu\text{m} - 0.5 \mu\text{m}$, $0.5 \mu\text{m} - 1 \mu\text{m}$, $1 \mu\text{m} - 3 \mu\text{m}$, $3 \mu\text{m} - 5 \mu\text{m}$, $5 \mu\text{m} - 10 \mu\text{m}$). In each source aerosol concentration measurement, three air cleaners with HEPA filters were turned on one hour before measuring source aerosol concentrations to reduce the background particle concentration from approximately $800 \text{ particles/cm}^3$ to $0.5 \text{ particles/cm}^3$. Air cleaners were kept on during measurements to ensure low background particle concentrations. In addition, air cleaners were placed at least two meters away from musicians to avoid interference with aerosol plume measurements. Each musician directed their aerosol plumes into a metal funnel to further minimize influences of the ambient air during

source aerosol concentration measurements. The funnel was also used to help collect particles in the related experimental studies on exhaled aerosols[26], [28], [60]–[62]. We prepared three funnels with diameters 10.4 cm, 12.7 cm and 14.5 cm to fit various dimensions of the mouth and instrument outlet. The funnel was connected to the particle counter with a tube as short as 3 cm to minimize losses of particles due to adhesions to tube surface. To avoid interferences of ambient air entrainments, the funnel was placed as close as possible to aerosol sources, i.e., the mouth or instrument outlet. The particle counter was fixed on a tripod when measuring exhaled aerosols from a singer, whose mouth was entirely covered by the funnel. When playing instruments, it was difficult to conduct measurements with the particle counter fixed on the tripod. Therefore, a researcher would hold it and ensure that the funnel could sufficiently capture expelled aerosols. If the bell of the instrument was smaller than the funnel, it would be entirely covered by the funnel. This was also the case for mouth measurements. If the bell was larger than the funnel, the funnel was placed inside the bell outlet without direct contact but with their centers aligned. Figure 5 illustrates aerosol measurements with funnels. Each measurement continued for the whole musical performance at one second sample interval for each trial.



Figure 5 Source aerosol measurements with funnels for singing (left) and instrument (right)

The source velocity of aerosol plumes was measured by a hot-wire anemometer with an omni-directional probe (Kanomax 6543-2G, measuring range: 0.01 - 5 m/s). The velocity was measured at the center of a singer's mouth or an instrument's bell. To avoid the measurement error introduced by the movement of the participants during performances, a researcher held the probe to follow the movement of the singer's mouth or the instrument's outlet. The sampling interval was one second. Importantly, to avoid influence of the background environment, air cleaners were not running in this experiment.

The source airflow rate was calculated by multiplying the measured source velocity by the effective opening area available in Table 2. The effective opening area calculation used the PIV flow visualization to identify mouth and bell areas discharging the airflow jet. This area is actually a cross-sectional area of the airflow jet at its source. Furthermore, we calculated the source aerosol emission rate by multiplying the source airflow rate with the source aerosol concentration. It was important to recognize that the singer/instrument airflow rates could be higher or lower than the sample airflow rate of the particle counter (0.047 L/s). If the source airflow rate was higher than the

particle counter's sample airflow rate, some amount of the source airflow was bypassing the particle counter. In this case, the source aerosol concentration is equal to the aerosol concentration measured by the particle counter. If the source airflow rate was lower than the particle counter's sample airflow rate, the particle counter captured the entire source airflow, plus additional airflow from the ambient air that had a negligible particle concentration. The additional ambient airflow made the measured aerosol concentration to be lower than the source aerosol concentration. In this case, we derived the source aerosol concentration according to the mass balance of the particle counter's sampling volume.

Table 2 Effective flow area of musical performances

	Category	Effective Opening Area (cm ²)	Total Area (cm ²)	Effective Area Percentage
Singing	Singing	3.40	3.40	100%
Brass Instrument	French horn	6.90	515.39	1%
	Trumpet	5.27	71.13	7%
	Trombone	10.16	210.50	5%
Woodwind Instrument	Flute End	2.84	2.84	100%
	Flute Mouth	1.00	1.00	100%
	Clarinet	9.38	29.64	32%
	Saxophone	9.19	99.36	9%
	Oboe	3.21	11.48	28%

Experiments to Characterize Convective Transport Capability

This experiment visualized and derived the detailed information of aerosol plumes from the singing and instrument by utilizing Background-Oriented Schlieren (BOS) and Particle Image Velocimetry (PIV).

The BOS system consists of four components: a scientific camera (sCMOS), a light, a BOS board made of four 2D BOS Random Dot Pattern Targets ($1\text{m} \times 1\text{m}$), and the BOS software. During measurements, the sCMOS camera was placed four meters away from the BOS board, and the participant was required to stand at one meter to the camera and three meters to the BOS board. Figure 6 shows the experiment setup of the BOS. The BOS visualized airflows by detecting density gradients between airflows and ambient air due to temperature differences. At each time step, the camera took two images with the second as the reference image to show the background (BOS board) without airflows. By comparing the two images, the certain pixel that appears at a different place was used to derive the density gradients[63]. In this study, it was not applicable to conduct BOS to visualize aerosol plums from instrument performances because the temperature differences to the ambient air were too small to be used to detect density gradients. Thus, the BOS visualization was only conducted for the singers.

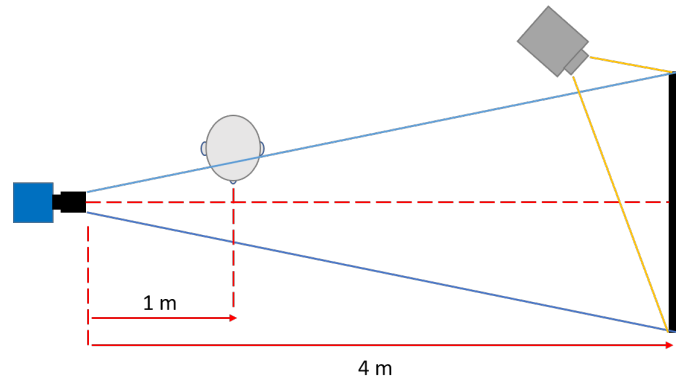


Figure 6 Description of BOS experiment setup

The PIV can provide detailed velocity distributions of aerosol plumes from singing and instrument performances. For a typical PIV recording, small tracer particles are added to the flow field. The plane of interest is illuminated twice by a laser light sheet. The light scattered by the tracer particles is recorded by a high-speed camera. The local displacement vector of the tracer particles of the first and second illumination is determined by the cross-correlation. Velocities are computed taking into account the time interval between two illuminations[64].

In this study, the measuring area was in the PIV chamber built with transparent plexiglass acrylic sheets ($1.2 \text{ m} \times 1.2 \text{ m} \times 0.003 \text{ m}$) for the bottom and side walls, thick Styrofoam sheets ($1.2 \text{ m} \times 1.2 \text{ m} \times 0.05 \text{ m}$) for the top and back walls, and thin Styrofoam ($2.4 \text{ m} \times 1.2 \text{ m} \times 0.03 \text{ m}$) for the front wall. The front wall had an opening for exhaled aerosol plumes to flow through. The height and size of the opening were adjustable with respect to musical performances to fit the location and dimension of singers' mouths and instruments' bells. The front wall separated human subjects from the PIV measuring area to protect human subjects from laser hazards and avoid disturbances to aerosol plumes by ambient airflows, such as ascending thermal plumes

and air movements caused by respirations. Front, top, back, and side walls were covered by non-scattering black papers to avoid reflections of laser beams. The bottom was uncovered to let laser beams through. The wall faced to the camera was also uncovered, so that the camera could take photos for particles' movement highlighted by laser sheets. In addition, an airflow outlet was opened on the back wall, which helped maintain a constant pressure in the PIV chamber during measurements. The PIV system in our experiment was a 2-D PIV, which captured the plane of the flow of interest. The test section was illuminated by a high speed pulsed Nd:YAG laser ($\lambda = 532 \text{ nm}$) with a pulse intensity of 200 MJ. The light sheet thickness was 2.5 mm. To allow the laser emitting from bottom to top, the laser emitter was placed on the floor, under the bottom of the PIV chamber. Before the experiment, tracer particles (DEHS, mineral oil, 1 μm diameter) were generated by an aerosol generator and uniformly spread in the PIV chamber to achieve an optimal concentration. The PIV chamber made it possible to keep seedings at a relatively steady state during measurements. As the experiment started, the light scattered by tracer particles were captured by a high-speed camera (5.5 Megapixel scientific CMOS camera with double-frame mode for cross correlation PIV) with an exposure of 15 μs . The camera faced perpendicular to the light sheet. The imaging frequency was 15 Hz, and the time interval between image pairs was set according to estimated velocities of exhaled airflow. The laser was aligned to the vertical midline of the opening on the front wall. The camera synchronized with the laser would record image frames of particles in the highlighted area of 0.76 m \times 0.64 m in size, and then the processor would calculate velocity vectors with the 32 pixels \times 32 pixels interrogation window. The window had a 75% overlap and noise filtration

with 5×5 Gaussian smoothing based on particles' moved distances during the pulse interval[64]. During the experiment, participants were required to wear laser goggles for eye protection and to stand in front of the PIV chamber's front wall. They were requested to put their mouths against the opening of the front wall, or insert instruments' outlets into the PIV chamber. Figure 7 illustrates the PIV experiment setup. Specifications of measurement equipment can be found in Table 3.

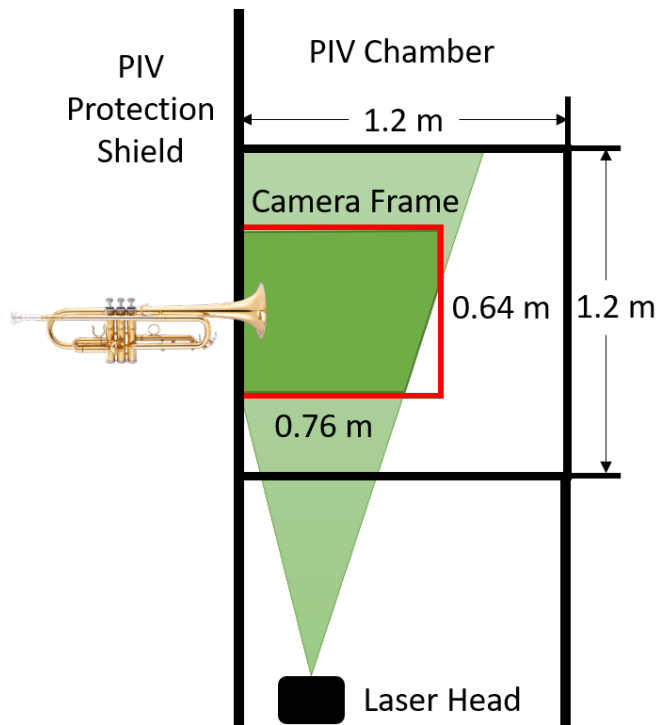


Figure 7 Description of PIV experiment setup

Table 3 Specifications of experiment equipment

Experiment	Equipment	Specification

Aerosol Concentration Measurement	Optical Particle Counter (TSI AEROTRAK 9306)	Channel Size: 0.3, 0.5, 1.0, 3.0, 5.0, 10.0 μm Counting Efficiency: 50% at 0.3 μm ; 100% for particles > 0.45 μm
Air Velocity Measurement	Hot-wire Anemometer (Kanomax, ClimateMaster Series 6501 with 6543-2G probe)	Range: 0.01 to 5 m/s Accuracy: 0.01 to 0.99: ± 0.02 , 0.99 to 5.00: $\pm 2\%$
Background- Oriented Schlieren (BOS)	Background	Board with randomly distributed black squared dots on a white surface. Supplied by Lavigation Inc.
	High-speed Camera	5.5 Megapixel scientific CMOS camera with Nikon 50 mm, F1.4. Supplied by Lavigation Inc.
Particle Image Velocimetry (PIV)	Laser	Nd:YAG Dual Cavity pulsed laser, 2 x 200 MJ/pulse at 532 nm, 15 Hz imaging frequency. Supplied by Lavigation Inc.
	High-speed Camera	5.5 Megapixel scientific CMOS camera with Nikon 50 mm, F1.4. Supplied by Lavigation Inc.

	Processor	CPU: Intel(R) Xeon(R) W-2135 CPU @ 3.70GHz, 6 cores Ram: 64 GB. Supplied by Lavision Inc.
	Aerosol Generator	DEHS (mineral oil, 0.91 g/cm ³ , 1 μm). Supplied by Lavision Inc.

Data analysis

For the source strength characterization, the temporal data of source aerosol concentrations and source velocities collected at singers' mouths or instrument outlets were averaged over the period of musical performance to get the time-averaged data for each trial. The statistics were conducted on the time-averaged data of trials of musical performances. For the convective transport capability characterization, the maximum value of the jet length was selected from the temporal data over the period of musical performance for data analysis. Because of the limited sample size, outliers were defined to be further than $3 \times \text{IQR}$ (where IQR is the inter-quartile range, or the distance between the first and third quartiles). Most of the data were not normally distributed, so the Kruskal-Wallis H Test, which is a rank-based nonparametric test, was conducted to analyze the significance of difference between each group. The significant level α was selected to be 0.05. Python was used as the programming language for the data analysis. In figures, box and whiskers plots are for the statistics of measured data, bar charts are for calculated data.

3.3 *Results*

Source Strength Characterization

Here we present the source strength characterization of aerosol plumes from musical performances with source aerosol concentrations, source velocities, source airflow rates, and source aerosol emission rates as shown in Figure 8 and Figure 9. For aerosol plumes generated by flute players, the source velocities at flautist's mouth and the end opening of the flute have noticeable differences. Thus, the measurements were conducted at both locations separately, as shown in Figure 8a. One French horn player generated much higher source aerosol concentration than the other players. This subject's data was categorized as “high shedder FH”, “FH” represents the French horn. Given that a high source aerosol concentration influences the source aerosol emission rate, the data of the “high shedder FH” was shown both in Figure 8c and 7d.

Figure 8a compares source velocities of the aerosol plumes from musical performances and shows significant differences ($p = 0.013 < \alpha$). Note that the source velocity of the aerosol plume from the flautist's mouth was one to two magnitudes higher than those from the other instruments. Figure 9 shows the same data averaged over instrument categories. By treating the flautist mouth data as an outlier and excluding it from the dataset, Figure 9a shows the source velocity of singing was the highest. It was around three times higher than that of woodwind instruments and six times higher than that of brass instruments ($p = 1e-4 < \alpha$). Figure 8b and Figure 9b show the source airflow rates of aerosol plumes. Overall, woodwind instruments—except for the oboe which uses a double reed—generated higher source airflow rates than brass instruments. Figure 8c compares source aerosol concentrations of aerosol

plumes from musical performances and shows significant differences ($p = 1.2e-5 < \alpha$) between categories. The source aerosol concentrations greatly varied in the orders of magnitude: 104 ~ 105 particles/L for the “high shedder FH” and trombone; 103 ~ 104 particles/L for trumpet, clarinet, oboe, French horn, singing, and saxophone; and 101 ~ 102 particles/L for flute. The size distribution of the source aerosol concentrations can be found in Figure 9. Figure 9c shows that the source aerosol concentration from brass instruments was about two times higher than that from singing and woodwind instruments ($p = 0.02 < \alpha$). Figure 8d shows the source aerosol emission rates of aerosol plumes. The clarinet had the highest source aerosol emission rate up to 1658 particles/s because of its relatively high source aerosol concentration and source airflow rate. Notably, due to the low source airflow rate of the French horn, the “high shedder FH” was ranked as first for the source aerosol concentration but second for the source aerosol emission rate. Figure 9d demonstrates that even though aerosol plumes of woodwind instruments had low source aerosol concentration, it still had about 20% higher source aerosol emission rates than the average of singing and brass instruments due to higher source airflow rates. These results illustrate that only measuring particle concentrations but ignoring source airflow rates will cause the source strength characterization to be incomplete. Table 4 presents the measured data for the source strength characterization that also represent important boundary conditions for future numerical studies of musical performances.

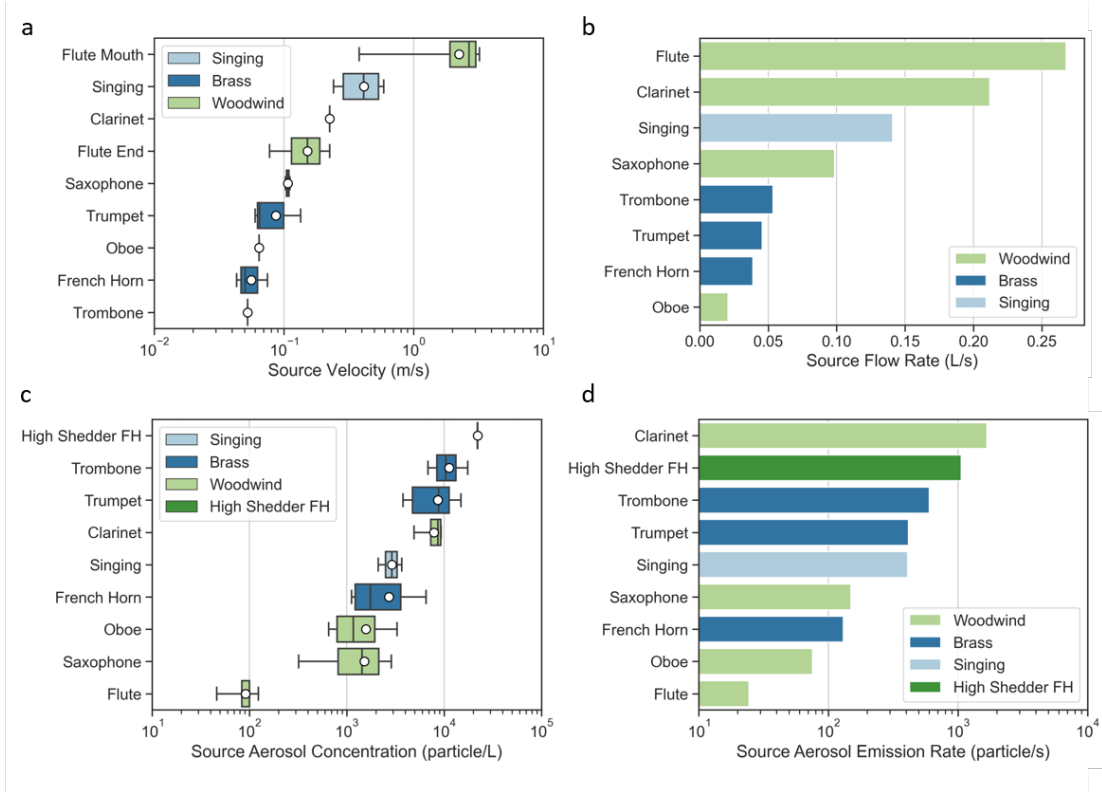


Figure 8 Source strength characterization of aerosol plumes from musical performances. a. Source velocity. b. Source airflow rate. c. Source aerosol concentration including high shedder. d. Source aerosol emission rate including high shedder. (note: “source” refers to the time-averaged data collected at singer mouth or instrument outlet)

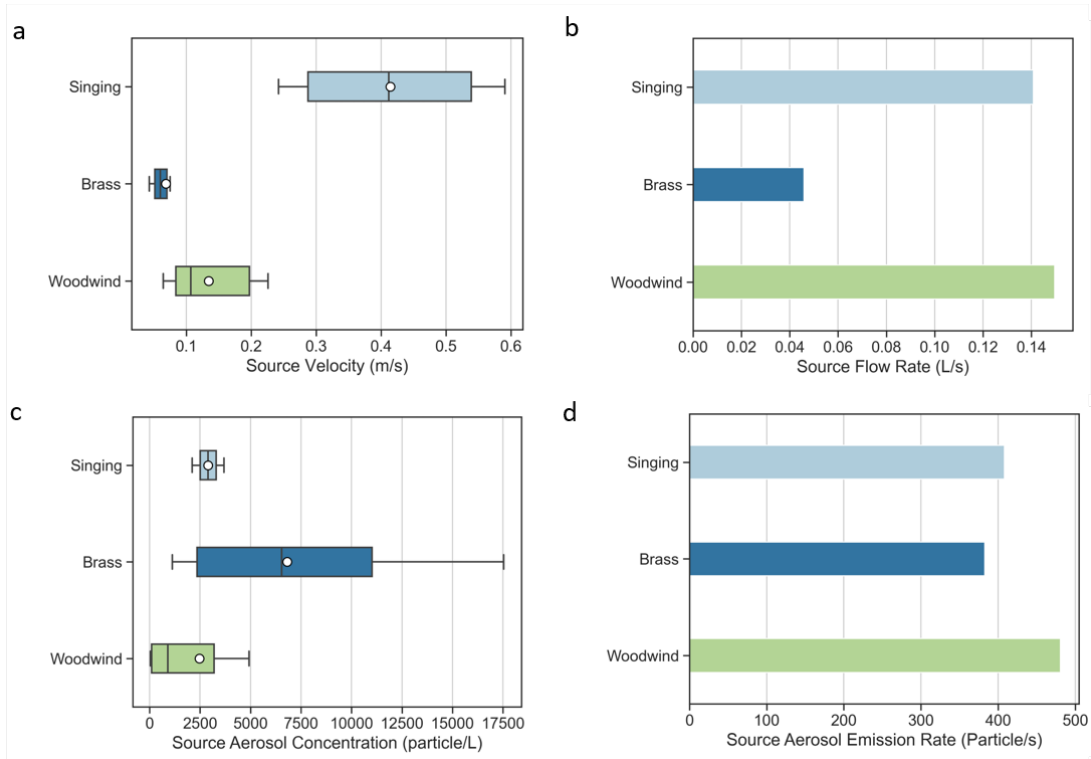


Figure 9 Source strength characterization of aerosol plumes from performance categories (singing, brass instrument and woodwind instrument). a. Source velocity. b. Source airflow rate. c. Source aerosol concentration. d. Source aerosol emission rate (note: “source” refers to the time-averaged data collected at singer mouths or instrument outlets).

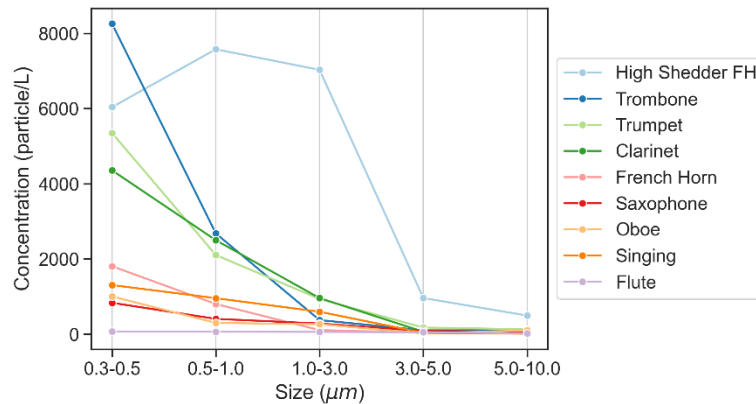


Figure 10 Size distribution of aerosol from musical performances

Table 4 Source characterization data of aerosol plumes from musical performances

Performance	Source Velocity (m/s)	Source Airflow Rate (L/s)	Source Aerosol Concentration (particle/L)	Source Aerosol Emission Rate (particle/s)
Flute	2.24	0.22	91	20
Oboe	0.06	0.02	3698	74
French horn	0.06	0.04	3197	128
Saxophone	0.11	0.10	1519	152
Singing	0.41	0.14	2899	406
Trumpet	0.09	0.05	8636	432
Trombone	0.05	0.05	11277	564
High Shedder FH	0.06	0.04	25960	1038
Clarinet	0.23	0.21	7894	1658

Convective Transport Capability Characterization

For the convective transport capability characterization, aerosol plumes were visualized by Particle Image Velocimetry (PIV) and Background-Oriented Schlieren (BOS). During musical performances, we observed that the air jet was formed from the singer's mouth or the instrument's bell. It then left the outlet and traveled forward until it fully mixed with the ambient air. The plume influence distance was used for the

convective transport capability characterization. It was defined as the sum of the instrument length and the aerosol plume’s jet length in the horizontal direction, which provided a reference distance from the end of the aerosol plume to the music player. This length can be used to assess the minimum social distance that should be used between players to keep them out of each other’s plumes. The horizontal jet length was defined as the farthest horizontal distance of the aerosol plume maintaining a velocity greater than 0.05 m/s. This demonstrates the extent of the area potentially having a non-negligible infection risk. For singing and instruments with bells close to the player’s body, such as the French horn and saxophone, the horizontal instrument lengths were treated as zero. The detailed instrument dimensions can be found in Table 5. Only the horizontal dimension was considered, as it is the main flow direction which influences the risk of the infection. The description of the features of convective transport capability characterization can be found in Figure 2.

Table 5 Convective capability characterization data of aerosol plumes from musical performances

Performance	Horizontal Instrument Dimension (mm)	Horizontal Jet Length (mm)	Plume Influence Distance (mm)
French horn	0	253	253
Saxophone	0	319	319
Singing	0	604	604
Oboe	438	273	711

Trombone	400	338	739
Trumpet	483	331	814
Clarinet	467	407	874
Flute	660	522	1182

During a performance, the horizontal jet length changed over time. The jets produced by playing a whole song were more dynamic than those by playing a single note. Figure 11 shows the fully developed jets moments before they were dissipated in the surrounding environment. We can see that the jets were complex and unsteady. The length and direction of the air jets by musical performances varied due to different instrument orientations and source velocities. To simplify the analysis of the complex time-dependent flow, the maximum jet lengths from performances were selected for the data analysis. From Figure 12a, jets of aerosol plumes produced from singing and playing the flute (both from the flautist's mouth and flute end) horizontally traveled around 500 mm, farther than those from other instruments, which varied from around 100 mm to 400 mm. The differences were significant ($p = 1e-5 < \alpha$) between instruments. Figure 12b shows that the aerosol plume from singing had the longest horizontal jet length with an average of around 600 mm. The aerosol plume from brass instruments had the shortest horizontal jet length with an average of 300 mm. The difference between each performance category was also significant ($p = 8.16e-7 < \alpha$). From Figure 12c, due to the longer jet length and long horizontal instrument length, the plume influence distance of playing flute reached about 1200 mm, which was clearly the farthest. Thus, the plume influence distance of woodwinds was about 30% greater

than that of singing and brass instruments (Figure 12d). The data of plume influence distances can be found in Table 5.

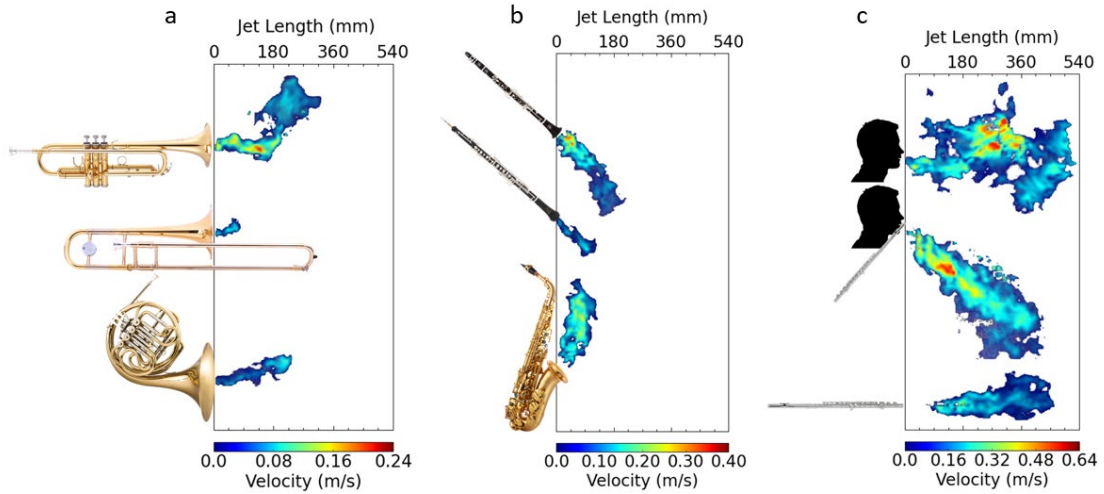


Figure 11 a. Jets of the aerosol plumes from brass instruments. b. Jets of the aerosol plumes from woodwind instruments. c. Jets of the aerosol plumes from singing and flute. Note that the velocity scale is different in each panel.

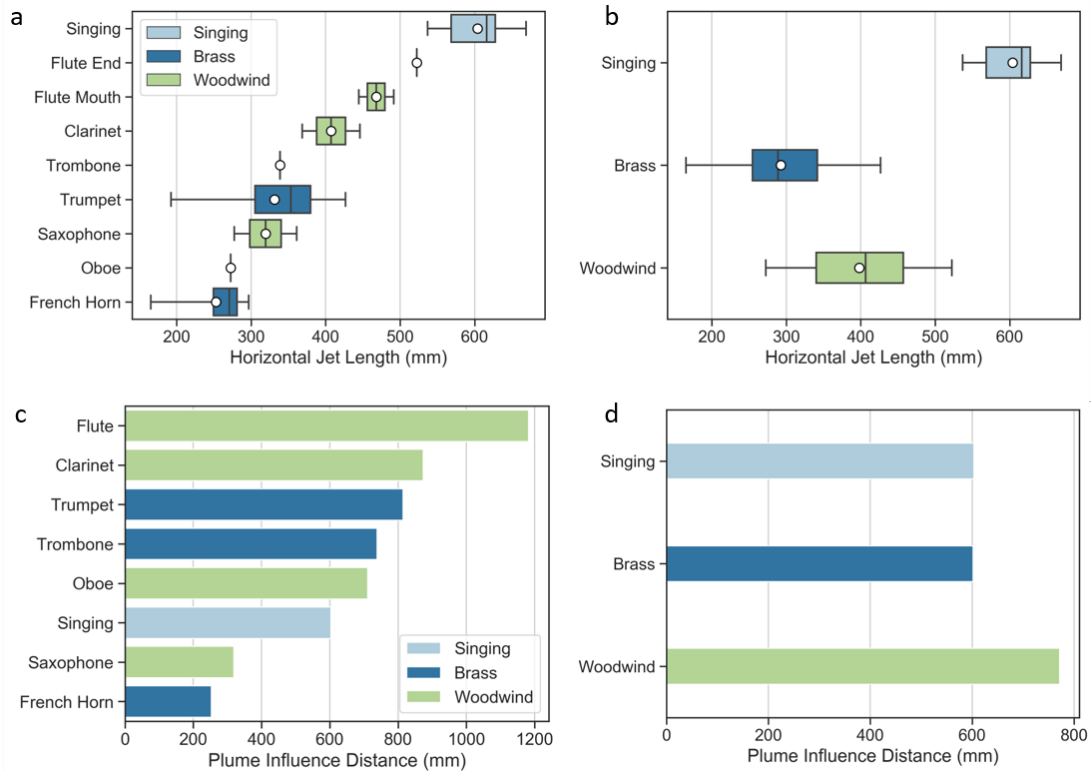


Figure 12 Convective transport capability characterization of aerosol plumes. a. Horizontal jet lengths (musical performance). b. Horizontal jet lengths (performance categories). c. Plume influence distances (musical performance). d. Plume influence distances (performance categories).

Comprehensive Characterization

According to our findings, it is insufficient to independently study the source strength and convective transport capability because such an evaluation would provide incomplete understanding of risk from playing an instrument and singing. Here, we comprehensively characterized the aerosol plumes from musical performances by combining the source strength and convective transport capability to the comprehensive characterization factor. The weight of these two plume characteristics was set to be equal. The characterization factors were calculated based on the weighted

sum method. Firstly, we normalized the source strength and convective transport capability data by their maximums to get values from zero to one. Secondly, the two normalized values were summed with weights to get the comprehensive characterization factor. The comprehensive characterization factor was classified into three categories: high (0.66-1), medium (0.33-0.66), and low (0-0.33). These bins are evenly distributed because they have equal importance. From Table 6, the clarinet was classified as high. The flute, trombone, trumpet, “high shedder FH”, and singing were classified as medium. The oboe, saxophone, and French horn were classified as low.

Figure 13 illustrates the comprehensive characterizations of the aerosol plumes. Figure 14 provides a qualitative visual comparison which allows simultaneous observation of plume size and averaged particle concentrations with the assumption of nearly real-time dispersion of aerosol.

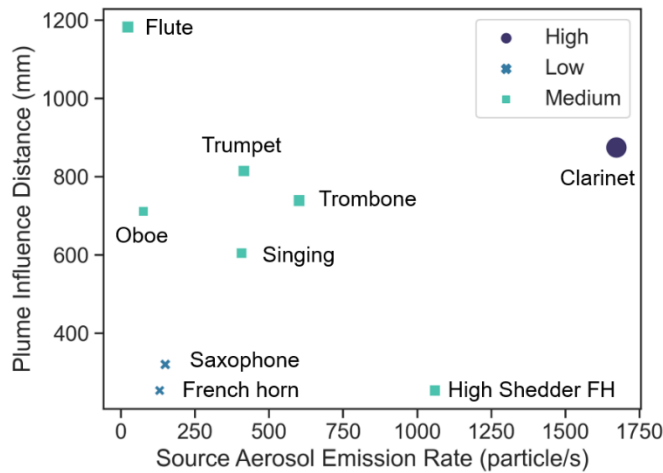


Figure 13 Comprehensive characterization of aerosol plumes

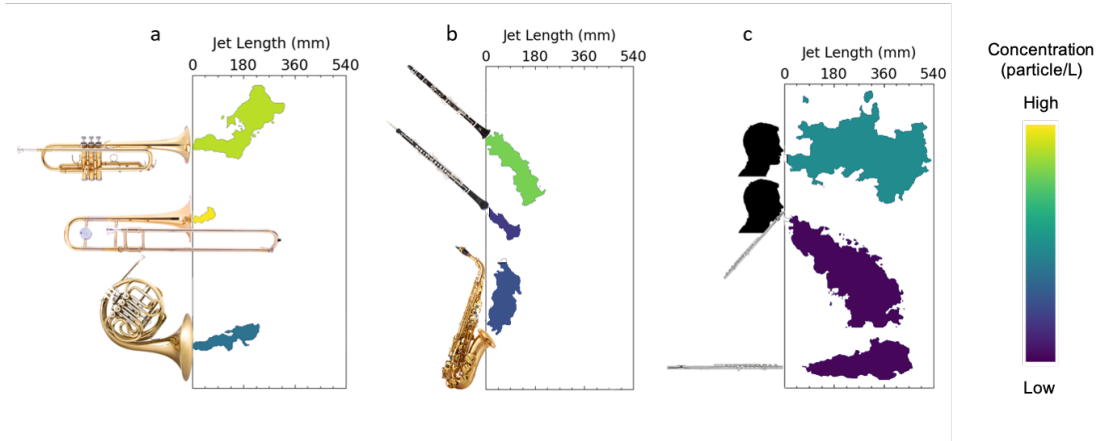


Figure 14 Qualitative comparison of measured average aerosol concentration in different jets of aerosol plumes. (Note: The values of the concentrations can be found in Table 4)

Table 6 Comprehensive characterization of aerosol plumes from musical performances

Performance	Aerosol Emission Rate (particle/s)	Normalized Aerosol Emission Rate	Plume Influence Distance (mm)	Normalized Plume Influence Distance	Comprehensive Characterization Factor	Comprehensive Characterization Category
French horn	128	0.08	253	0.21	0.15	Low
Saxophone	152	0.09	319	0.27	0.18	
Oboe	74	0.04	711	0.60	0.32	
Singing	406	0.24	604	0.51	0.38	Medium
High Shedder FH	1038	0.63	253	0.21	0.42	
Trumpet	432	0.26	814	0.69	0.48	
Trombone	564	0.34	739	0.62	0.48	
Flute	20	0.01	1182	1	0.51	
Clarinet	1658	1	874	0.74	0.87	High

Mitigation Methods

Mitigation methods, such as masks for singers and bell covers with MERV-13 filters for instruments, were tested in the experiments. Measurements were conducted in front of masks and bell covers, leakage areas were not considered in this study. Figure 15 shows the source aerosol concentration and the horizontal jet length comparison with and without mitigation methods for singing and clarinet performance. Based on the measurements, mitigation methods reduced source aerosol concentrations and the momentum of the airflow at the same time. All the other performances follow the similar trend shown in the figure. According to Table 7 and Table 8, for singing, wearing masks can bring source aerosol concentrations to the background level in front of a singer and reduce plume influence distances by 65%. For instruments, bell covers with filters can bring source aerosol concentrations to the background level in front of the instrument bells and reduce plume influence distances by up to 57%. It is noteworthy that only a bell cover without filters cannot promise the reduction of the source aerosol concentration.

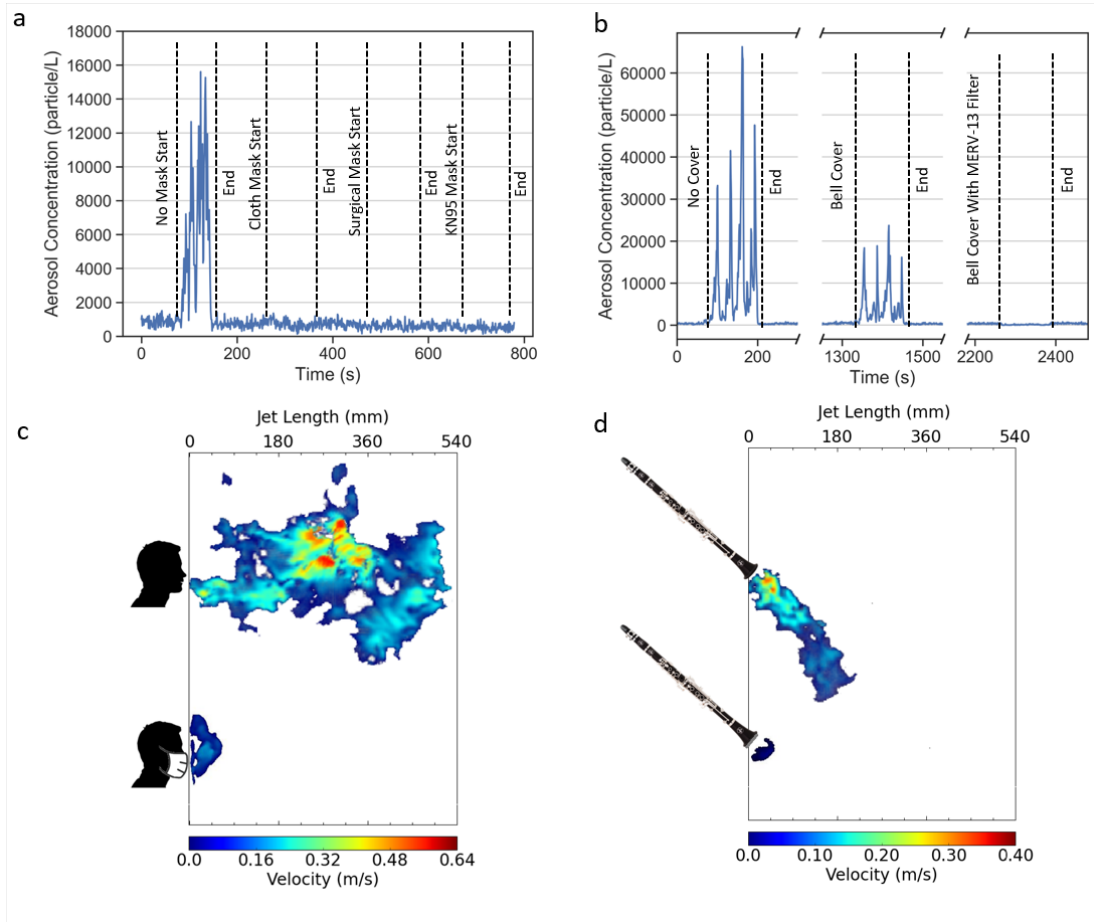


Figure 15 Source Aerosol concentration and horizontal jet length reduction by mitigation methods (singing and clarinet). a. Real-time source aerosol concentration of aerosol plumes from singing (with/without mitigation methods). b. Real-time source aerosol concentration of aerosol plumes from clarinet (with/without mitigation methods). c. horizontal jet length comparison of singing (with/without mitigation methods). d. horizontal jet length comparison of clarinet (with/without mitigation methods).

Table 7 Source Aerosol concentration (particle/L) reduction by mitigation methods

Category	Performance	No Mitigation Methods	With Mitigation Methods	Reduction Percentage
Singing	Singing	2899	~ 0	100%
Brass Instrument	French horn	3197	~ 0	100%
	High Shedder FH	25960	1657	94%
	Trumpet	8636	~ 0	100%
	Trombone	11277	~ 0	100%
Woodwind Instrument	Clarinet	7894	~ 0	100%
	Saxophone	1519	~ 0	100%
	Oboe	3698	~ 0	100%

Table 8 Horizontal jet length (mm) reduction by mitigation methods

Category	Performance	No Mitigation Methods	With Mitigation Methods	Reduction Percentage
Singing	Singing	604	211	65%
Brass Instrument	French horn	253	157	38%
	Trumpet	331	175	47%
Woodwind Instrument	Clarinet	407	260	36%
	Saxophone	319	253	21%

	Oboe	273	117	57%
--	------	-----	-----	-----

3.4 *Discussion*

The acoustics of musical performances may partly account for the generation of aerosol plumes. Brass instrument players produce sound by vibrating the lips[65], while the woodwind instrument players produce sound by reed or air vibration[66], and the singer vibrates vocal cords[67]. The lip vibration may generate more aerosols than the vibration of the reed and the vocal cord. This may be due to frequent accumulations of saliva in the instrument requiring release through water valves; brass instruments would then produce higher source aerosol concentrations than singing and wood instruments. Another cause could be condensations inside the brass tube due to the low surface temperature of brass instruments. Additionally, a curved, long, and keyhole-less instrument means that more aerosols would impact the walls than in the case of woodwinds. Moreover, the instrument's body resonates with the air flowing through it during performances[65]; as a result, the vibration may lead to more aerosols being generated from the condensate on the walls. The tube of a woodwind instrument is usually short, straight, and has a number of keyholes on the tube where exhaled air may contact ambient air. Therefore, compared to the brass instrument, when playing a wood instrument, there is much less water condensations in the tube and aerosols can spread faster by air mixing.

The airflow of aerosol plumes from musical performances may also be influenced by the acoustics. The flute had the highest source air velocity and source airflow rate among the instruments because it produces sound by air vibration[68]. The

air jet formed by singing also had a relatively high source velocity, because it was directly released to indoor air without periodic valving actions of reeds or lips. The air jets formed by playing woodwind instruments with a single reed had higher velocities than those of brass instruments. This may result from different interactions of the reed and lips. A single reed may have an opening area greater than one formed by lipping on a brass instrument, allowing more air flow. The oboe, which uses a double reed, had the lowest velocity among woodwind instruments and the lowest source airflow rate among all the instruments. Compared to air-jet instruments (flute) and single-reed instruments (clarinet and saxophone), double-reed instruments can generate much higher intraoral pressure with decreased source airflow rate for exhaled air because of the smaller gap between the blades of the reed[69]. Playing posture could be a source determinant for the horizontal length of the aerosol plume, as it would affect the direction of the jet. Furthermore, the length and shape of an air jet are determined by the physical characteristics of the instruments and the musicians' blowing techniques. Future research is needed to focus on the aerosol generation and airflow formation mechanisms influenced by the acoustics of musical performances.

Aerosol plumes created by the same instrument can vary widely in the source aerosol concentration, source velocity, and horizontal jet length for different human subjects. For the French horn, we measured source aerosol concentrations to be approximately 26000 particle/L, 6700 particle/L and 1800 particle/L, respectively, for three human subjects. The high shedder had the highest concentration at about five times higher than the average concentration of the other two French horn players. Notably, this player was observed to more frequently remove condensations in the

instrument in comparison to the other players. This could confirm that the accumulated condensation generates a significantly greater amount of aerosol or indicate that the player employed wetter lips, generating more aerosol at the mouthpiece. Therefore, even though singing and brass instruments produce a measurably lower risk on average than the woodwind instruments, it is possible to have an individual musician with high particle shedding rate and associated risk. However, the occurrence of this phenomenon was roughly 5% in this study, the sample was too small to make any conclusions regarding the general population of musicians. Different characteristics of aerosol plumes between each human subject might have been caused by diverse playing techniques and personal features. Further work is required to explore the variances caused by individual musician differences.

Implementing mitigation strategies is strongly recommended in musical performances to prevent airborne microorganism transmission. The comprehensive characterization factors and categorization can offer a reference for the protection strategies in musical performances. For example, if the musical performance has multiple instruments, which were listed in different categories, the decision maker can customize the protection strategy with the help of the comprehensive characterization. Higher level protection, such as a greater social distancing amount, could be implemented for the instruments with higher comprehensive characterization factors.

Aerosol measurements should consider the evaporation of particles because it influences particle diameters[70]–[73]. The present study focused on particles with diameters between 0.3 μm and 10 μm because of their potential for aerosol transmission of viruses that is much more difficult to control than a spray of virus droplets

characterized by larger particles. The measured air velocities were lower than 5 m/s, indoor air temperatures were at $22^{\circ}\text{C} \pm 2^{\circ}\text{C}$, and relative humidity levels were between 30% and 40%. Under these environmental conditions, the evaporation of particles is almost instantaneous[70], so particles were fully-evaporated before reaching the particle counter. Nicas et al.[74] identified that evaporation of aerosols rapidly reaches steady state with the particle diameter equal to half of its original size in typical indoor environmental conditions, similar to the experimental conditions in the present study. Therefore, the diameters of the sampled fully-evaporated aerosols were roughly half of their original diameters at the musician mouth openings or instrument outlets. However, high uncertainties are possible because the one-half shrinkage factor was a rough estimation from Nicas et al.[74], and no other studies directly investigating the shrinkage of expelled respiratory particles were found[74].

Importantly, the transport of aerosols close to the source with resultant near-field aerosol concentrations is dominated by the source aerosol emission rate and a plume primarily driven by the initial air jet momentum. Further from the source, the transport of aerosols with resultant far-field aerosol concentrations is also impacted by the indoor airflow field. The present study focuses on characterizing the near field aerosol plume properties because this is the first step in analyzing the far field aerosol concentrations and transport. Future research could use the findings in the present study to predict and analyze far field aerosol concentrations and transport.

Previous studies provided valuable data to evaluate our measurements. Importantly, in the present study, the data collection instrument allowed for collection of aerosols with particle diameters between $0.3\ \mu\text{m}$ and $10\ \mu\text{m}$, which is a typical range

for airborne aerosols. Therefore, the comparative analysis between the current and existing studies used 0.3 μm to 10 μm range of aerosol diameters. Smaller aerosols than this range are also important[75], but were not collected because the particle counter used in this study cannot collect particles smaller than 0.3 μm . Larger particles are droplets that were outside of the scope of the present study. During each of aerosol measurement experiments, the background concentration of particles was maintained at a very low level of 0.5 particle/cm³. The saturation limit of the data collection device[76], of 210 particle/cm³, was never reached during our experiments. In the comparison, most of our results are in the same magnitude as the results of Alsved et al.[17], Gregson et al.[26], He et al.[28], Stockman et al.[29], and McCarthy et al.[30]. The differences might be caused by different sampling sizes, sample variances, and different measuring equipment and setups in each experiment. For the source air velocity, our measurements are comparable to Stockman et al.[29], Bahl et al.[31], and Becher et al.[32]. For the jet length, our measurements are in the same magnitude of the result from Becher et al.[32]. However, the plume influence distance is shorter than the result from Gantner et al.[34]. The differences may be caused by different experiment methods and setups. Our experimental investigation could be limited by the number of human subjects. Also, for the convective transport characterization, the PIV imaging area may not fully cover the whole flow area of the musical performances with high velocities. Finally, some laser reflections by the instrument body during the PIV experiment, e.g. trombone, could also influence the accuracy of the measurements.

3.5 *Summary*

This study concluded that the characterization of aerosol plumes requires the source strength, characterized by the aerosol emission rate (brass 383 particle/s, singing 408 particle/s, woodwind 480 particle/s), and the convective transport capability, characterized by the plume influence distance (brass 0.6 m, singing 0.6 m, woodwind 0.8 m), to indicate risk of airborne virus transmission. The source strength, characterized by the source aerosol emission rate, requires the measurements of both source aerosol concentrations and source airflow rates. If only the source aerosol concentration is measured, important information about the air flow is ignored, so the source strength characterization will be incomplete. For example, the clarinet showed medium source aerosol concentration, but the highest source aerosol emission rate due to a high source airflow rate. Therefore, the source strength of aerosol plumes from clarinet would have been underestimated, if the source airflow rate had not been measured. From the results of the convective transport capability, the study found that the length and direction of the aerosol plumes in front of the musicians varied due to different instrument orientations and source velocities. To offer comprehensive information on the aerosol plume within a specified musical performance, it is necessary to comprehensively consider its source strength and convective transport capability simultaneously. As an example, playing flute generated aerosol plumes with the lowest source strength, but the highest convective transport capability. If we only considered the characteristic of the source strength, the risk assessment of the infection transmission caused by the aerosol plume from flute playing would be biased in an unsafe way. It is important to note that the comprehensive results show that airflow

from musical performances is a critical component which influences the risk of airborne microorganism transmission. Overall, woodwind instruments showed the highest risk with around 20% higher source aerosol emission rates and 30% higher plume influence distances compared to the average of the same risk indicators for singing and brass instruments.

4. Data-driven thermal comfort identification

This chapter is reproduced from the following journal paper:

L. Wang, D. A. Dalgo, N. Mattise, S. Zhu, and J. Srebric, “Physiological responses and data-driven thermal comfort models with personal conditioning devices (PCD),” *Building and Environment*, p. 110290, Apr. 2023, doi: 10.1016/J.BUILDENV.2023.110290.

4.1 Introduction

One of the primary functions of building systems is to provide an acceptable indoor thermal environment to the occupants [35]. Based on the thermal comfort standard of American Society of Heating, Refrigerating and Air-Conditioning Engineers (ASHRAE) [77], the state of art centralized heating, ventilation, and air-conditioning (HVAC) system is designed to satisfy 80% of the building occupants, but the common real satisfaction rate is only about 50% [78]. One main reason is that the uniform indoor environment with the centralized HVAC can be perceived differently by its occupants because of large individual differences in actual occupant needs. Thus, personalized air conditioning has been proposed to regulate the microenvironment in the proximity of occupants in accordance with their thermal preferences [46]. As an expression of this concept, a personal conditioning device (PCD) was developed to provide both localized thermal comfort and simultaneously allowed for energy savings [79], [80]. The PCD units created comfortable microenvironment due to the forced convection of local air-conditioning given the fact that occupants prefer higher levels of air movement in hot environmental conditions [81]. Importantly, the PCD-based

thermoregulation in an occupant's microenvironment allow for a potential increase of the indoor setpoint temperatures in the uniform environment, resulting in overall energy savings and reduced carbon footprint for future building that might use this technology coupled with the central HVAC systems [80].

Modeling of thermal sensation and comfort is critical to the design, evaluation, and control of indoor thermal environment. Thermal comfort of occupants in uniform environments with centralized HVAC systems have been investigated for decades. The most popular thermal comfort model is Fanger's Predicted Mean Vote/Predicted Percentage of Dissatisfied (PMV/PPD) model [37], which is adopted in the domestic and international standards, such as ASHRAE-55 [77] and ISO-7730 [82]. Fanger's model was based on the mathematical deduction of heat transfer process, originally developed for a group of people in uniform, steady, and thermally neutral indoor environments [83]. However, due to the frequent changes of the indoor environment and activity levels, people's thermal comfort is unsteady most of the time. Moreover, because of the influences of social, cultural, and personal factors [84], individual occupant's thermal sensation and comfort may differ from one another when exposed to the same thermal stimulation [85]. In recent years, personal thermal comfort models were developed to predict thermal comfort requirements of individual occupants more accurately than the predictions with aggregate models in uniform environments. Studies have shown that the personal thermal comfort models can increase energy benefits and occupant associated acceptability in both single-occupant and shared built environment [44].

The development of sensor techniques has made it possible for the real-time monitoring of physiological data, such as skin temperature, heart rate, and skin conductivity, which are associated with a person's thermoregulatory process [86]. As a result, studies presented data-driven models to predict personal thermal comfort based on physiological data collected in real time [45], [87], [88]. Multiple review papers [45], [89], [90] summarized the commonly used machine learning methods for data-driven thermal comfort model development. The machine learning methods used in relevant studies include regression methods [91], k nearest neighbor (KNN) [92], support vector machine (SVM) [93], artificial neural network (ANN) [94], random forest (RF) [95], decision tree (DT) [96], naïve Bayes (NB) [97], etc. Among these machine learning methods, SVM, ANN, and RF are the most frequently used ones [89]. SVM can find the optimal margin between classes and obtain good performance with a relatively small data set [98]. ANN has strong power to effectively solve non-linear and complex problems [99]. RF ensembles multiple decision trees to avoid the possible overfitting caused by a single decision tree [100]. In addition, KNN was also used by relevant studies because of its simplicity and good performance [96], [101], [102].

The existing aggregate or personal thermal comfort models, either physical or data-driven, were mostly developed for the occupants in a uniform environment controlled by the centralized HVAC system. Several studies [103], [104] used thermal comfort models developed for uniform environment on the cases of PCDS, such as Fanger's model [37] and bio-heat comfort model [105]. However, the PCD aims to only condition a relatively small space of the user, microenvironment, with nonuniform or non-steady-state thermal conditions. Thus, the thermal comfort models for

microenvironments created by centralized HVAC may not be applicable to the occupant comfort in nonuniform microenvironments [106]–[109]. Only few studies focused on the thermal comfort modeling with PCD [102], [110]. A study compared different machine learning methods and sensing techniques to build personal comfort models with a local fan or heater [102]. It shows that the data-driven thermal comfort model for centralized HVAC system had low accuracy (about 0.5) in PCD conditions. Based on this, this study suggested better sensing and modeling methods for the PCD with 0.88 overall prediction accuracy. Another study [110] quantitatively described the occupant thermal preference adaptation method, and proposed a classification method of occupant thermal preference recognition in personal microenvironment. Overall, it is necessary to develop high accuracy thermal comfort models that can quickly and effectively capture the thermal comfort variation triggered by local thermal stimulation caused by a PCD [102], no matter PCD is used alone or together with centralized HVAC.

Most of the thermal comfort models take the skin temperature, heart rate, and skin conductance, etc., as thermal physiological inputs [86]. However, these parameters may be not good enough to account for one's thermoregulatory process, which is specifically controlled by the autonomic nervous system [111]. The autonomic nervous system consists of the parasympathetic nervous system (PNS), accounting for the rest/digest activities and the restoration of in vivo thermal balance, and the sympathetic nervous system (SNS), responsible for the fight-or-flight response when exposed to stressful environments, such as a hot environment. The balance between the PNS and SNS can be assessed by the heart rate variability (HRV) [112]. HRV indices include

time-domain, frequency domain, and non-linear variables [113]. Time-domain HRVs quantify the amount of variability in measurements of time intervals between successive heartbeats, which is called inter-beat interval (IBI). Frequency-domain HRVs estimate the distribution of absolute or relative power of the IBI into four frequency bands, which are ultra-low-frequency (ULF, ≤ 0.003 Hz), very-low-frequency (VLF, 0.003-0.04 Hz), low-frequency (LF, 0.04-0.15 Hz), and high-frequency (HF, 0.15-0.40 Hz). Non-linear HRVs are usually used to quantify the unpredictability of the time series, which represents the complexity of the HRV regulation mechanisms. Earliest in 1995, Hasebe et al. [114] used R-R interval and the coefficient of variation in R-R intervals (CVR-R) to point out the potential to evaluate thermal comfort with HRV. The R-R interval is defined as the time elapsed between two successive heartbeats. After that, the frequency domain HRV LF/HF was focused by numerous follow-up studies, because it is the key parameter that represents the ratio of the sympathetic nervous activity and parasympathetic nervous activity. A number of studies show that LF/HF is high for people staying in a cold or hot environment, and low for people in a comfortable thermal environment [115]–[120]. Thus, it becomes a representative HRV index to evaluate human thermal comfort. Another HRV index, pNN50, was also investigated by a study [121]. The results show that pNN50 decreased when human subjects feel hot. Some studies explored the feasibility to evaluate occupant thermal sensation and comfort with multiple HRV indices by data-driven methods for the uniform environment created by centralized HVAC system [122]–[124]. The prediction accuracies achieved by these studies vary from 0.79 to 0.93. Hilbert Transform was used by a study to extract the instantaneous amplitude (iA) of

the LF and HF, the highest prediction accuracy reached 0.73 [125]. However, it is also found that the variations of indoor air temperatures may not cause significant changes on LF/HF [122], [126]. Time-domain, frequency-domain, and non-linear HRV indices can show various trends with the change of the room temperature [122]. In addition, most of the relevant studies were conducted for the whole-room environment created by the centralized HVAC systems [122]–[124]. Almost no study was found considering HRV indices with the PCD. Accordingly, the HRV responses and the possibility of using HRV to evaluate thermal comfort with the PCD need to be investigated.

Based on the above literature review, we can see the lack of a high-performance model to predict thermal comfort in real time when using a PCD. HRV indices appear useful for such a model as they represent the principle of the thermoregulatory process to thermal stimulation. Therefore, this study considers HRV indices in addition to the wrist temperature to be the physiological variables for the thermal comfort prediction. We conducted human subject experiments to monitor human subjects' time-domain, frequency-domain HRV indices, as well as wrist temperature using a self-made non-invasive bracelet sensor. The thermal sensation and comfort were collected by the questionnaire survey. The changes of physiological variables with the PCD may be not as obvious as the cases with the centralized HVAC system due to the nonuniform thermal environment. In this case, data-driven modeling may provide the possibility to predict thermal comfort from the continuous physiological variables. Therefore, we explored the responses of the collected physiological data and surveys, at the same time used machine learning methods to develop data-driven models for the real-time thermal sensation and comfort prediction with the PCD.

4.2 Methodology

Figure 16 presents a graphical illustration of the research scheme applied in this study, which includes the data collection, data analysis, and machine learning. In this section, we provide the details of the methodology of this study, including human subject information, sensor information, experimental setup and procedure, HRV indices, data process, and machine learning methods. The human subject experiment was approved by the Institutional Review Board (IRB) of the University of Maryland (IRB: 655690).

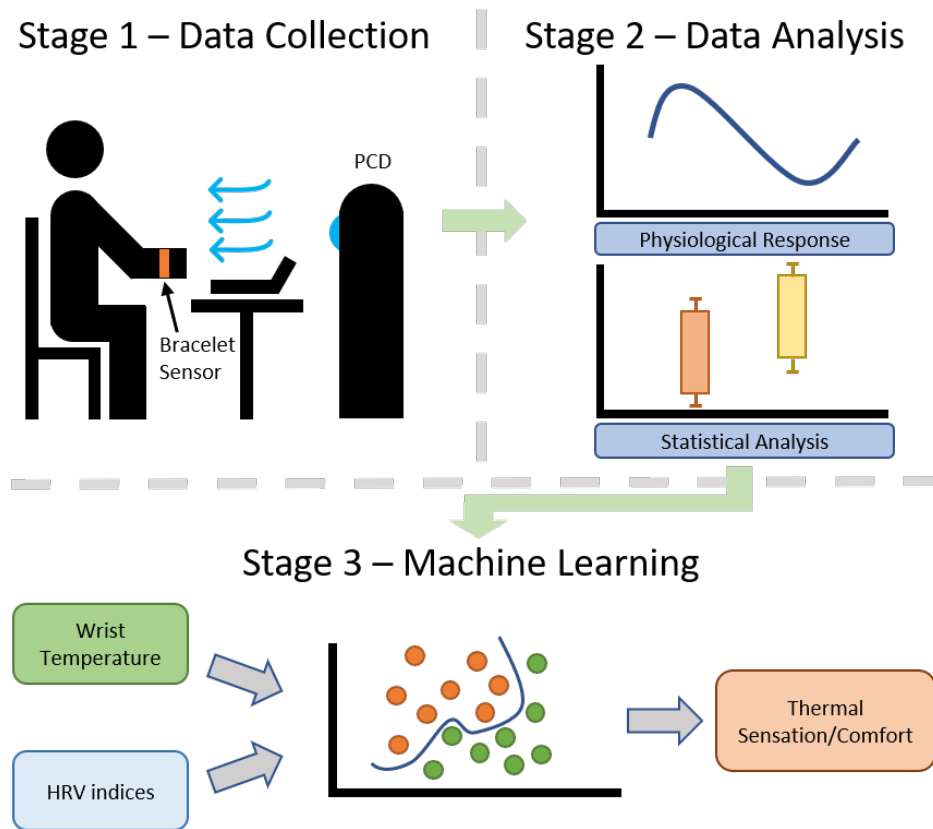


Figure 16 Research scheme of this study

Human subject information

In our study, the human subjects were randomly sampled to represent the target population. The genders were balanced in the sampling. The selection criteria for human subjects specified healthy adults with no ongoing fever, cold/flu symptoms, or chronic diseases that could potentially affect the physiological variables being monitored. A total of 14 human subjects participated in the experiments. Each human subject provided information about their physical attributes, such as body weight, height, age, and gender. According to their Body Mass Index (BMI), all the human subjects were classified as normal weight (18.5 – 24.9). The human subjects were aged from 20 to 29, and most of them were undergraduate students. Table 9 lists the information of human subjects. Each human subject was required to wear office type clothing (pants, shirt, and closed-toe shoes), which resulted in a clothing level of approximately 1.0 clo [77]. The thermal resistance of the office chair is important when considering thermal comfort in a quiescent fluid resulting in natural convection around the whole human body. In our experiments, the same chair was used to keep its thermal resistance identical for each human subject. Therefore, both chair and clothing thermal resistance were constant in our experiments and did not influence measurements of comfort and physiological outcomes with the changing personal environmental conditions.

Table 9 Information of human subjects.

Information	Values
Number of Human Subjects	14
Weight (kg)	Mean: 65.6, Min: 54.0, Max: 79.4, SD: 8.8
Height (cm)	Mean: 172.3, Min: 156.0, Max: 185.9, SD: 9.1

Gender	6 Male 8 Female
--------	-----------------

Sensor information

It is increasingly popular and important to monitor physiological data with wearable technologies without interfering with people in real-world applications. Therefore, we designed and developed a bracelet sensor to non-invasively collect the wrist temperature and HRV of the human subjects with the sensors controlled by a processor (Arduino pro-mini 5V) and packaged in a 3D printed bracelet-type housing, as shown in Figure 17. With the bracelet sensor device, wrist temperature was measured by 2 DS18B20 sensors at a frequency of 2 Hz, and the photoplethysmography (PPG) signal was measured by the pulse sensor at a frequency of 230 Hz. PPG uses a light source and a photodetector to measure the volumetric variations of blood circulation. This bracelet sensor was able to measure the PPG signal with a similar trend compared to the more intrusive and expensive electrocardiograms used in other studies [127]. The HRV indices were calculated by the python package HeartPy [128] based on the collected PPG signal. Importantly, wearing the bracelet did not increase the wrist temperature by producing heat or cause skin sweating at the wrist during the experiment. The ambient temperature and relative humidity were measured by the temperature transmitter and relative humidity transmitter located in the return air duct of the environmental chamber. To secure privacy of the human subjects, all the data was sent, stored, and analyzed in a local server. The technical specifications of the bracelet sensor components are shown in Table 10.

Table 10 Technical specification of the sensors.

Components	Technical information	Accuracy
Processor	Arduino Pro Mini, 5 Volts, 16 MHZ	N/A
PPG Sensor	Pulse sensor, 5 Volts	N/A
Wrist Temperature Sensor	DS18B20, 0.5 °C resolution	± 0.5 °C from -10 °C to +85 °C
Ambient Temperature Sensor	Temperature Transmitter, ACI, 0.1 °C resolution	$\pm 0.2\%$ of full scale for spans < 275 °C
Ambient RH Sensor	Humidity Transmitter, ACI, 0.1% RH resolution	$\pm 1\%$ over 20% span (between 20 to 90%)

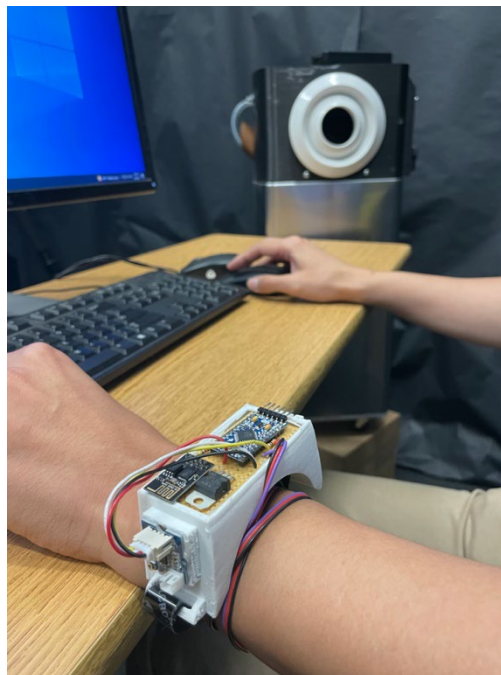


Figure 17 Human subject wearing the bracelet sensor.

Experimental setup and procedure

The experiments were conducted from April 2017 to March 2018. We conducted experiments with human subjects in an environmental chamber ($4 \times 4 \times 4.5$ m) with two desks and two computers. During the design phase of the experiment, we examined the spatial variability of the air temperature and relative humidity in the environmental chamber. The DHT22 sensors were placed on the locations suggested by ASHRAE standard 55 [77]. The measured variation range of the air temperature and relative humidity were ± 0.5 °C and ± 5 %, respectively. No significant spatial variabilities were detected. Because of the same experimental setup, the spatial variabilities were identical in each experiment. Therefore, they were not repetitively measured. The air temperature and relative humidity sensors in the return air duct can accurately represent the uniform environment of the environmental chamber. Before each experiment, the human subjects were arranged to stay in the anteroom, an office room maintained at a temperature of 24 °C, for 15 minutes to acclimatize to a neutral thermal condition. In the anteroom, first a visual inspection was carried out to make sure that human subjects had appropriate clothing. Then a detail explanation of the experiment and appropriate documentation were provided to the human subjects to ensure full consent. A relevant study [129] showed that, human's thermal sensation/comfort and skin temperature can reach near steady-state in 15 minutes after a step temperature change. 10-15 minutes time interval is commonly used for the pre-experimental acclimatization in multiple relevant studies conducted human subject thermal comfort experiments [102], [129]–[132]. After 15 minutes, the human subjects would be introduced into the environmental chamber and stayed there for 100 minutes.

As the studies investigated the dynamic thermal comfort [132]–[134], in the experiment, we dynamically changed the uniform indoor environmental conditions to make human subjects experience thermal discomfort. In this case, human subjects would consider to request the PCD to adjust their personal microenvironmental conditions to relieve thermal discomfort. The air temperature in the chamber was maintained at 28 ± 0.5 °C during the first 50 minutes, then increased and maintained at 30 ± 0.5 °C during the latter 50 minutes. Moreover, the relative humidity during the experiments was maintained at $50 \pm 5\%$. To simulate a real-world office environment, throughout the 100-minute period, each human subject was asked to perform office type activities, such as reading, writing, and typing, with an activity level of around 1.0-1.2 Met [77]. Each human subject had a PCD located approximately 1 ± 0.1 m away at his/her left or right side, and was provided the option to use the PCD at any point in time upon request, except during the time interval of the indoor air temperature change from 28 °C to 30 °C. Specifically, the PCD device used in this study was the Prototype Y2V1 Ice RoCo with technical details available in the literature [79], [135]. It was reported that local thermal sensation of upper body is more weighted to the overall thermal sensation than the local thermal sensation of head and lower body, with the weights of 0.6, 0.21, and 0.19, respectively [136]. Therefore, the PCD supplied cooled air towards the upper torso with about 5 °C lower than the room air temperature and at airflow rates varying between 18.8 ± 5 L/s and 28.3 ± 5 L/s. The outlet diameter of the PCD is 7.62 cm. The area is 45.6 cm². The air velocities vary between 4.12 ± 1 m/s and 6.21 ± 1 m/s. The temperature and flow rate of the supplied air were designed based on the thermal comfort study using CFD [137]. Moreover, the human subjects

continuously reported their thermal sensation and thermal comfort levels every 10 minutes. The thermal sensation levels were based on a -3 to 3 scale used in the ASHRAE Standard 55 (hot, warm, slightly warm, neutral, slightly cool, cool, and cold) [77]. The thermal comfort levels were based on a 5-point scale (very uncomfortable, uncomfortable, neutral, comfortable, very comfortable) used in relevant studies [123], [138].

HRV Indices

HRV can be analyzed in terms of time domain or frequency domain. Time-domain HRV indices quantify the amount of variability of the time period between successive heart beats, while Frequency-domain HRV indices transfer the time series data of the heartbeat to frequency domain to calculate its power by using transforming methods, e.g., Fast Fourier Transform (FFT). This study adopted both the time domain and frequency domain HRV indices [113] as introduced below.

Time-domain indices

Four time-domain indices were used in this study:

SDNN, the standard deviation of intervals between normal heartbeats:

$$SDNN = \sqrt{\frac{1}{N-1} \sum_{i=1}^N (RR_i - \overline{RR})^2} \quad (1)$$

SDSD, the standard deviation of successive differences between adjacent R-R intervals:

$$SDSD = \sqrt{\frac{1}{N-1} \sum_{i=1}^N (RR_{diff_i} - \overline{RR_{diff}})^2} \quad (2)$$

RMSSD, the root mean square of successive differences between adjacent R-R intervals:

$$RMSSD = \sqrt{\frac{1}{N-1} \sum_{i=1}^N (RR_{diff_i})^2} \quad (3)$$

pNNx, percentage of R-R interval that differ by x milliseconds, 20 and 50 are the typical value of x:

$$pNNx = \frac{1}{N-1} \sum_{i=1}^N (|RR_i - RR_{i+1}| > x) \quad (4)$$

where RR is the time interval between two successive heart beats (ms), RR_{diff} is the difference between the adjacent heartbeat time intervals (ms).

Frequency-domain index

LF/HF ratio can well represent the cooperation of PNS and SNS because LF power may be generated by the SNS, and HF power may be produced by the PNS. Homeostasis based on the complementary actions of PNS and SNS represents a human body's ability to uphold optimum conditions when encountering the changes in external stimuli [139]. Therefore, in this study, we used the LF/HF ratio as frequency-domain index, with LF (0.04–0.15 Hz) and HF (0.15–0.4 Hz) signals extracted from the measured PPG signals.

In this study, all the time domain and frequency domain HRV indices were calculated as the short-term in a 5-minute window.

Data process and analysis

Due to individual differences in thermal tolerance, the PCD usage varied among human subjects. For data process, we mark the moment of turning on the PCD, i.e.,

PCD requesting, as time 0. Negative and positive time value represents the time before and after the moment of PCD requesting. To avoid the disturbance and noise brought by the start and the end of the experiments, we calculated and visualized the mean and 95% confidence interval of the 60-minute effective time series data among all human subjects, 30-minute time interval before and after the moment of PCD requesting. To statistically study the significance of the PCD requesting impact, we selected the data in a 10-minute time interval before and after the moment of PCD requesting to conduct the two-sample t-test. The significant level α was selected to be 0.05. Python was used as the tool of data process and analysis.

Machine learning

To implement the machine learning methods to develop the data-driven models, we did the pre-processing to clean data, resample data and normalize data. First, data was cleaned by replacing the outliers with the medium of the dataset. Next, we resampled raw data measured in different sampling frequencies, with linear interpolation for up-sampling and mean value method for down-sampling. Finally, the Min-Max scaler was used to scale the data to be with zero mean and unit variance. The dataset was split in training (75%) and test (25%) using stratified sampling. After the pre-processing, the python machine learning package, scikit-learn, was used as the tool for model development and performance evaluation. The dataset of the present study has labels, which are thermal sensation and comfort indices, so we used supervised learning methods. The thermal sensation and thermal comfort indices are categorical, therefore the machine learning methods we selected are classifiers. Based on the relatively small size of our dataset, this study did not use the machine learning methods

for large datasets, such as the neural network. Importantly, because different datasets have their own properties, such as different complexities and dimensionalities, there are no strict rules on selecting the machine learning methods for a supervised classification problem. It is common to try multiple machine learning methods and selected the one with the highest accuracy [140]. Therefore, due to the uniqueness and high dimensionality of our dataset, which includes the wrist temperature and 6 HRV indices in time and frequency domains, we believe it is important to investigate the performances of multiple commonly used machine learning classification methods mentioned in relevant studies. Based on the literature review of the machine methods in thermal comfort studies, we selected four most commonly used methods including linear support vector machine (SVM_L), k nearest neighbor (KNN), random forest (RF), and support vector machine with RBF kernel (SVM_RBF). We did not use the neural network due to its complexity of hyperparameter tuning.

Linear support vector machine (SVM_L)

The linear support vector machine is one of the most widely used machine learning classification methods. It separates data using hyperplanes as decision boundaries based on the linear combination of input features. The hyperplanes are optimized to have the largest margin between the data and the decision boundary. We selected the linear support vector machine as the baseline model to compare with the other machine learning methods, because it can achieve acceptable performance in most applications. The regularization parameter C was tuned in the model development. The candidate values of C were 0.1, 1, 10, and 100.

K-Nearest Neighbour (KNN)

The KNN is a non-linear supervised machine learning method. The principle behind the KNN is to find a predefined number of training samples closest in distance to the new point and predict the label. The Euclidean distance is the most common choice to measure the distance of between data points. We tuned k , the hyperparameter of the KNN model, which decides the number of closest training samples. The value range of k was from 2 to 50.

Random forest (RF)

Random forest is an ensemble of decision trees. It trains a group of decision trees based on different random subset of the training set, and makes the prediction by selecting the most voted class among the predictions of all individual trees. To optimize the model performance, the hyperparameters we tuned for random forest include the number of trees and the maximum depth of trees. The number of trees was selected from 10, 50, 100, 200, and 300. The maximum depth of trees was selected from 3, 5, and 10.

Support vector machine with RBF kernel (SVM_RBF)

Even though the linear support vector machine works well with the linear separable data, a lot of real-world data sets are nonlinear. Therefore, a non-linear kernel can be used to help solve this issue. We used the Gaussian Radial Basis Function (RBF) as the non-linear kernel. The regularization parameter C and kernel coefficient γ are the hyperparameters needed to be tuned. The candidates of C and γ were 0.1, 1, 10, and 50.

Feature selection

Table 11 shows the value range of the measured physiological variables (input features) and thermal comfort/sensation indices (output). During the machine learning model fitting, all the input features were scaled to be with zero mean and unit variance.

Table 11 Value range of the physiological variables and thermal comfort/sensation indices.

Name	Unit	Minimum	Maximum
Wrist Temp	°C	30.10	36.65
SDNN	ms	40.06	147.29
SDSD	ms	11.52	107.18
RMSSD	ms	17.96	160.98
pNN20	%	33.01	99.77
pNN50	%	1.17	92.76
LF/HF	-	0.03	3.82
Thermal Sensation	-	-1.00	3.00
Thermal Comfort	-	-1.00	1.00

One of the objectives of our study is to explore the performance improvement by using HRV indices. The skin temperature is commonly used for thermal comfort modeling by relevant studies [141], [142], because it is the most straightforward physiological variable related to human thermal regulation. Therefore, we developed M1 as the baseline feature group which only using the wrist temperature. Time domain and frequency domain HRV indices may have different influences on the thermal sensation/comfort prediction. To explore these effects of HRV indices in different

domains, we developed the feature groups M2 and M3. with one typical HRV indices in time domain (SDNN) and frequency domain (LF/HF) in addition to wrist temperature. Because the feature space is high-dimensional, we evaluated the feature importance using the random forest. Figure 18 shows the feature importance of thermal sensation and comfort. The wrist temperature has the highest score for thermal sensation, while the pNN20 is the most important feature for thermal comfort. We selected the first four important features (wrist temperature, pNN20, pNN50, and SDNN) for both thermal sensation and comfort as the feature group M4. Finally, we developed M5 using the wrist temperature and all calculated HRV indices to evaluate the performance improvement, including SDNN, SDSD, RMSSD, pNN20, pNN50 and LF/HF. The feature groups (M1-M5) were introduced in Table 12.

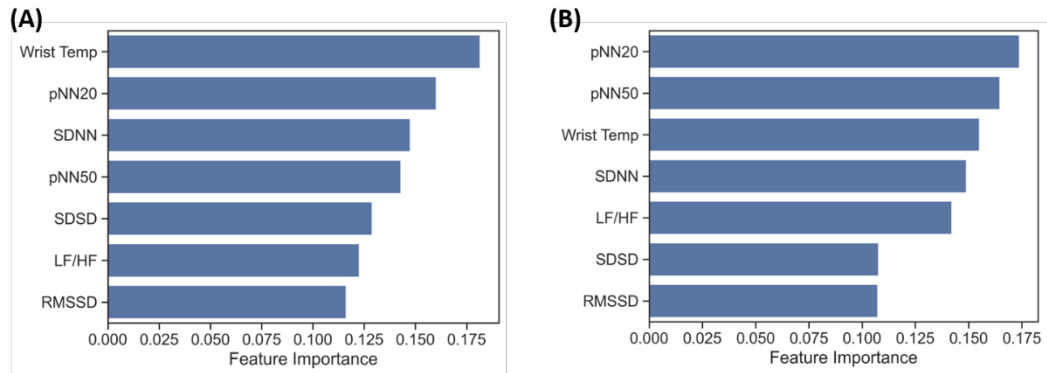


Figure 18 Feature importance analysis of (A) thermal sensation (B) thermal comfort

Table 12 Feature group description.

Groups	Feature Description
M1	Wrist Temperature
M2	Wrist Temperature + SDNN

M3	Wrist Temperature + LF/HF
M4	Wrist Temperature + SDNN + pNN20 + pNN50
M5	Wrist Temperature + SDNN + SDSD + RMSSD + pNN20 + pNN50 + LF/HF

Hyperparameter tuning

We used the exhaustive grid search with the 5-fold cross validation to tune the hyper parameter of the machine learning models. The optimal hyperparameters of thermal sensation and thermal comfort models with different feature groups are listed in Table 13.

Table 13 Optimal hyperparameters of machine learning models

	SVM_L	KNN	RF		SVM_RBF	
	C	k	max depth	number of trees	C	γ
TS-M1	10	15	10	300	50	50
TS-M2	100	7	10	300	50	50
TS-M3	100	6	10	100	50	50
TS-M4	100	2	10	200	50	50
TS-M5	100	2	10	300	10	50
TC-M1	0.1	25	10	200	50	50
TC-M2	0.1	3	10	200	50	50
TC-M3	0.1	3	10	300	50	50
TC-M4	0.1	3	10	300	50	50

TC-M5	10	3	10	100	10	50
-------	----	---	----	-----	----	----

Performance evaluation

To validate the generalizability of the models, the k-fold cross-validation was implemented on the training dataset with 5 folds ($k=5$). Multiple indices were used to evaluate the performance of the machine learning classification models:

- **Accuracy:** The accuracy score is a widely-used performance evaluation method of machine learning models defined as the fraction of correct predictions. If the entire set of the prediction matches with the true values, the accuracy is 1. Otherwise, it is 0.
- **F1 score:** If the imbalance of the classes exists in the datasets of a classification problem, the commonly used accuracy score may fail to evaluate the performance of the model. Thus, we also report the F1 score [143], which is a suitable measure of models with imbalanced classes, to evaluate the model performances. The F1 score is a way to combine the precision and recall of the model. It is defined as the harmonic mean of the model's precision and recall. Because each class is treated to be equally important in our case, the F1 score of the model is the macro average of those among all classes.
- **AUC:** The AUC is defined as the area under curve of the receiver operating characteristic (ROC) curve, a graphical plot illustrates the performance of classifier as its discrimination threshold is varied [144].

A perfect classifier has an AUC equal to 1, a worst classifier has an AUC equal to 0.5.

4.3 *Results*

This section introduces the data analysis of the thermal sensation/comfort patterns and physiological responses with the PCD, as well as the performances of the data-driven models.

Thermal Sensation Responses

Figure 19(A) shows the mean and 95% confidence interval of the time-series thermal sensation data among all the human subjects. Time 0 on the x axis represents the moment of PCD requesting. Negative and positive values on the x axis represent the time before and after PCD requesting. From the plot we can see that the mean thermal sensation before PCD requesting started from around 1.5 (slightly warm to warm), and gradually increased to be higher than 2 (warm to hot) right prior to PCD requesting. Then, the mean thermal sensation dropped to around 0.5 (neutral to slightly warm) soon after starting to use the PCD and decreased to around 0 (neutral). Figure 19(B) visualizes and compares the thermal sensation distribution in 10-minute time intervals before and after PCD requesting. The mean value of thermal sensation was about 2 (warm) before PCD requesting, and 0.5 (neutral to slightly warm) after PCD requesting. The p-value of the two-sample t-test was $3.83e-6 < 0.05$, which shows a significant difference in thermal sensation before and after PCD requesting. According to these results, in our experiment, the PCD can significantly change people's thermal sensation from warm to neutral.

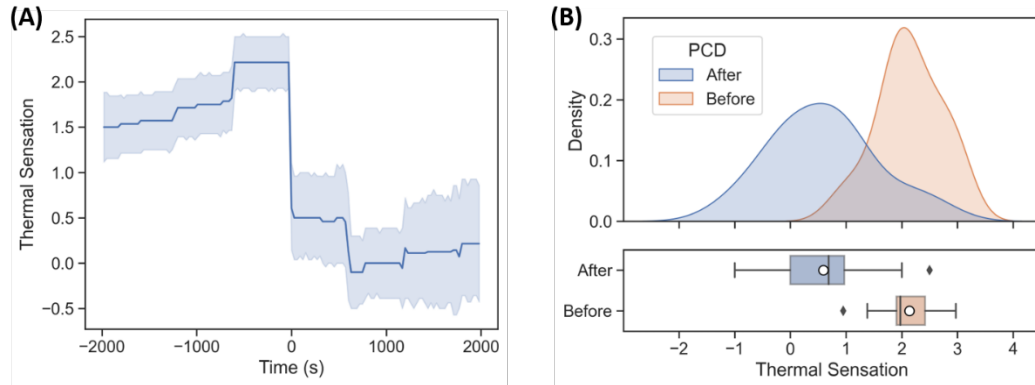


Figure 19 Statistical analysis results for thermal sensation. (A) Mean and 95% confidence interval of thermal sensation. (B) Comparison of the thermal sensation distribution before and after PCD requesting.

Thermal Comfort Responses

Figure 20(A) shows the mean and 95% confidence interval of the time-series thermal comfort data among all the human subjects. From the plot we can see that the mean thermal comfort before PCD requesting started from about 0 (neutral); however, it continuously decreased due to the high temperature environment, and reached around -0.5 (uncomfortable) before using PCD. Soon after PCD requesting, the mean thermal sensation jumped to be higher than 0.2 (neutral to comfortable) and maintained in the comfortable region. Figure 20(B) visualizes and compares the thermal comfort distribution in 10-minute time intervals before and after PCD requesting. The mean value of the thermal comfort was about -0.4 (uncomfortable) before PCD requesting, and 0.2 (neutral to comfortable) after PCD requesting. The p-value of the two-sample t-test was $4.7e-5 < 0.05$, which shows a significant difference in thermal comfort before and after PCD requesting. These results show that running the PCD can significantly

change the thermal comfort of the human subjects from uncomfortable to neutral or comfortable.

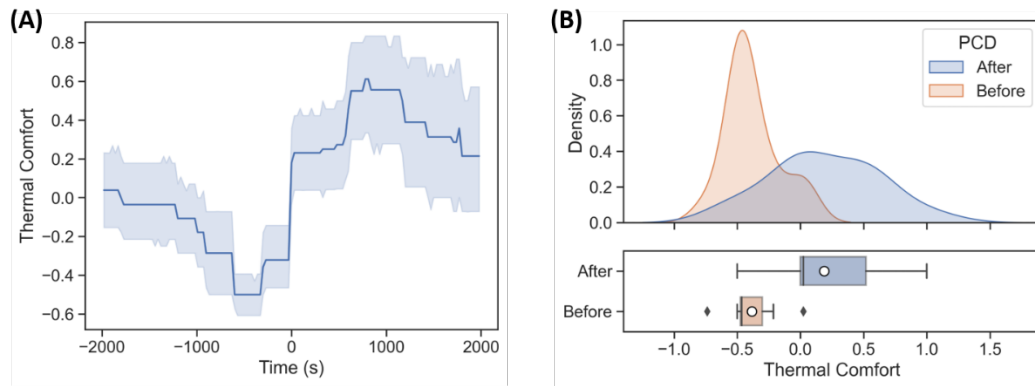


Figure 20 Statistical analysis results for thermal comfort. (A) Mean and 95% confidence interval of thermal comfort. (B) Comparison of the thermal comfort distribution before and after PCD requesting.

Wrist Temperature Responses

Figure 21(A) shows the mean and 95% confidence interval of the time-series wrist temperature data among all the human subjects. The wrist temperature fluctuated randomly between 33 °C to 34 °C. No clear patterns of wrist temperature response can be identified from the time-series data. Figure 21(B) visualizes and compares the wrist temperature distribution in 10-minute time intervals before and after PCD requesting. The mean wrist temperatures before and after requesting the PCD were both about 34 °C. The use of PCD could not make an observable change. The p-value of the two-sample t-test was $0.11 > 0.05$, which shows the difference between the two samples were non-significant.

The non-significant change on wrist temperature can be explained as follows. Varying the indoor air setpoint temperature controlled by the centralized HVAC can

cause the heat transfer on human's overall body surfaces, thus the wrist temperature follows the pattern of the setpoint temperature. However, using the PCD particularly affects the limited body surfaces exposed to the personalized airflow [145]. In our experiment, the convective heat transfer caused by the PCD mainly happened on the upper torso, not the overall human body. As a result, the wrist temperature cannot show a clear pattern with using the PCD. In this case, the traditional thermal comfort models based on skin temperatures for uniform indoor environment may not be compatible with this unclear wrist temperature pattern to provide successful prediction with the PCD.

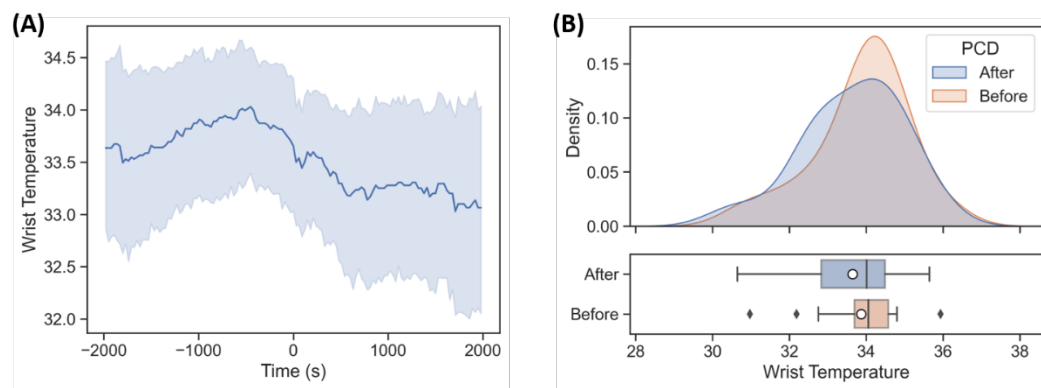


Figure 21 Statistical analysis results for wrist temperature. (A) Mean and 95% confidence interval of the wrist temperature. (B) Comparison of the wrist temperature distribution before and after PCD requesting.

Heart Rate Variability (HRV) Responses

The mean and 95% confidence interval time series data are shown in

Figure 22(A) for SDNN and in

Figure 22(C) for LF/HF. Some spikes can be noticed, but only a noisy pattern

of SDNN and LF/HF responses can be found on the time-series data. The visualization

and comparison of the distributions in a 10-minute time interval before and after PCD requesting are shown on

Figure 22(B) for SDNN and

Figure 22(D) for LF/HF. From the box plots, we can find that the mean values of SDNN and LF/HF are close to each other. The p-values of the two-sample t-test were $0.75 > 0.05$ for SDNN and $0.22 > 0.05$ for LF/HF, both showing non-significant differences before and after PCD requesting.

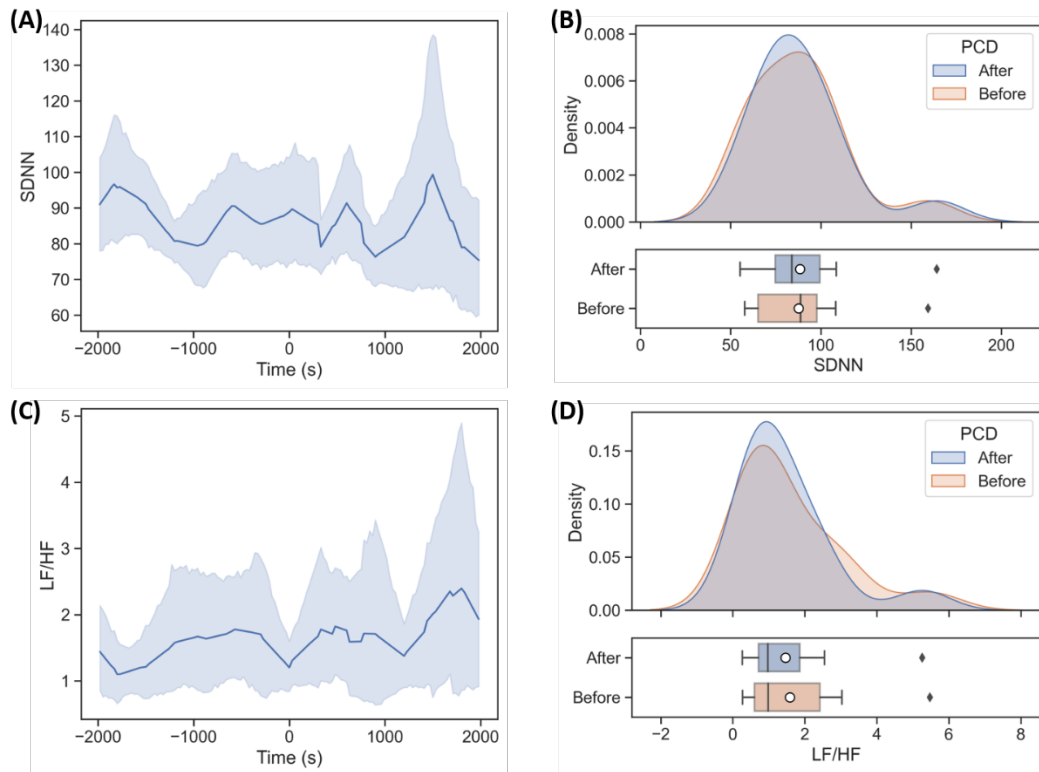


Figure 22 Statistical analysis results for SDNN and LF/HF. (A) Mean and 95% confidence interval of the SDNN. (B) Comparison of the SDNN distribution before and after the PCD requesting. (C) Mean and 95% confidence interval of the LF/HF. (D) Comparison of the LF/HF distribution before and after the PCD requesting.

Machine Learning

The physiological responses with unclear patterns measured in the nonuniform environments created by the PCD could be incompatible with traditional thermal comfort models for uniform environments. Therefore, this study implemented machine learning methods as powerful tools to predict thermal sensation and comfort for PCD users based on these physiological responses with unclear patterns.

Table 14 - Table 17 show the values of performance indices of machine learning methods with different feature groups for thermal sensation and thermal comfort prediction. No big deviations were found among the training, cross-validation, and test accuracies, which shows no overfitting happened. The test accuracy, test F1 score and test AUC show similar patterns. However, in some cases, especially for the Linear SVM, the test F1 scores are significantly lower than the test accuracies because of the class imbalance. Therefore, the F1 score could be a more suitable performance index than the other two to objectively represent the classification performance with our dataset.

Table 14 Values of performance indices of the linear SVM models.

	Training Accuracy	Cross Validation Accuracy	Test Accuracy	Test F1 Score	Test AUC
TS-M1	0.219	0.206	0.215	0.093	0.614
TS-M2	0.245	0.246	0.227	0.094	0.646
TS-M3	0.274	0.270	0.272	0.125	0.677
TS-M4	0.321	0.322	0.331	0.179	0.700

TS-M5	0.330	0.329	0.316	0.158	0.757
TC-M1	0.398	0.398	0.398	0.114	0.576
TC-M2	0.398	0.398	0.398	0.114	0.630
TC-M3	0.398	0.398	0.398	0.114	0.560
TC-M4	0.398	0.398	0.398	0.114	0.628
TC-M5	0.422	0.419	0.426	0.166	0.707

Table 15 Values of performance indices of the KNN models.

	Training Accuracy	Cross Validation Accuracy	Test Accuracy	Test F1 Score	Test AUC
TS-M1	0.439	0.419	0.392	0.288	0.802
TS-M2	0.600	0.455	0.499	0.488	0.851
TS-M3	0.646	0.501	0.553	0.527	0.860
TS-M4	0.939	0.799	0.836	0.848	0.948
TS-M5	0.968	0.866	0.884	0.900	0.972
TC-M1	0.535	0.509	0.519	0.381	0.749
TC-M2	0.743	0.563	0.569	0.476	0.770
TC-M3	0.753	0.570	0.648	0.546	0.793
TC-M4	0.939	0.845	0.881	0.900	0.974
TC-M5	0.970	0.884	0.924	0.917	0.988

Table 16 Values of performance indices of the RF models.

	Training Accuracy	Cross Validation Accuracy	Test Accuracy	Test F1 Score	Test AUC
TS-M1	0.470	0.431	0.410	0.297	0.852
TS-M2	0.805	0.538	0.577	0.547	0.917
TS-M3	0.800	0.554	0.577	0.530	0.914
TS-M4	0.956	0.767	0.835	0.834	0.980
TS-M5	0.984	0.830	0.852	0.856	0.986
TC-M1	0.563	0.548	0.539	0.406	0.828
TC-M2	0.844	0.623	0.615	0.536	0.889
TC-M3	0.850	0.647	0.692	0.603	0.907
TC-M4	0.960	0.822	0.841	0.778	0.973
TC-M5	0.967	0.844	0.869	0.760	0.981

Table 17 Values of performance indices of the SVM with RBF kernel models.

	Training Accuracy	Cross Validation Accuracy	Test Accuracy	Test F1 Score	Test AUC
TS-M1	0.366	0.327	0.320	0.209	0.759
TS-M2	0.536	0.460	0.471	0.416	0.870
TS-M3	0.560	0.504	0.501	0.459	0.879

TS-M4	0.968	0.860	0.881	0.889	0.989
TS-M5	0.989	0.922	0.918	0.922	0.996
TC-M1	0.436	0.416	0.438	0.238	0.720
TC-M2	0.575	0.510	0.495	0.423	0.805
TC-M3	0.616	0.559	0.608	0.521	0.854
TC-M4	0.963	0.884	0.900	0.878	0.987
TC-M5	0.989	0.935	0.958	0.966	0.997

Analysis of feature groups

We calculated the average test F1 score of each feature group among all the machine learning methods to evaluate the performance of the feature groups. With the baseline feature group M1, which only includes the wrist temperature, the average test F1 scores are poor on predicting TS (0.222) and TC (0.285). This confirms that the commonly used temperature-based thermal comfort models for the uniform indoor environment may not work well for the nonuniform microenvironment created by the PCD. Comparing to the baseline feature group M1, adding additional HRV features (M2-M5) can improve the performance of most models. We calculated the percentage to assess the performance improvements. The average test F1 scores of M2, with one time-domain HRV (SDNN) and wrist temperature, are 0.386 for both TS and TC prediction. Comparing to M1, the performances are improved by 74% for TS and 35% for TC. The average test F1 scores of M3, with one frequency-domain HRV (LF/HF) and wrist temperature, are 0.410 for TS prediction and 0.446 for TC prediction. The performances are improved by 85% for TS and 56% for TC versus M1. M4 includes

the top four features selected according to the feature importance, which has the average test F1 scores to be 0.688 for TS and 0.668 for TC. The improving percentages reach 210 % for TS and 134% for TC in comparison with M1. M5 uses all the HRV indices in addition to the wrist temperature as features. The average test F1 scores of M5 achieve the highest values, which are 0.709 for TS and 0.752 for TC. The performances are increased by 219% for TS and 164% for TC against the baseline feature group. Figure 23 shows the average performance indices of different feature groups. The results demonstrate that, even though the patterns of physiological responses were unclear in the nonuniform microenvironment created by the PCD, adding HRVs can still provide useful information of human's thermoregulation system to improve the model performance.

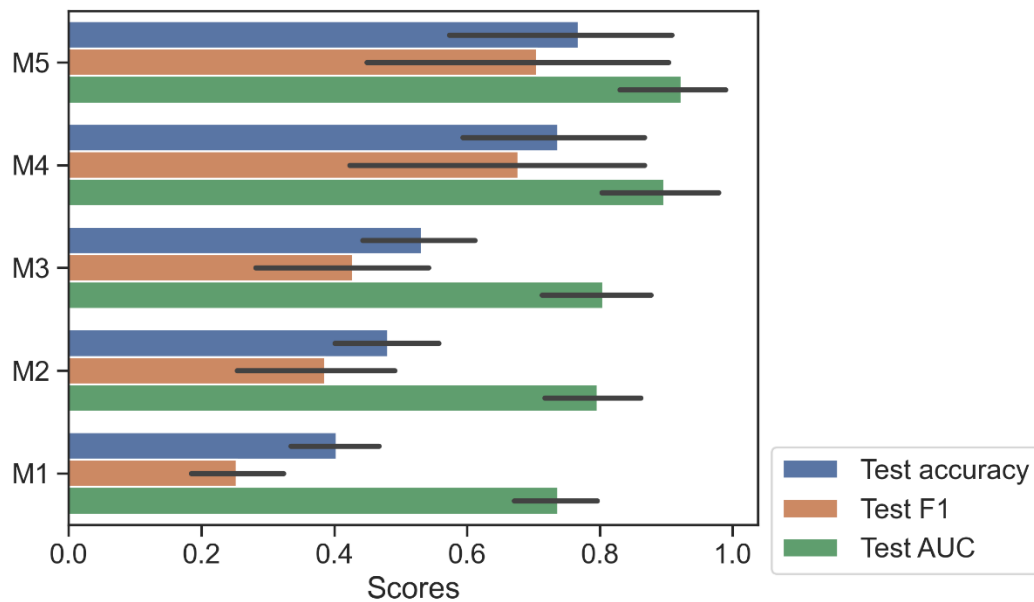


Figure 23 Average performance indices of different feature groups

Analysis of machine learning methods

Among all the machine learning methods, the linear SVM has the lowest performance because of the nonlinearity of the dataset. The highest test F1 scores of linear SVM were 0.179 for TS and 0.166 for TC. In addition, with linear SVM, adding part of the HRV indices cannot improve the performance of the TC prediction (TC-M2 ~ TC-M4) comparing to TC-M1. RF has the highest test F1 scores of 0.856 for TS and 0.778 for TC. These scores are higher than those of linear SVM, but lower than those of KNN and SVM with RBF kernel. The highest test F1 scores of KNN reach 0.900 for TS and 0.917 for TC, about four times higher than the those of the linear SVM. The SVM with RBF kernel achieves the best performance among all the machine learning methods, with the highest test F1 scores to be 0.922 for TS and 0.966 for TC. Figure 24 shows the average performance indices of different machine learning methods with feature group M5.

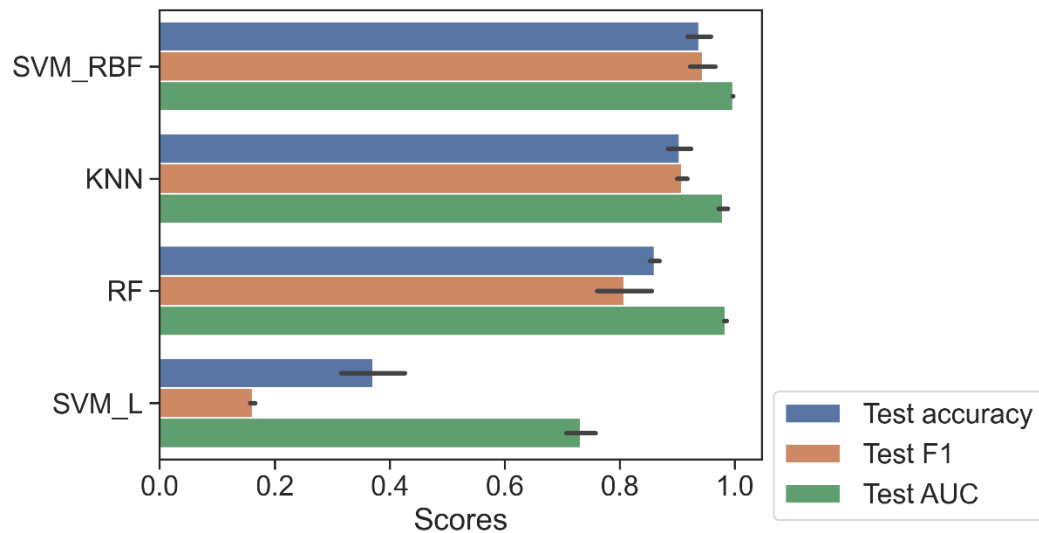


Figure 24 Average performance indices of different machine learning methods with M5

4.4 Discussion

Multiple studies [103], [104] used thermal comfort models developed for uniform environment on the cases of PCDs. To our best knowledge, only one study [102] is found to publish results directly comparable to the present study results. This prior study developed data-driven thermal comfort models for personal conditioning systems using machine learning methods. The models were developed with RF, KNN, SVM with a cubic kernel, and decision trees based on environmental information and skin temperature. The highest accuracy was about 0.88 achieved by KNN for using the PCD (Fan Segment). In present study, the KNN also achieved good performance, which is consistent to the findings of the prior study. However, there are differences in two research findings, such as model performances, which could be due to a variety of factors. The main reason could be the feature selection. The prior study stated that using environmental sensors resulted in slightly better accuracy than physiological sensors. However, the present study did not use any environmental information as features, because the area of the jet region on user's chest created by the personalized conditioning device's is small (10-20 cm²). If the environmental sensor is not placed closed to the center line of the jet, the collected data would not represent the microenvironment created by the PCD. Users could find it difficult to position the sensors correctly in actual applications. Instead, the present study used six HRV indices in addition to the wrist temperature to provide comprehensive information of the human thermoregulation system. The results show that only using physiological data can provide high thermal sensation and comfort prediction performance. The other reasons

for the result differences could be the distinctions between the personal conditioning devices and machine learning methods used in these two studies.

Importantly, the developed models can be potentially used in the occupant-centric autonomous control agent of the PCD. Specifically, the control agent can reliably predict user's thermal sensation and comfort based on collected wrist temperatures and HRVs. The costs of environmental sensors can be saved because only physiological sensors are needed for this system. The flow rate and temperature of the PCD supplied air could be automatically adjusted based on the predicted thermal sensation and comfort from the model. This autonomous control of the PCD with the developed models could allow a possible increase of the indoor setpoint temperatures in the uniform environment. The setpoint temperature increase would result in overall energy savings and reduced carbon footprint for future building that might use PCD coupled with central HVAC systems. With regards to the machine learning methods, the SVM with RBF kernel and KNN could be used in actual application scenarios because both of them achieved high performances and the hyperparameters are relatively easy to tune. Overall, coupled PCD and central HVAC systems integrated with these developed models could provide sustainable energy savings.

One of the limitations of this study is that it involved 14 human subjects. Even though the dataset is comparable to similar previous studies [87], [88], [95], [102], [146], the performance of the machine learning models trained on our dataset may be slightly different from the models trained on a bigger dataset. Longer observations and larger number of human subjects are needed for future investigation.

4.5 *Summary*

This study conducts human-subject experiments to collect physiological data and thermal sensation/comfort surveys for occupants who used a personal conditioning device (PCD) to provide localized cooling based on individual thermal preferences. Specifically, the physiological data allow the development of data-driven thermal sensation and comfort models for occupants using a PCD device. The thermal sensation and comfort data show significant differences before and after requesting the PCD. However, because the thermal stimulus of the PCD are nonuniform and localized compared to the thermal stimuli of the centralized HVAC system, the physiological responses of the PCD users do not show clear patterns as those measured by studies conducted in uniform environments only controlled by centralized HVAC systems. Therefore, the physiological responses with PCD could be incompatible with the traditional aggregate or personal thermal comfort models developed for uniform environments. In this case, this study develops a new set of data-driven models based on occupant physiological responses to nonuniform thermal environments created by the PCD.

The skin temperature, especially the wrist temperature, is a common physiological variable for the thermal sensation and comfort modeling. However, our results show that only using wrist temperature for the data-driven model development cannot achieve sufficient accuracy. Adding HRV indices as additional features can improve the model performance even though the patterns of the physiological responses could be unclear to an observer. Among machine learning methods, the SVM with RBF kernel produced the best performance with the feature group M5, which

combines wrist temperature and six HRV variables. The F1 scores of models based on feature group M5 are more than four times higher than those of the models only using the wrist temperature as the feature (M1). The highest test F1 scores achieved by this study are higher than 0.9 for both thermal sensation and thermal comfort predictions. We suggested using the SVM with RBF kernel based on the feature group M5 in actual applications to provide the reliably solution for predicting users' thermal sensation and comfort variations triggered by local nonuniform thermal stimuli from the PCD units. Future research studies could collect additional data to increase the generalizability of the models.

5. Simultaneous air quality, thermal comfort, and building energy controls

This chapter is reproduced from the following papers:

L. Wang, S. A. Romo, E. Sanico, H. Da Costa, T. Lin, N. Rabchevsky, M. Kern, S. Zhu, J. Srebric, “A Wearable Micro Air Cleaner for Occupant-oriented Indoor Environmental Controls,” *Building and Environment*, (Under Review)

L. Wang, T. Hensel, P. Chanpiwat, S. Zhu, and J. Srebric, “Occupant-centric Control of Building Systems based on Real-time Optimization by Extremum Seeking,” in *2022 IEEE International Conference on Environment and Electrical Engineering and 2022 IEEE Industrial and Commercial Power Systems Europe (EEEIC / I&CPS Europe)*, 2022, pp. 1–6. doi: 10.1109/EEEIC/ICPSEurope54979.2022.9854615.

5.1 Introduction

The air pollution has emerged as a significant global health challenge in recent years, affecting millions of people on a daily basis [147]. The air pollution has been linked to various of illnesses and health conditions, such as respiratory diseases [148] including asthma [149] and chronic obstructive pulmonary disease (COPD) [150], as well as cardiovascular diseases [151], lung cancer [152], and other serious health problems. Despite the growing awareness of the health risks associated with air pollution, progress in reducing pollution levels is still slow in many parts of the world [153], [154]. In addition to air pollution, airborne diseases pose another significant health threat. These diseases are caused by airborne infectious microorganisms, such as bacteria or viruses, which can spread through the air from one person to another

[155]. These pathogens are usually present in respiratory secretions, such as mucus or saliva, and can be released into the air when an infected person talks, coughs, or sneezes [156]. Examples of airborne diseases include COVID-19 [1], tuberculosis [157], and influenza, etc. Because airborne infectious microorganisms can spread easily from person to person, they can be highly contagious and have the potential to cause widespread outbreaks if appropriate prevention and control measures are not taken [11].

Ensuring a healthy indoor environment is essential for public health, considering that people spend a significant amount of time indoors [158]. Poor indoor air quality poses a greater health risk in enclosed spaces with higher population density, such as hospitals [159] and schools [160]. Prior studies showed that higher ventilation rate may reduce the risk of the air pollution and airborne infectious microorganisms [161]. However, centralized ventilation systems may not be able to provide enough protection, especially in situations where the short-range transmission occurs within people's breathing zone, such as music performances [11], [162], [163] and health care in hospitals [164]. In fact, such systems may even contribute to the transmission of infectious diseases by recirculating contaminated air throughout the building [165]. Other technologies, such as ultraviolet (UV) [166] have been investigated for their protective performance. However, their effectiveness depends on range and coverage, and there may be safety concerns regarding human exposure. Recently, by characterizing the aerosol plumes generated from the potential airborne microorganism source [162], [163], studies show that it is imperative to implement effective mitigation methods that specifically target the breathing zone of individuals.

Respirators could be worn by individuals and provide physical barrier between the user and the contaminants in their breathing zone [167]. The N95 respirator is most commonly used for preventing the inhalation of contaminants and airborne infectious microorganisms [168]. However, N95 respirators rely on users' lungs to push the air against the filtering surfaces, which may cause increased facial skin temperature, breathing difficulties and thermal discomfort [169] for prolonged use. Other types of respirators, such as powered air-purifying respirators (PAPRs) [170] etc., utilize head gears of facepieces. These physical components have been found to interfere with many physical, physiological, and psychological aspects of user's task performance. The interference can affect respiration, thermal equilibrium, vision, communication, feelings of well-being, and everyday activities such as eating and sneezing [167]. On the other hand, personalized ventilation systems offer an alternative approach to prevent the spread of pollution and airborne infectious microorganisms without relying on a physical barrier directly on the individual's breathing zone [46], [171]. Typical personalized ventilation systems supply the localized airflow to the occupant at a fixed location [172]–[178]. However, slight variations in positioning, orientation, and height of the person may impact the effectiveness of the fixed personalized ventilation [178]. In situations where individuals need to move or walk around, such as healthcare and laboratory workers or those in high-density and congested workplaces like manufacturing facilities, relying solely on fixed personalized ventilation may not be sufficient.

A wearable air cleaner could be a solution for providing protection to the moving users with the minimum interference due to lack of the physical barrier on

human's breathing zone. Patented wearable air cleaner could be found in the market [179], but there is limited documentation on their performance. Among prior studies, Alshitawi et al. [180] conducted CFD simulations of a personalized air curtain concept. More recently, a helmet-based personalized air curtain was presented, and a series of studies were conducted to assess its performance [181]–[183]. Wei et al. [181] studied multiple influencing factors, such as opening angle, tilt angle, velocity, and width of the helmet-based personalized air curtain by CFD simulations and experiments. They also optimized the air outlet and the flow rates of this device under the static condition (without human movement)[182]. Ma et al. [183] investigated the impact of human body heat, breathing modes and air curtain characters on protective efficiency of the helmet-based personalized air curtain by using CFD. However, the air supplying system of the device, such as the fan could be worn by the user, was not introduced in the studies. The recommended flow rate of helmet-based personalized air curtain is 8-10 L/s [182]. The size and weight of the fan providing this recommended flow rate could be challenging for the user to wear. An applicable and wearable micro air cleaner with appropriate fan and diffuser size is needed to be developed. In addition, the jet of the wearable personalized ventilation device could cause significant convective heat transfer on user's face. User's thermal comfort during the usage of the device also needed to be investigated.

The present study develops a wearable micro air cleaner [184] for occupant-oriented indoor environmental controls, which allows for safety and comfort for the users during moving and prolonged use. The device operates by driving air through a supplying fan mounted on the user's waist. A filter is attached to the supplying fan to

effectively filter out particles and airborne infectious microorganisms. The clean air is then supplied directly into the user's breathing zone through a diffuser mounted on a safety goggle. Since the interaction between airflow and the human breathing zone is intricate and can affect the protective performance and thermal comfort, the supplied air location and flow rate must be carefully designed. The present study conducted tracer gas experiments to optimize the design of the air supply and to evaluate the protective performance. Additionally, human subject experiments were conducted to investigate the thermal comfort experienced by the users during the usage of the wearable micro air cleaner.

Besides the challenge of the indoor air quality, buildings also account for a significant fraction of global electrical energy consumption [54]. The total energy consumption of building is expected to grow at least 40% by 2040 [8]. At the same time, buildings are designed to maintain homogeneous indoor ambient condition, especially for a comfortable thermal and visual environment [54]. The American Society of Heating, Refrigerating and Air-Conditioning Engineers (ASHRAE) defines the thermal comfort as an important aspect in representing human satisfaction [38]. Thermal comfort is the state of mind that indicates a person's perceived equilibrium with their environment. The overall comfort level of a building's occupants has a direct impact on their energy consumption patterns. However, even though a state-of-the-art building system is expected to satisfy 80% of the building occupants based on the ASHRAE standard, the average satisfaction rate is still much lower than expectation [4]. Overall, traditional building heating, ventilation, and air-conditioning (HVAC) systems, which ignore real-time occupant behavior and requirements, are exactly the

cause of the waste of energy and unsatisfied human thermal comfort. There is a need to develop the technologies considering the individual expectation to the indoor thermal environment.

To address the conflict between indoor comfort demand and energy consumption, research on occupant-centric controls (OCC) have increased significantly over the past decade [55]. The OCC is a control strategy for the indoor environment, which specifically focuses on decreasing building energy consumption while meeting the current needs of building occupants. It acquires various data from the occupant and indoor environment, and sends the optimal control signals to actuators according to occupants' requirements [56]. Most OCC algorithms for HVAC were incorporated in either conventional reactive controllers [57] or model predictive controls [58]. However, the conventional controllers cannot handle the uncertainties well. Additionally, the insufficient accuracy of the models is the main weakness of the model-based controller [185].

To overcome the limitations of conventional control strategies, the extremum seeking control (ESC), which is a model-free real-time adaptive control algorithm, becomes popular due to its independence to the system models. ESC is also useful to solve static optimization problems and to optimize parameters of dynamic systems. For building systems, ESC has been implemented in heat pump systems [186], [187], chilled water systems [188], air-side economized systems [189], [190], lighting systems [191], and a virtual thermal environment by Computational Fluid Dynamics (CFD) [192]. However, there is no prior study to apply ESC for the OCC of building systems. Therefore, in this study, we evaluate and analyze the performance of

implementing ESC as the OCC to optimize the building operations based on occupant behavior in an office environment.

5.2 Methodology

This section outlines the methodology used in the air quality and thermal comfort controls.

Air quality control

Both the protective performance and thermal comfort evaluation were carried out within a biosafety level 1 (BSL-1) environmental chamber (4.5 m × 4.1 m × 4.6 m), situated at the University of Maryland, College Park, USA. It is worth mentioning that the thermal comfort evaluation experiments involving human subjects received approval from the Institutional Review Board (IRB) of the University of Maryland (IRB: 1973659).

Figure 25 shows the user wearing the wearable micro air cleaner. A supporter with an air diffuser was mounted on a safety goggle to supply clean air to user's breathing zone. The diffuser was connected to a portable fan mounted on users' waist by a flexible tube. The area of the diffuser is about 5 cm². A filter made by the material of the surgical mask was placed on the fan to clean the air. The filtration efficiency of the filter is 70% - 99% depends on particle sizes [193]. The design of the fan is critical to make the whole device wearable. By balancing the trade-offs between the wearability and performance, the dimension of the fan selected for the wearable micro air cleaner is 120 mm x 112 mm x 32 mm. The flow rate of this wearable micro air cleaner is about 4 L/s. With this flow rate, the air velocity at the diffuser is about 8 m/s.

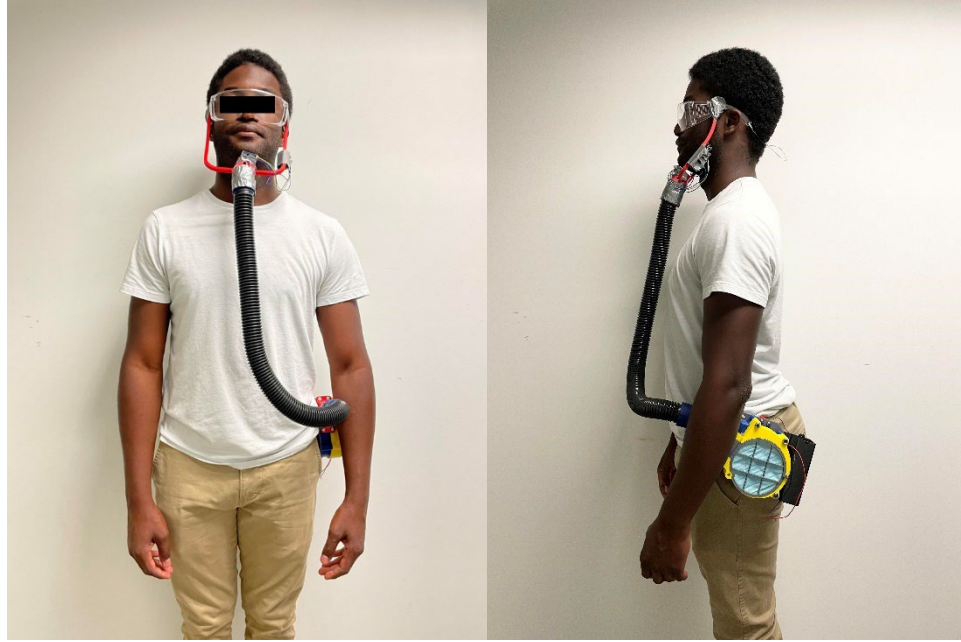


Figure 25 User wearing the wearable micro air cleaner

Protective Performance Evaluation

The protective performance of the wearable micro air cleaner was evaluated by conducting the tracer gas experiments. Multiple indices were developed by prior studies to assess the protective performance, such as personal exposure effectiveness [194], intake fraction [195], and the personal exposure reduction effectiveness (PER) [196]. The present study supplied high concentration tracer gas from the diffuser of the wearable micro air cleaner to manikin's breathing zone. Therefore, the AQI [197] was used as the protective performance index. This index represents the percentage of the tracer gas inhaled by the human subject, which is defined as the following equation:

$$AQI = \frac{C_i - C_a}{C_d - C_a} \quad (5)$$

where C_i is the tracer gas concentration of the inhaled air, C_d is the tracer gas concentration at the diffuser of the wearable micro air cleaner, C_a is the tracer gas concentration of the ambient air.

To simulate human's inhalation, a 3-D printed NIOSH standard manikin head was connected to a pump. Both the nasal and mouth inhalation were considered. The flow rate of the inhalation was set to about 8 L/min [198]. CO₂ was used as the tracer gas in the experiment. High concentration CO₂ (about 5000 ppm) was supplied to the wearable micro air cleaner fan through a hose, then supplied to manikin's breathing zone through the diffuser. No mixing happened between the high concentration CO₂ and ambient air in the chamber during the supplying. Because the CO₂ concentration in the hose is the same to the CO₂ concentration at the diffuser, a CO₂ sensor was placed next to the the wearable micro air cleaner fan in the hose to measure C_d . One CO₂ sensor was placed at the end of the inhalation loop to measure the inhaled air concentration C_i . Another CO₂ sensor was placed in the chamber to measure the ambient air concentration C_a . The spatial variability of the CO₂ was verified before the experiment. No significant spatial variability was detected. Figure 26 shows the diagram of the experimental setup.

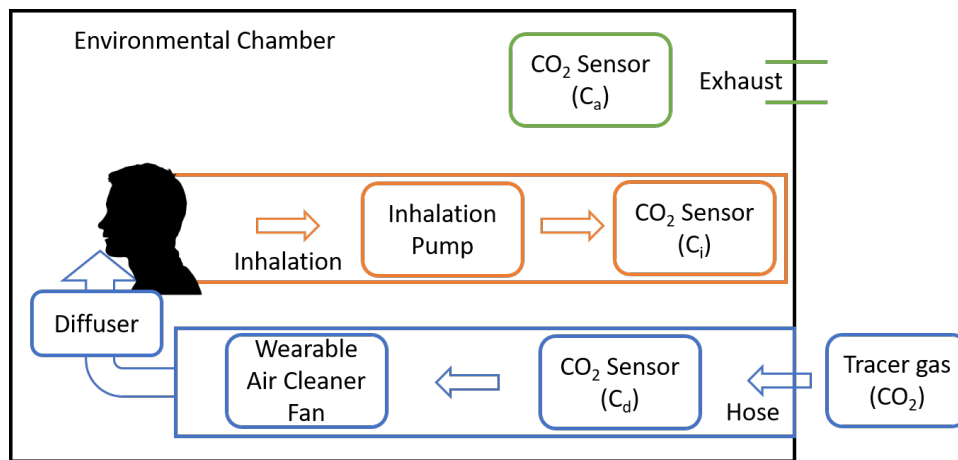


Figure 26 Experimental setup of the protective performance evaluation

Thermal Comfort Evaluation

The objective of the thermal comfort evaluation is to investigate the thermal sensation/comfort and physiological response of users resulting from the operation of the wearable micro air cleaner. Data-driven thermal comfort models were developed using collected environmental and physiological data. The human subjects were randomly selected to ensure representation of the target population. The genders were balanced. The selection criteria for human subjects specified healthy adults who were free from fever, cold/flu symptoms, or chronic diseases that could potentially impact the monitored physiological variables. A total of 20 human subjects participated in the experiments. Each human subject provided information about their physical attributes, such as body weight, height, age, and gender. Each human subject was required to wear office-type clothing (pants, shirt, and closed-toe shoes), resulting in a clothing level of approximately 1.0 clo [77]. Please refer to Table 18 for detailed information of the human subjects.

Table 18 Information of human subjects.

Information	Values
Number of Human Subjects	20
Weight (kg)	62.7
Height (cm)	169.45
Gender	10 Male, 10 Female

Because the wearable micro air cleaner may cause significant convective heat transfer on user's face, both the overall and local (face) thermal sensation and comfort were collected by the questionnaire. The face temperature, a commonly used

physiological variable for thermal comfort evaluation, was measured using a MLX90640 thermal camera at a sampling rate of 1 second. An averaged face temperature was calculated based on the measured temperature array. Previous studies have demonstrated the benefits of incorporating heart rate variability (HRV) in predicting thermal sensation/comfort [199], [200]. Therefore, multiple HRV indices in the time and frequency domains were measured, including SDNN, SDSD, RMSSD, pNN20, pNN50, and LF/HF [113]. The photoplethysmography (PPG) signal was measured by a pulse sensor at the sample rate of 230 Hz. The HRV indices were calculated by the python package HeartPy [128] based on the collected PPG signal. The ambient temperature and relative humidity within the environmental chamber were measured using temperature and relative humidity transmitters located in the return air duct. To ensure the privacy of the human subjects, all data was transmitted, stored, and analyzed on a local server. The technical specifications of the sensor are shown in Table 19.

Table 19 Technical specification of the sensors.

Components	Technical information	Accuracy
Processor	Arduino Nano, 5 Volts, 16 MHZ	N/A
PPG Sensor	Pulse sensor, 5 Volts	N/A
Face Temperature Sensor	MLX90640 thermal camera	± 1 °C from 0 °C to 100 °C

Ambient Temperature Sensor	Temperature Transmitter, ACI, 0.1 °C resolution	$\pm 0.2\%$ of full scale for spans < 275 °C
Ambient RH Sensor	Humidity Transmitter, ACI, 0.1% RH resolution	$\pm 1\%$ over 20% span (between 20 to 90%)

The experiments were conducted from April 2023 to June 2023. Prior to each experiment, the human subjects were instructed to spend 15 minutes in the environmental chamber maintained at a temperature of 25 °C to acclimate to a neutral thermal condition. A visual inspection was conducted to ensure that the human subjects were appropriately dressed. Detailed explanations of the experiments were provided, and appropriate documentation was given to the subjects to ensure their full consent. As the wearable micro air cleaner can be used in various indoor air temperatures, the experiments were divided into three sections, each conducted at a different indoor air temperature: 22 °C, 25 °C, and 28 °C. Each section lasted approximately 40 minutes. For the first 20 minutes of each section, the wearable micro air cleaner was turned off, while for the second 20 minutes, it was turned on. The relative humidity was maintained at $50 \pm 10\%$ throughout the experiments. To simulate a typical office environment, the human subjects were allowed to engage in office-type activities such as reading, writing, and typing, with an activity level ranging from 1.0 to 1.2 Met [77]. At regular intervals of 5 minutes, the human subjects provided continuous reports of their overall and local thermal sensation/comfort levels. The thermal sensation levels were assessed on a scale of -3 to 3, as defined in the ASHRAE Standard 55 (ranging

from hot, warm, slightly warm, neutral, slightly cool, cool, to cold) [77]. The thermal comfort levels were evaluated using a 7-point scale based on relevant studies [123], [138].

In the present study, the mean values of the time series data were calculated and visualized across all human subjects. To examine the statistical significance of the impact of the wearable micro air cleaner on thermal comfort and physiological variables, paired t-tests were performed on the data collected before and after the operation of the wearable micro air cleaner. The significant level α was selected to be 0.05. Additionally, Cohen's d value was calculated to assess the effect size. An absolute Cohen's d value below 0.3 indicates a small effect size, while values between 0.3 and 0.5 represent a moderate effect size. If the absolute Cohen's d value exceeds 0.7, the effect size is considered large. Positive and negative values indicate positive and negative relationships, respectively. Python was used as the tool of data process and analysis.

In order to develop data-driven models using machine learning methods, the present study performed several data pre-processing steps, including data cleaning, data resampling, and data normalization. Firstly, the data was cleaned by replacing outliers with the median value of the dataset. Subsequently, the raw data, which was measured at different sampling frequencies, was resampled to a frequency of 30 seconds. Linear interpolation was used for up-sampling, while the mean value method was applied for down-sampling. Finally, the Min-Max scaler was employed to normalize the data, ensuring zero mean and unit variance. After the pre-processing stage, the machine learning models were developed and evaluated using the scikit-learn package in

Python. The dataset was divided into training (75%) and test (25%) sets using stratified sampling. Given the unique nature and high dimensionality of the dataset, three commonly used nonlinear machine learning algorithms were selected: k nearest neighbor (KNN), random forest (RF), and support vector machine with RBF kernel (SVM_RBF). The feature importance was calculated based on the random forest method. The hyperparameters of the machine learning methods were tuned using grid-search, and cross-validations were performed to exam overfitting. Multiple model performance evaluation metrics, such as accuracy, F1 score, and AUC (Area Under the Curve), were chosen as indices to assess the performance of the machine learning models.

Thermal comfort control

Thermal Comfort Model

In this study, Fanger's Predicted Mean Vote (PMV) and Predicted Percent Dissatisfied (PPD) model [37], on which the ISO and ASHRAE thermal comfort standards are based, is selected to develop the extremum seeking controller. The PMV-PPD was originally developed to predict thermal comfort at steady states, so it does not account for the dynamic response to the changes in indoor thermal environment. To apply this model, we assume that the occupants' thermal comfort changes immediately with the indoor environment. The PMV-PPD model accounts the following heat transfer processes on a human body:

Rate of convective heat loss from the skin (C):

$$C = f_{cl}h_c(T_{cl} - T_a) \quad (6)$$

Rate of radiative heat loss from the skin (R):

$$R = -3.96 * 10e^{-8} f_{cl} [(T_{cl} + 273)^4 - (T_r + 273)^4] \quad (7)$$

Dry respiration heat loss (C_{res}):

$$C_{res} = 0.014M(34 - T_a) \quad (8)$$

Latent respiration heat loss (E_{res}):

$$E_{res} = 0.0173M(5.867 - P_a) \quad (9)$$

Heat loss by vapor diffusion through skin (E_{dif}):

$$E_{dif} = 3.05[5.733 - 0.007(M - W) - P_a] \quad (10)$$

Rate of evaporative heat loss from the skin through sweating (E_{rsw}):

$$E_{rsw} = 0.42(M - W - 58.2) \quad (11)$$

where f_{cl} is clothing area factor (non-dimensional), h_c is convective heat transfer coefficient ($Wm^{-2}K^{-1}$), T_{cl} is mean temperature over the clothed body ($^{\circ}C$), T_a is air temperature ($^{\circ}C$), T_r is mean radiant temperature ($^{\circ}C$), M is rate of metabolic energy production (Wm^{-2}), P_a is partial pressure of water vapor in air (kPa), and W is rate of mechanical work (Wm^{-2}).

All heat transfer terms provide the PMV equation:

$$PMV = (0.303e^{-0.036M} + 0.0275)\{M - W - [(C + R + E_{rsw} + E_{dif}) + (C_{res} + E_{res})]\} \quad (12)$$

PMV evaluates the thermal sensation. There are seven scales from hot (+3) to cold (-3). $PMV = 0$ is the neutral thermal sensation. PPD establishes a quantitative prediction of the percentage of thermal dissatisfaction, and it can be determined as a function of PMV:

$$PPD = 100 - 95e^{[-(0.03353PMV^4 + 0.2179PMV^2)]} \quad (13)$$

The PPD can range from 5% to 100%, depending on the PMV value. Intuitively, the PMV metric indicates the predicted thermal sensation that respondents would experience in a given environment, and the PPD translates the PMV metric to a measure of what percentage of respondents are expected to be satisfied with their perceived thermal sensation. A PMV between -0.5 and 0.5 is considered satisfactory. It is important to note that PPD transforms PMV into a symmetric, convex function representing thermal comfort. This is necessary to establish the optimality of temperature setpoints in later sections.

To simplify the model, some parameters in the PMV model are treated as constant. The assumptions are listed in Table 20.

Table 20 Assumptions for thermal comfort model

Index	Assumptions
1	Constant heat transfer coefficient [201]: $h_c = 3 \text{ W/m}^2\text{K}$
2	Constant cloth temperature [202]: $T_{cl} = 32 \text{ }^\circ\text{C}$
3	Mean radiant temperature [203]: $T_r = T_a + 1 \text{ }^\circ\text{C}$
4	Clothing insulation [201]: 0.6 clo (1 clo = 0.155 m ² K/W)
5	Constant relative humidity: 40%

Energy Model

Multiple tools have been developed for building energy modeling, e.g., EnergyPlus. However, the tools usually consider detailed geometry and thermal zones which make the calculation expensive. Also, the discontinuity of the simulation results can make it more challenging to solve the optimization problem. In our study, we

selected the building environment to be an office room. The energy model is simplified to be a steady-state heat balance equation:

$$Q = hA(T_{out} - T_{in}) \quad (14)$$

where h is the heat transfer coefficient ($Wm^{-2}K^{-1}$), A is the surface area (m^2), and Q is the energy consumption (W).

The convective heat transfer area of the office was assumed to be one exterior wall, which was 5 m x 4 m. The heat transfer coefficient h is calculated by Chartered Institute of Building Services (CIBS) Guide Book [204]:

$$h = 4.1V_{loc} + 5.8 \quad (15)$$

The V_{loc} is the local wind velocity, which is assumed to be 3 m/s for typical outdoor environment.

Optimization Problem

Before designing the extremum seeking controller, the static multi-objective optimization should be formed. The weights of objective functions in the extremum controlled can be selected according to the optimization results. Two optimization problems are formulated. The first one is a two-objective optimization problem that considers the thermal comfort of two types of occupants with different metabolic rates. The second is a three-objective optimization problem that includes an additional objective on energy consumption.

Two-objective Optimization Problem

Figure 27 shows thermal comfort responses of two types of occupants with different metabolic rates. We found that both the optimal temperatures and the steepness of PPD profile are different between the two types of occupants. To explore

the inherent trade-offs between minimizing the thermal comfort index of each occupant, we formulated the optimization objective as a linear combination of two occupants' PPD models. Using a parameter β as the weight, the two-objective optimization problem can be expressed as follows:

$$\min \beta * PPD_1(T_a, M) + (1 - \beta) * PPD_2(T_a, M) \quad (16)$$

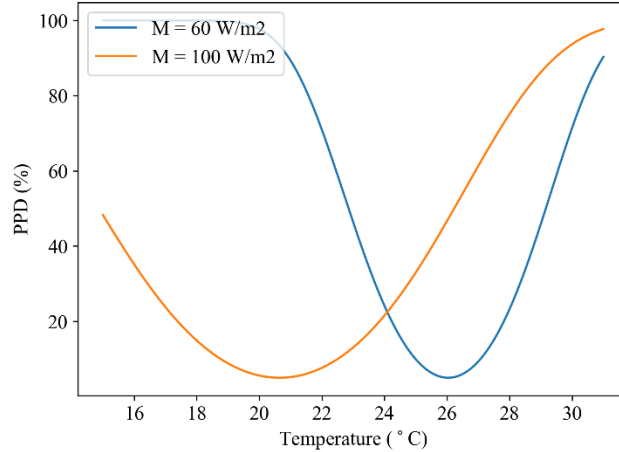


Figure 27 Thermal Comfort Response of Occupants with Different Metabolic Rate
Three-objective Optimization Problem

Energy usage should be considered in addition to occupant comfort in building system control. The most energy-efficient ways to condition the room is to use the outdoor air temperature, but it will have a direct impact on the occupant thermal comfort. The three-objective optimization problem is formulated as a linear combination of two occupants' PPD model and the squared energy consumption.

$$\min w_1 * PPD_1(T_a, M) + w_2 * PPD_2(T_a, M) + w_3 Q(T_a)^2 \quad (17)$$

Extremum Seeking Control

The ESC is developed to optimize an objective function, which can be a function of unknown input parameters, or to determine the targeted states to maintain an operation at the extreme value of a function [205]. Its goal is to find input $u_{opt}(t)$ in

real time that optimizes the online measurement of the generally unknown and/or time-varying objective function, $f(t,u)$, see Eqn. 13.

$$u_{opt} = \operatorname{argmin} f(t, u) \quad (18)$$

u is the input vector. The objective function of the ESC is assumed to be convex and linear. The general setting of the ESC with dither is shown in Figure 28. The transfer function $F_I(s)$ is the input dynamics, and the transfer function $F_O(s)$ is the sensor dynamic. y is the output of the objective function that can be perturbed by noise n . However, the noise is not considered in this study. This output y can be directly measurable for the feedback. $d_1(t)$ and $d_2(t)$ are demodulation and signals dither, respectively, where α and ω are phase angle and frequency.

In this diagram, the dither outputs signal $d_2(t)$ that goes through the high-pass filter $F_{HP}(s)$. Then, it is multiplied by the demodulating signal $d_1(t)$ and low-pass filter $F_{LP}(s)$. As a result, the signal is proportional to the gradient $df/du(\hat{u})$. When closing the loop, the integrator helps eliminate the gradient. The stability or transient performance can be enhanced with the compensator $K(s)$.

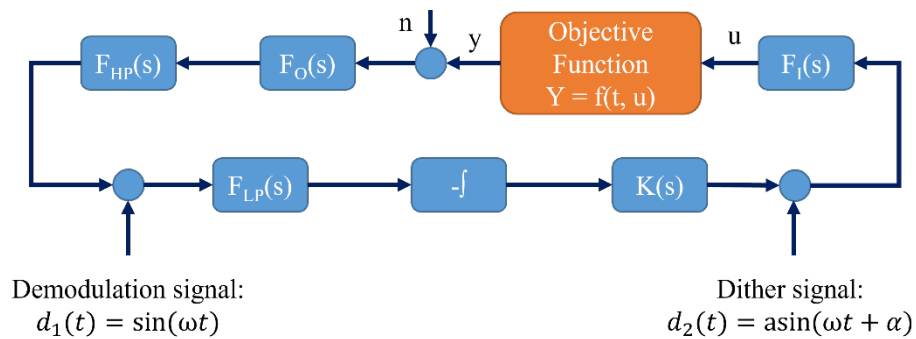


Figure 28 Extremum seeking control system

In this study, the extremum seeking controller solves the same optimization problems we formed in the previous section without the constraints. The outputs of the

plant are the weighted linear combination of energy and thermal comfort models. If considering the real-world implementation, the real-time thermal comfort index can either be collected from questionnaires provided from the occupants or be estimated by models based on physiological data collected by sensors. The energy consumption can be sensed by the energy meter. The input is indoor air temperature. The extremum seeking controller keeps tracking the optimum temperature, which balances the trade-offs between different occupants' thermal comfort and building energy consumption.

5.3 Results

Air quality control

The fan of the wearable micro air cleaner achieved a maximum flow rate of approximately 4 L/s. In terms of the protective performance of the wearable micro air cleaner, the location of the diffuser and the flow rate of the supplied air are crucial factors. We tested two diffuser locations, one is above user's eyes (Figure 29 left), another is in front of user's face (Figure 29 right).

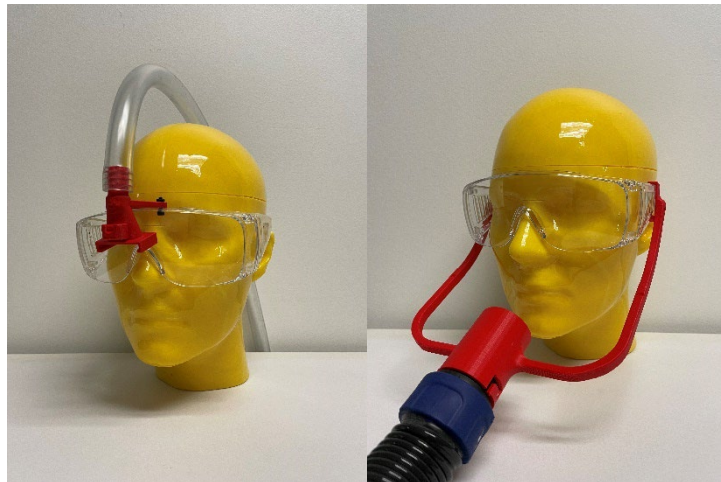


Figure 29 Diffuser locations, (left) Diffuser above the eyes, (right) Diffuser in front of the face

In the case of the diffuser located above the user's eyes, with the highest flow rate of 4 L/s, the protective efficiency for mouth breathing was approximately 50%, and for nasal breathing, it was only around 20%. These results did not meet the expectations, which were set at approximately 60%-70% for both mouth and nasal breathing. In the case of the diffuser location in front of user's face, this study investigated three different distances: 2.54 cm (1"), 3.81 cm (1.5"), 5.08 cm (2"). The diffuser was positioned at a horizontal angle of 45°, directed towards the nose and mouth. Table 21 shows the results of the protective efficiencies with the three locations of the air diffuser. With a distance of 2.54 cm (1"), the protective efficiency reached 77% for mouth breathing and 63% for nasal breathing. With the distance increased to 3.81 cm (1.5"), the protective efficiencies decreased to 60% for mouth breathing and 51% for nasal breathing. Further increasing the distance to 5.08 cm (2") resulted in a decline in protective efficiencies, reaching approximately 50% for both mouth and nasal breathing. Considering these findings, only the 2.54 cm (1") distance met the expected performance. Consequently, the diffuser was fixed at this distance for subsequent experiments.

Table 21 Protective efficiencies with different location for air diffuser.

Distance to face	Efficiency of mouth breathing	Efficiency of nasal breathing
2.54 cm (1")	77%	63%
3.81 cm (1.5")	60%	51%
5.08 cm (2")	48%	50%

After fixing the diffuser at a distance of 2.54 cm (1"), this study further examined the relationship between protective performance and flow rates. The flow rates were selected to be 2 L/s, 3 L/s, and 4 L/s. The corresponding air velocities at the diffuser were 4 m/s, 6 m/s, and 8 m/s. Table 22 shows the protective efficiencies at different flow rates. At the flow rate of 4 L/s, the protective performance achieved 77% for mouth breathing and 63% for nasal breathing. When the flow rate was reduced to 3 L/s, the protective efficiency dropped to approximately 69% for mouth breathing and 50% for nasal breathing. Similarly, at a flow rate of 2 L/s, the protective efficiency reached 61% for mouth breathing and 50% for nasal breathing. These results indicate that an airflow rate of 4 L/s is necessary to achieve the expected protective efficiency.

Table 22 Protective efficiencies with varied airflow rates for air supply.

Flow rates (Air velocity)	Efficiency of mouth breathing	Efficiency of nasal breathing
4 L/s (8 m/s)	77%	63%
3 L/s (6 m/s)	69%	50%
2 L/s (4 m/s)	61%	50%

Investigating the thermal comfort impacts resulting from the operation of the wearable micro air cleaner is another crucial factor addressed in this study. The present study visualized the thermal sensation/comfort questionnaires and physiological data. The average time series data among all the human subjects are shown in Figure 30 and Figure 31. In these figures, time 0 represents the moment when the wearable micro air cleaner was activated, while negative and positive values indicate the time before and

after its operation. To determine whether the wearable micro air cleaner operation had a significant impact on user's thermal comfort, paired t-tests were conducted to assess statistical significance, and Cohen's d values were calculated to measure the effect size. The p-values of the paired t-test and Cohen's d values are listed in Table 23. Figure 30 shows the responses of the overall/local thermal sensation and comfort. The overall thermal sensation exhibited a significant decrease at the indoor air temperature of 25 °C ($p = 0.02$, $d = -0.59$). No significant changes were observed at the indoor air temperature of 22 °C ($p = 0.18$, $d = -0.26$) and 28 °C ($p = 0.12$, $d = -0.43$). Regarding overall thermal comfort, a significant decrease was observed at the indoor air temperature of 22 °C ($p = 0.02$, $d = -0.72$), while no significant changes were found at 25 °C ($p = 0.25$, $d = -0.27$). At 28 °C, the overall thermal comfort can be observed slightly increased from the visualization, but this change was not statistically significant ($p = 0.21$, $d = 0.41$). Notably, all overall thermal comfort values were above 0 at all indoor air temperatures, indicating the absence of overall discomfort. The local thermal sensation significantly decreased at all three indoor air temperatures due to the strong convective heat transfer caused by the wearable micro air cleaner (22 °C: $p = 2e-4$, $d = -1.35$; 25 °C: $p = 2e-5$, $d = -1.40$; 28 °C: $p = 4e-3$, $d = -1.17$). At 22 °C, the local thermal comfort experienced a significant drop ($p = 2e-4$, $d = -1.36$) from about 1 (slightly comfortable) to -1 (slightly uncomfortable). At 25 °C, the local thermal comfort also significantly decreased ($p = 8e-3$, $d = -0.79$), but all values remained above 0. At 28 °C, the local thermal comfort did not have significant change ($p = 0.82$, $d = 0.08$). The results indicating the wearable micro air cleaner operation may generate

local thermal discomfort at 22 °C, but no overall and local discomfort were caused at the indoor air temperature of 25 °C and 28 °C.

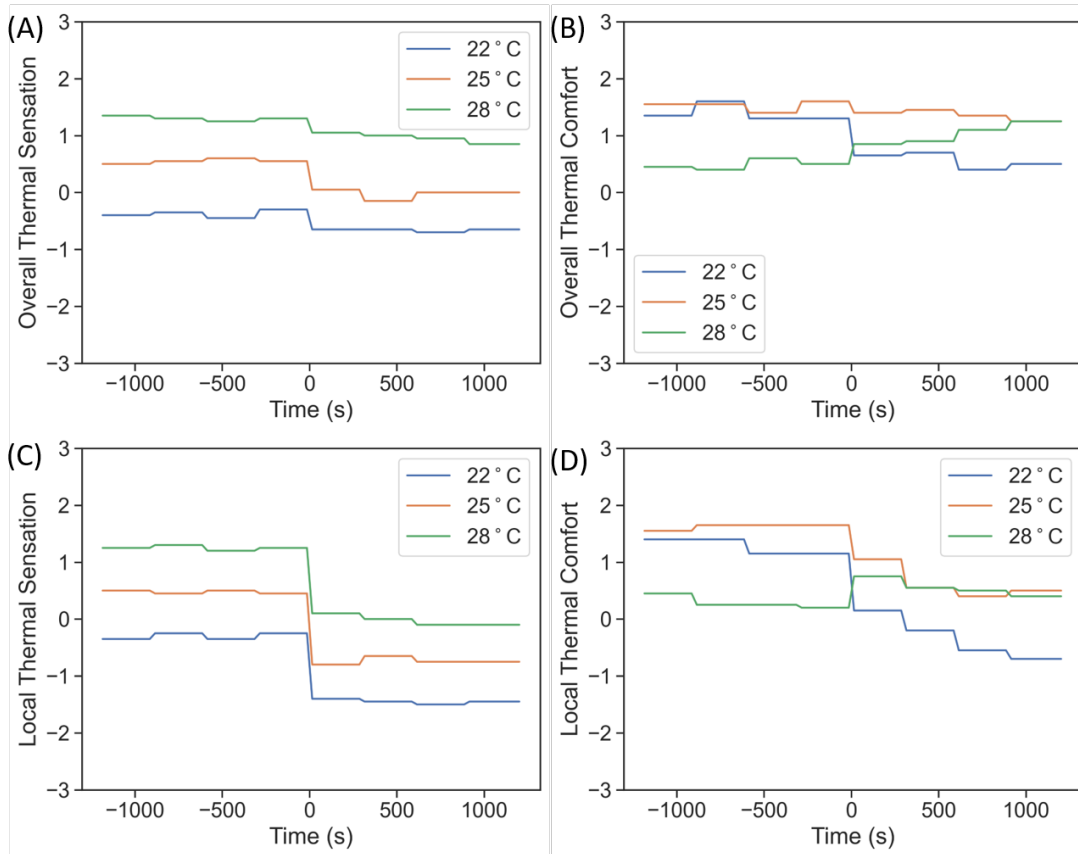


Figure 30 Thermal sensation and comfort responses at different indoor air temperatures. (A) Overall thermal sensation. (B) Overall thermal comfort. (C) Local thermal sensation. (D) Local thermal comfort.

Figure 31 displays the responses of some representative physiological variables, including the face temperature, heart rate, one typical time domain HRV (SDNN), and one typical frequency domain HRV (LF/HF). At all the indoor air temperatures, the face temperature significantly decreased because of the convective heat transfer caused by the jet of the wearable micro air cleaner (22 °C: $p = 2e-11$, $d = -4.90$; 25 °C: $p = 1e-13$, $d = -5.14$; 28 °C: $p = 1e-10$, $d = -3.31$). Because of the big temperature

differences between the face temperature and the indoor air temperature at 22 °C, the face temperature decreased by about 6 °C, from about 34 °C to 28 °C. The face temperature reductions were approximately 4 °C and 3 °C, at indoor air temperatures of 25 °C and 28 °C, respectively. For the heart rate, SDNN, and LF/HF, no clear patterns or significant changes were observed in the time-series data or statistical analysis.

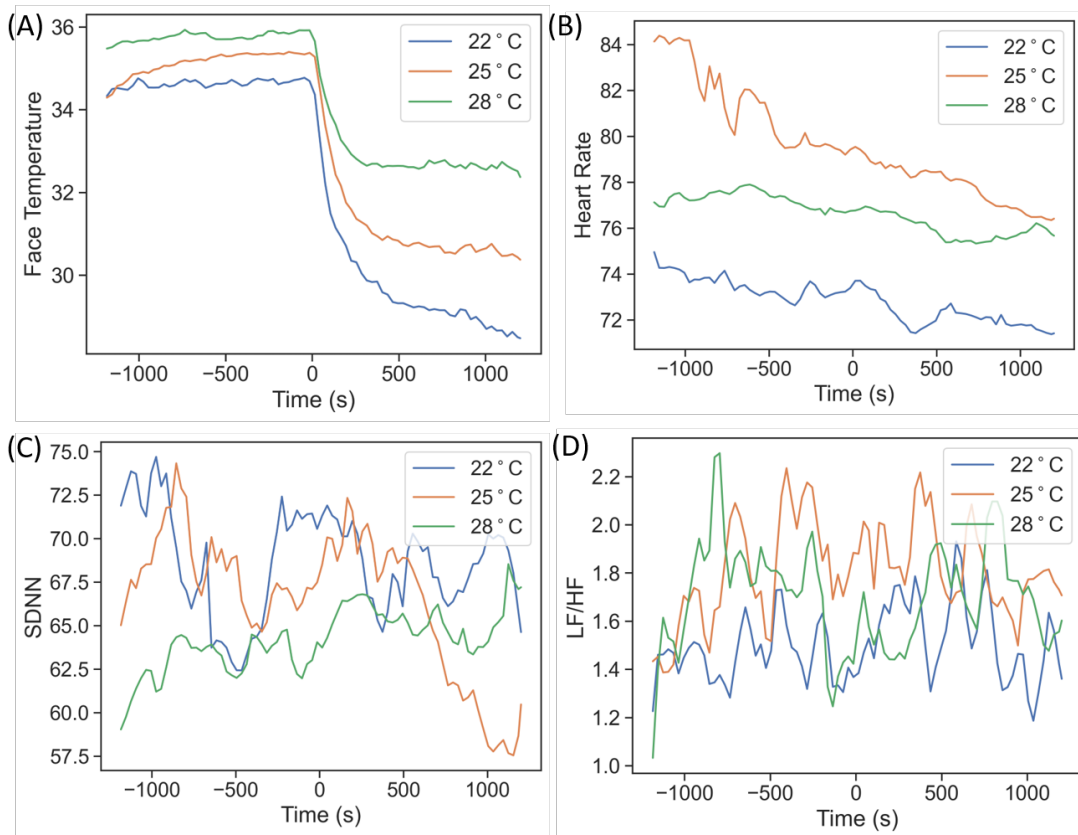


Figure 31 Physiological responses at different indoor air temperatures. (A) Face temperature. (B) Heart rate. (C) SDNN. (D) LF/HF.

Table 23 p-values and Cohen's d values of each variable at different indoor air temperatures

	22 °C		25 °C		28 °C	
	p-value	Cohen's d	p-value	Cohen's d	p-value	Cohen's d
Overall TS	0.18	-0.26	0.02	-0.59	0.12	-0.43
Local TS	2e-4	-1.35	2e-5	-1.40	4e-3	-1.17
Overall TC	0.02	-0.72	0.25	-0.27	0.21	0.41
Local TC	2e-4	-1.36	8e-3	-0.79	0.82	0.08
Face Temperature	2e-11	-4.90	1e-13	-5.14	1e-10	-3.31
Heart Rate	0.04	-0.21	0.01	-0.39	8e-5	-0.16
SDNN	0.39	0.15	0.44	-0.12	0.08	0.16
SDSD	0.63	-0.09	0.17	-0.22	0.50	0.09
RMSSD	0.66	-0.07	0.27	-0.19	0.41	0.08
pNN20	0.51	0.07	0.41	0.08	0.40	0.07
pNN50	0.87	0.02	0.54	-0.06	0.30	0.08
LF/HF	0.55	0.13	0.68	0.04	0.59	0.12

To develop machine learning models to predict the thermal sensation and comfort, the present study first conducted the feature importance analysis by using the random forest method. Figure 32 illustrates the feature importances for overall and local thermal sensation and comfort. Among all the features, heart rate and face temperature demonstrated relatively higher importance. Regarding the HRV indices,

several time domain measures, including pNN20 and pNN50, exhibited greater importance compared to other HRV indices. These findings indicate that these specific HRV indices may carry more significant information for predicting thermal sensation and comfort.

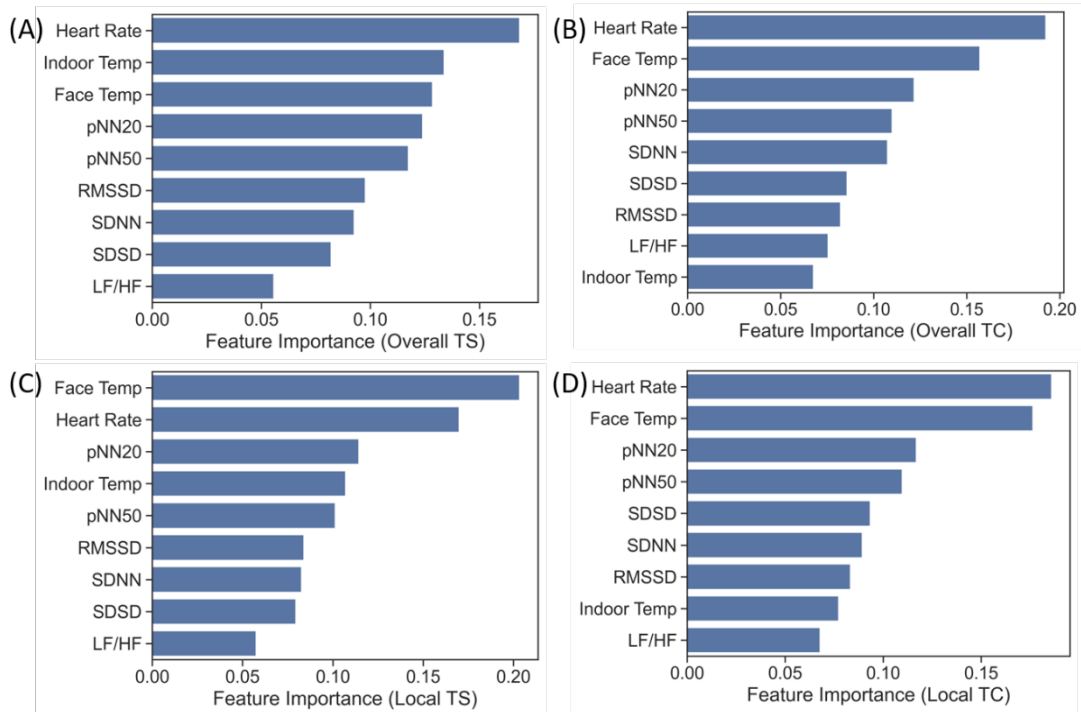


Figure 32 Feature importance of the overall and local thermal sensation and comfort

In order to assess the performance enhancements attributed to specific features, particularly heart rate and HRV indices, the present study developed five feature groups denoted as M1 to M5. The temperature, being a crucial and widely utilized variable in both physical and data-driven thermal comfort modeling, was chosen as the main focus for the baseline feature group, M1. This group incorporated indoor air and face temperature. Considering the high feature importance of heart rate, M2 included heart rate as an additional feature to M1. The objective was to investigate the extent to which heart rate could improve the performance of the baseline feature group. For M3,

culated HRV indices were added as supplementary features to M1. This was done to analyze the performance improvement brought by the inclusion of HRV indices. Taking into account the high feature importance of heart rate, face temperature, pNN20, and pNN50, these variables were selected to construct M4. Finally, M5 incorporated all variables available to develop a comprehensive feature group. Table 24 shows the descriptions of each feature group.

Table 24 Feature group descriptions

Group name	Features
M1	Indoor air temperature, Face temperature
M2	Indoor air temperature, Face temperature, Heart rate
M3	Indoor air temperature, Face temperature, pNN20, pNN50, SDNN, SDSD, RMSSD, LF/HF
M4	Face temperature, Heart rate, pNN20, pNN50
M5	Indoor air temperature, Face temperature, Heart rate, pNN20, pNN50, SDNN, SDSD, RMSSD, LF/HF

Among all the evaluation indices, the F1 scores was selected to analyze the model performances, as it can represent the model performance with imbalanced categories. Table 25 and Figure 33 present the test F1 scores of machine learning models developed based on different feature groups. It is observed that the model performances for different outputs are similar within the same feature group. The baseline feature group, M1, which solely employs indoor air temperature and face temperature, demonstrated the lowest performance ranging from 0.2 to 0.3. By

introducing heart rate as an additional feature, feature group M2 achieved a performance improvement to the range of 0.6 to 0.7. The average performance of M2 increased by approximately 140% compared to M1. Feature group M3, which includes multiple HRV indices, further enhanced the performance to the range of 0.8 to 0.9. The performance improvement of M3 over the baseline feature group M1 was around 207%. The comparison between M2 and M3 indicates that incorporating multiple HRV indices provided more information relevant to thermal comfort than using heart rate alone. Both feature groups M4 and M5 achieved similar performances, ranging from 0.8 to 0.9. Within the same feature group, the KNN, RF, and SVM_RBF models demonstrated comparable performances. Table 26, Table 27, and Table 28 show all the calculated training and test scores of KNN, RF, and SVM_RBF. It is observed that there were no significant differences between the training and test scores, suggesting that the models were not overfitting.

Table 25 Test F1 scores of machine learning models with different feature groups

	Machine Learning	M1	M2	M3	M4	M5
Overall TS	KNN	0.36	0.68	0.90	0.86	0.94
	RF	0.35	0.68	0.79	0.79	0.88
	SVM_RBF	0.34	0.67	0.92	0.87	0.96
Overall TC	KNN	0.24	0.65	0.88	0.84	0.91
	RF	0.20	0.62	0.72	0.79	0.84
	SVM_RBF	0.19	0.64	0.91	0.86	0.95
Local TS	KNN	0.31	0.69	0.91	0.84	0.94

	RF	0.30	0.71	0.84	0.78	0.89
	SVM_RBF	0.30	0.67	0.93	0.88	0.95
Local TC	KNN	0.32	0.70	0.83	0.80	0.87
	RF	0.25	0.74	0.80	0.80	0.89
	SVM_RBF	0.25	0.69	0.86	0.83	0.92

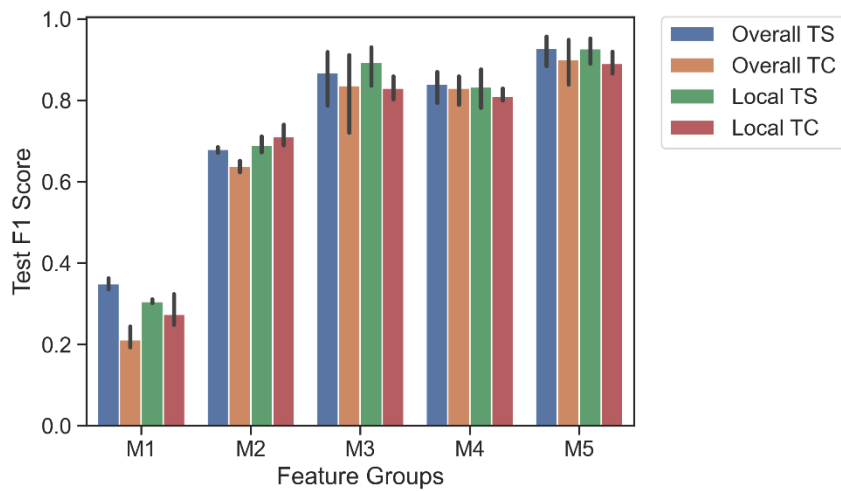


Figure 33 Test F1 scores of feature groups

Table 26 Training and test scores of KNN models

	Training Accuracy	Cross Validation Accuracy	Test Accuracy	Test F1 Score	Test AUC
Overall TS-M1	0.53	0.49	0.52	0.36	0.83
Overall TS-M2	0.87	0.75	0.76	0.68	0.9

Overall TS-M3	0.96	0.87	0.89	0.9	0.98
Overall TS-M4	0.93	0.82	0.86	0.86	0.96
Overall TS-M5	0.98	0.91	0.93	0.94	0.99
Overall TC-M1	0.53	0.51	0.50	0.24	0.81
Overall TC-M2	0.82	0.76	0.75	0.65	0.94
Overall TC-M3	0.96	0.88	0.89	0.88	0.97
Overall TC-M4	0.93	0.85	0.85	0.84	0.95
Overall TC-M5	0.98	0.92	0.93	0.91	0.98
Local TS- M1	0.55	0.51	0.49	0.31	0.84
Local TS- M2	0.87	0.75	0.74	0.69	0.88
Local TS- M3	0.95	0.86	0.91	0.91	0.97

Local TS- M4	0.93	0.82	0.85	0.84	0.95
Local TS- M5	0.97	0.90	0.94	0.94	0.98
Local TC- M1	0.48	0.46	0.46	0.32	0.82
Local TC- M2	0.82	0.74	0.73	0.70	0.92
Local TC- M3	0.96	0.86	0.87	0.83	0.97
Local TC- M4	0.92	0.83	0.84	0.80	0.94
Local TC- M5	0.97	0.90	0.91	0.87	0.98

Table 27 Training and test scores of RF models

	Training Accuracy	Cross Validation Accuracy	Test Accuracy	Test F1 Score	Test AUC
Overall TS-M1	0.52	0.49	0.49	0.35	0.83
Overall TS-M2	0.88	0.75	0.76	0.68	0.95

Overall TS-M3	0.93	0.83	0.82	0.79	0.98
Overall TS-M4	0.92	0.79	0.81	0.79	0.97
Overall TS-M5	0.97	0.87	0.87	0.88	0.99
Overall TC-M1	0.53	0.51	0.51	0.2	0.8
Overall TC-M2	0.92	0.77	0.76	0.62	0.96
Overall TC-M3	0.94	0.81	0.81	0.72	0.98
Overall TC-M4	0.95	0.81	0.81	0.79	0.97
Overall TC-M5	0.97	0.87	0.87	0.84	0.99
Local TS- M1	0.55	0.52	0.5	0.3	0.85
Local TS- M2	0.89	0.75	0.74	0.71	0.95
Local TS- M3	0.93	0.83	0.84	0.84	0.98

Local TS- M4	0.94	0.82	0.81	0.78	0.97
Local TS- M5	0.97	0.89	0.89	0.89	0.99
Local TC- M1	0.47	0.45	0.46	0.25	0.82
Local TC- M2	0.9	0.74	0.75	0.74	0.96
Local TC- M3	0.94	0.79	0.82	0.8	0.98
Local TC- M4	0.92	0.79	0.79	0.8	0.97
Local TC- M5	0.96	0.86	0.87	0.89	0.99

Table 28 Training and test scores of SVM_RBF models

	Training Accuracy	Cross Validation Accuracy	Test Accuracy	Test F1 Score	Test AUC
Overall TS-M1	0.51	0.49	0.49	0.34	0.82
Overall TS-M2	0.76	0.72	0.7	0.67	0.94

Overall TS-M3	0.99	0.91	0.91	0.92	0.99
Overall TS-M4	0.94	0.83	0.87	0.87	0.98
Overall TS-M5	0.99	0.94	0.95	0.96	1
Overall TC-M1	0.52	0.51	0.51	0.19	0.79
Overall TC-M2	0.78	0.73	0.73	0.64	0.95
Overall TC-M3	0.98	0.91	0.91	0.91	0.98
Overall TC-M4	0.94	0.85	0.85	0.86	0.98
Overall TC-M5	1	0.94	0.95	0.95	0.99
Local TS- M1	0.53	0.52	0.49	0.3	0.84
Local TS- M2	0.77	0.73	0.72	0.67	0.94
Local TS- M3	1	0.89	0.93	0.93	0.99

Local TS- M4	0.93	0.85	0.87	0.88	0.98
Local TS- M5	0.99	0.93	0.95	0.95	0.99
Local TC- M1	0.46	0.46	0.46	0.25	0.81
Local TC- M2	0.75	0.7	0.72	0.69	0.95
Local TC- M3	0.99	0.89	0.9	0.86	0.99
Local TC- M4	0.94	0.84	0.83	0.83	0.97
Local TC- M5	1	0.93	0.94	0.92	1

Thermal comfort control

Static Optimization

Two-objective Optimization: The occupant with lower metabolic rate (60 W/m²) is named as Occupant 1, the occupant with a higher metabolic rate (100 W/m²) is named as Occupant 2. Figure 34 shows the Pareto front of the two-objective optimization. From Figure 27, we can see that the thermal comfort changes at different rates as the occupants have different metabolic rate. Occupant 1 has more thermal sensitivity than the Occupant 2. The Pareto front in Figure 34 verifies this, because as

the weight changes from 0 to 1, the thermal comfort of Occupant 1 with lower metabolic rate changes more quickly.

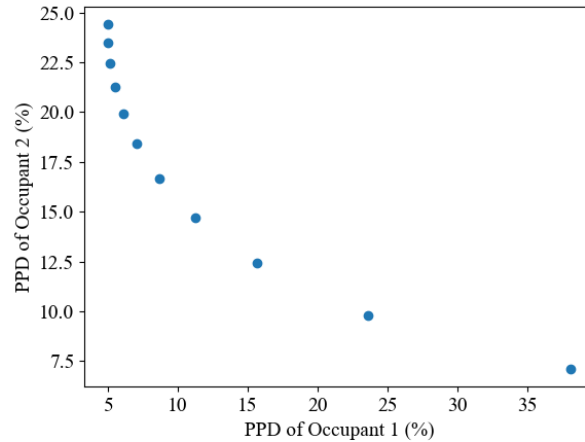


Figure 34 Pareto Front of Two-objective Optimization (PPD of Occupant 1 Vs. PPD of Occupant 2)

Three-objective Optimization: Figure 35 shows the Pareto front of the three-objective optimization problem. When the instantaneous energy consumption is low, both PPD of Occupant 1 and PPD of Occupant 2 tend towards almost 100, which is far less acceptable than the alternative of high energy consumption. Conversely, as the thermal comfort index of the two occupants decreases, the energy consumption starts to increase.

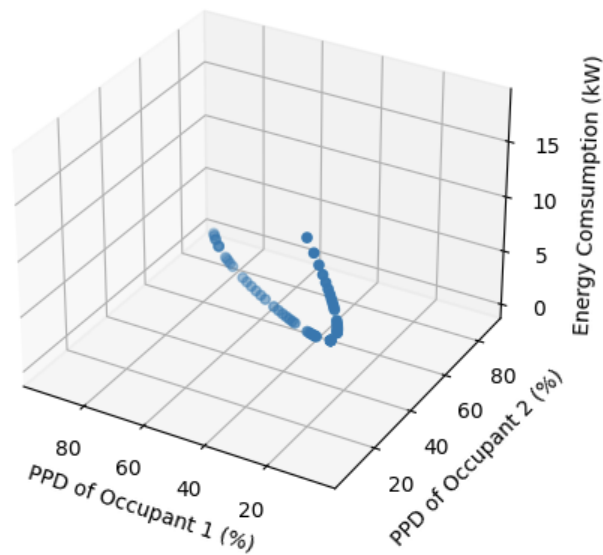


Figure 35 Pareto Front of Three-objective Optimization (PPD of Occupant 1 vs. PPD of Occupant 2 vs. Energy consumption)

Extremum Seeking Control

Weight Selection: In this study, the weights used in the extremum seeking control were selected according to the results obtained by mapping the two and three-objective Pareto fronts. However, users can adjust the weights in different implementation cases according to specific practical purposes.

Scenarios: Five scenarios were simulated in a Simulink model of PPD of Occupants 1 and 2. The outdoor temperature was set to be 35 °C. The simulated time was nine hours, which was a typical working hour. The following optimization objective functions were used: 1. energy usage only; 2. single-occupant with no energy usage; 3. two occupants; 4. two occupants + energy usage; and 5. "staggered" (time-

dependent) two occupants + energy usage. The initial air supply temperature was set to be 21 °C.

Energy Usage: This simulation result presents the baseline optimization problem of minimizing energy usage. As seen in Figure 36, the optimal result is to let the air supply temperature changing from the initial temperature to the ambient temperature, which is about 35 °C. If human thermal comfort is not a concern, there is no need to adjust the environmental conditions in a manner suitable for occupants.

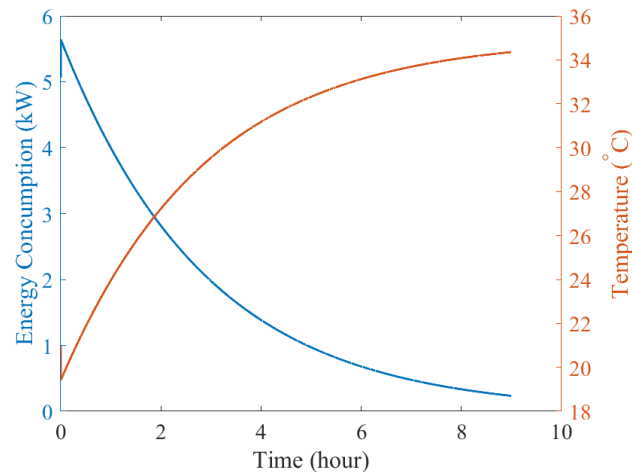


Figure 36 Energy Consumption and Temperature for Energy Usage Optimization

Single-Occupant Thermal Comfort: The model of single occupant was exercised, with the results shown in Figure 37. The optimum temperature corresponding to thermal equilibrium for Occupant's BMR of 100W/m² is reached within three to four hours. The steady state temperature is about 23.3 °C, which is much lower than the optimal temperature in the energy usage case.

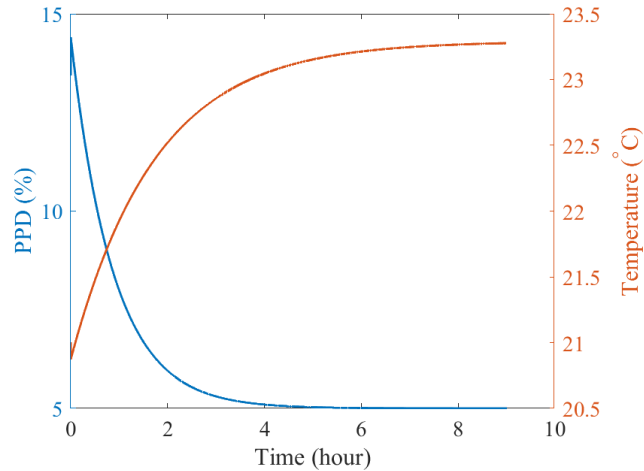


Figure 37 Thermal Comfort and Temperature for Single-Occupant Thermal Comfort Optimization

Two-objective Extremum Seeking Control: The weights for the two types of occupants' thermal comfort metrics (PPD) should consider their individual physiology. According to the two-factor Pareto Front (Fig. 3), the range of the thermal comfort change of Occupant 1 ($M = 60 \text{ W/m}^2$) is larger than Occupant 2 ($M = 100 \text{ W/m}^2$). Occupant 1 is more thermally sensitive than Occupant 2. Based on the above reasoning, we selected the weight with $\beta = 0.6$, $1 - \beta = 0.4$. Even though the thermal comfort of Occupant 2 factors less into the controller's behavior, the resulting loss of comfort will not be very large due to their comparatively lower thermal sensitivity.

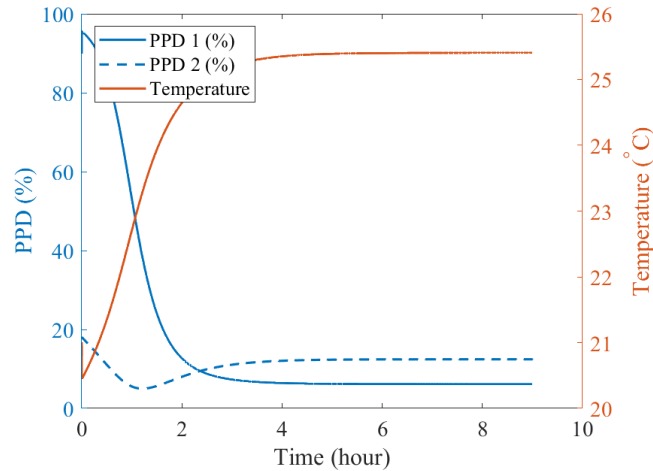


Figure 38 Thermal Comfort and Temperature for Two-objective Extremum Seeking Control

In the simulation results for this scenario shown as Fig. 7, we see the controller drives the air supply temperature to about 25.4 °C. This temperature falls reasonably within the optimum temperature range for both occupants. The temperature is slightly skewed towards Occupant 1's optimal temperature due to their higher weighting in the objective function. The steady state temperature is about 2 degrees higher than the single-occupant thermal comfort case.

Three-objective Extremum Seeking Control: The three-objective problem balances the two types of occupants' thermal comfort and the instantaneous energy usage. When the energy consumption is minimized, the air supply temperature and outdoor temperature are the same, and both occupants feel extremely uncomfortable. In the three-objective optimization, we found that when the objective weight of energy is higher than 0.1, the resulting air temperature action tends strongly towards energy minimization (resulting in high PPDs). Based on this rationale, a weight of 0.1 for energy consumption should be selected, which can promise reasonable thermal comfort values while keeping energy usage low. The rationale of the weights on the occupants'

thermal comfort is the same as the two-objective extremum seeking control: two roughly similar weights, with one higher to reflect Occupant 1's higher thermal sensitivity. The weights are selected to be $w_1 = 0.5$, $w_2 = 0.4$, $w_3 = 0.1$.

The three-objective extremum seeking control simulation results are shown in Fig. 8. In the first few hours, the energy usage is high due to the large difference in air supply temperature and ambient temperature. After two to three hours, the thermal comfort metrics for both occupants have improved---however, Occupant 2 has slightly higher PPD than Occupant 1 due to the higher final temperature. This is simply the result achieved by the above selection of weights on each term in the objective function. The steady state temperature is about 25.8 °C. That means in this case, the temperature is higher than the two-objective case because it tends to increase the temperature to save energy. Even though the occupants may not be as comfortable as in the two-objective case, the thermal comforts are still in an acceptable range.

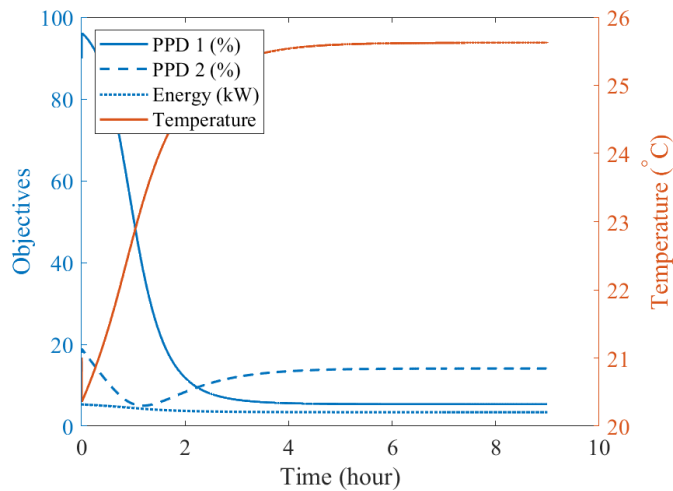


Figure 39 Thermal Comfort, Energy Consumption, and Temperature for Three-objective Extremum Seeking Control

Staggered Three-objective Extremum Seeking Control: This scenario involved staggering the two occupants' presences throughout the workday, with Occupant 1 working the first two-thirds of the day; Occupant 2 working the middle third of the day; and only the energy management system for the last third of the day. The weights were set to be $w_1 = 0.9$, $w_2 = 0$, $w_3 = 0.1$ for the first one-third of the day; $w_1 = 0.5$, $w_2 = 0.4$, $w_3 = 0.1$ for the second one-third of the day; and $w_1 = 0$, $w_2 = 0$, $w_3 = 1$ for the last one-third of the day. As is seen in Fig. 9, the entrance of Occupant 2 impacted the ESC temperature result to have about 0.2 degrees decreasing. The PPDs shown in this figure indicate the thermal comfort experienced by the occupants when present. After both occupants leave, the energy usage sub-objective is the only one active and rises to meet the ambient temperature.

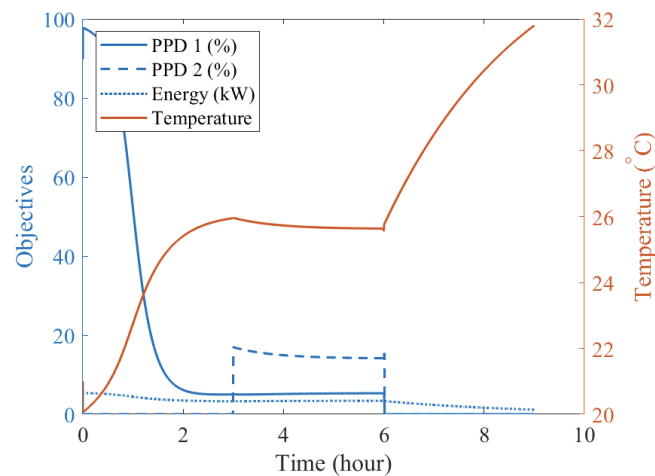


Figure 40 Thermal Comfort, Energy Consumption and Temperature for Staggered Three-objective Extremum Seeking Control

From the results, we can see that the staggered three-objective extremum seeking control can optimize the temperature setpoint in real-time based on occupant behavior. We also compared the energy consumption of the staggered ESC to that of a

constant temperature setpoint (assuming 24 °C) case, which is widely used in a lot of real-world buildings. In nine hours, the constant temperature setpoint case consumed 35.8 kWh, while this staggered ESC consumed 28.0 kWh. The energy consumption reduction was 22%.

5.4 Discussion

With the diffuser location above user's eyes, the low performance could be due to the relatively small diffuser area comparing to the device developed by the prior study [182]. The generated jet from the small diffuser might not adequately cover the mouth and nose region, resulting in reduced effectiveness in providing protection. Additionally, when the diffuser is positioned in front of the user's face, it could potentially lead to dryness of the eyes and lips. Furthermore, the weight of the tube connecting the goggle may exert pressure on the user's ears and nose, which could affect wearing comfort. Future research could focus on exploring the comfort aspects of wearing this device. In terms of thermal comfort, the visualization results indicate that the wearable micro air cleaner has the potential to improve the overall and local thermal comfort of users at 28 °C. If multiple occupants within a building wear the wearable micro air cleaner, it may be possible to increase the indoor air temperature setpoint to 28 °C. This relatively higher setpoint temperature has the potential to reduce energy consumption for cooling in the building during warmer seasons.

By incorporating HRV as additional features, the data-driven thermal comfort models exhibited improved performance compared to the baseline feature group, which only considered indoor and face temperatures. This finding aligns with the previous study [199], which confirms that HRV indices could provide valuable information

regarding human thermal comfort. Feature groups M3, M4, and M5 achieved similar performance, with test F1 scores ranging from approximately 0.8 to 0.9. Among these feature groups, M4 could be considered the preferable choice due to its lower number of features. The low feature dimensionality in M4 has the potential to save computational resources and avoid overfit.

For the extremum seeking control, the present study only focuses on verifying the theoretical feasibility. For the actual applications, the parameters of the controller need to be tuned to meet the performances of the actuators and the sensors, such as responding speed, etc. Future studies are needed to implement the extremum seeking controller in environmental chambers or real buildings to test the performance of the controller. The wearable micro air cleaner and the extremum seeking control provides the simultaneous occupant-oriented environmental controls which considers occupant health, thermal comfort, and building energy consumptions.

5.5 Summary

The present study introduced a novel wearable micro air cleaner designed for occupant-oriented indoor environmental controls, which effectively provides personalized protection in the breathing zone without disrupting the user's behavior and thermal comfort. Tracer gas experiments were conducted to investigate the protective performance of the device. Through optimization of the diffuser location and flow rate, the wearable micro air cleaner achieved a maximum protective efficiency of 77% for mouth breathing and 63% for nasal breathing. To investigate the impact of the device operation on user's thermal comfort, this study conducted human subject experiments with 20 participants at different indoor air temperatures. The findings indicate that the

device reduced the thermal comfort at an indoor air temperature of 22 °C. However, when the indoor air temperature exceeded 25 °C, the operation of the device did not significantly affect user's thermal comfort. Comparing to traditional personal ventilation at fixed locations, the protective performance of the wearable micro air cleaner would not be influenced by user's movements and daily behaviors. Moreover, this study developed data-driven thermal comfort models based on the collected physiological data in the human subject experiments. HRV indices showed the capability to improve the model performance. With the highest performance exceeded 0.9, these models could be potentially implemented in the automatic control of the wearable micro air cleaner based on occupant thermal comfort requirements.

The present study also presents a novel application of the extremum seeking control in multiple occupant-central scenarios for real-time optimization of building system operation. Based on different scenarios, we demonstrated that the extremum seeking control is effective at managing multiple occupants' thermal comfort preferences and the energy consumption simultaneously. Even though we only considered a small office with two types of occupants in this paper, this implementation shows that extremum seeking control in actual buildings is possible. In actual buildings, the thermal comfort preferences become more complicated because of the much higher occupant density. However, the problem can be simplified by classifying the thermal comfort preferences of all occupants into several categories, e.g. two categories presented in this study. According to the results, the staggered ESC, which can be realized with modern building sensor systems that detect occupant presences, saved

about 22% of energy compared to the building energy usage with the constant temperature setpoint.

The wearable micro air cleaner and extremum seeking provides a comprehensive occupant-oriented indoor environmental control framework which simultaneously considers the air quality, thermal comfort, and building energy consumptions. The developed simultaneous control could provide a healthy, comfort, and energy-efficient indoor environment for building occupants.

6. Discussion

This chapter presents the implications of the dissertation findings, limitations, and future work.

6.1 Implications of the dissertation findings

For the air quality characterization in occupant breathing zone, previous aerosol plume studies only characterized either source strength or convective transport capability. This study comprehensively analyzes the aerosol plumes associated with the transmission of airborne infectious microorganisms by combining the aerosol generation rate and convective transport capability into one factor. The measured aerosol concentration, air velocity, and airflow rate could be used as boundary conditions for CFD simulations related to aerosol transmission in indoor environment. The implications of this study extend beyond the characterization of aerosol plumes. Specifically, the findings provide valuable insights into the design and implementation of air quality control strategies. Understanding the aerosol dispersion and the factors influencing source strength and convective transport can inform the development of more effective mitigation measures. The tested effectiveness of different mitigation methods shows the importance of the protection of users breathing zone, which highlights the objectives of the occupant-oriented indoor air quality control.

For data-driven thermal comfort identification, even though several studies showed the potentials of HRV to be correlated to thermal comfort, few studies used HRVs to develop thermal comfort models. The present dissertation conducted two sets of human subject experiments with the personal condition device to collect HRV data

and develop data-driven models. With the possible thermo-regulation system information provided by HRVs, the performances of the thermal comfort predictions are significantly improved comparing to traditional models. The incorporation of HRV indices as additional features enhances the predictive capabilities, enabling a more precise understanding of how users perceive and experience thermal conditions in nonuniform environments. In the present study, the HRV data were not collected by medical devices but by portable Arduino-based sensors, which shows the convenience of using HRV-based thermal comfort models in actual occupant-oriented thermal comfort controls.

Traditional centralized HVAC system does not effectively control the airborne microorganism transmission in indoor environment. The wearable micro air cleaner provides the next generation occupant-oriented air quality control method for occupant breathing zone. In addition, with the convection caused by this device, occupant does not need to experience the thermal discomfort and breath hardness caused by traditional protection device, such as masks. For some occupants, this device could increase the thermal comfort in high indoor air temperature, such as 28 °C. In this case, the indoor air set point temperature could be potentially increased to save the building energy consumption during the cooling seasons. Resolving the conflicts between occupant individual thermal preferences are challenging for traditional building controllers. This study firstly implements the extremum seeking control on occupant-oriented building controls. By running real-time multi-objective optimization, the extremum seeking control successfully tracks the optimal indoor air set point temperature which makes all the occupant feel relatively comfortable, at the same time saves the building energy

consumption. By effectively addressing air quality concerns, enhancing thermal comfort, and optimizing energy usage, these approaches offer a comprehensive framework for creating energy-efficient indoor environments that prioritize the well-being and comfort of occupants.

6.2 Future work

For the air quality characterization, future research could explore the reason of the diverse source strength and convective transport capability of aerosol plumes generated by different human subjects or instruments. For thermal comfort identification, more studies could be conducted to validate the effect of heart rate variability on thermal comfort prediction. Future studies could use the HRV-based data-driven thermal comfort model in thermal comfort prediction scenarios or building control applications to test the model performance with unknown data. Future research could also further explore the impact of nonuniform thermal stimuli on physiological responses and investigate the generalizability of the developed model across diverse populations and settings. Continued efforts in this field will contribute to the development of more effective and personalized approaches to thermal comfort management. For the air quality controls, future studies could optimize the design of the wearable micro air cleaner according to user's wearing comfort. The potential performance improvement of the wearable micro air cleaner could also be explored. The optimal parameters of the extremum seeking control are needed to be found by considering the dynamic of the building system, e.g. the response speed of the HVAC actuators and occupant thermal sensation. Future studies could experimentally implement the extremum seeking control in environmental chamber or actual building

applications. Additionally, assessing the air quality and thermal comfort control performance across diverse building types and occupant profiles will contribute to their wider adoption and application in real-world scenarios. Overall, future studies could experimentally integrate multi-scale building systems and technologies developed by the present dissertation.

7. Conclusions and contributions

7.1 Conclusions

The present dissertation developed the comprehensive research framework for next generation occupant-oriented indoor environmental control, which simultaneously considers the air quality, thermal comfort, as well as building energy consumptions.

For air quality characterization in occupant breathing zone, the present dissertation conducted the aerosol concentration measurements, airflow rates measurements, and flow visualization to characterize the source strength and convective capability of the aerosol plumes associated with airborne microorganism transmission. The findings underscore the importance of considering both the source strength and convective transport simultaneously when characterizing aerosol plumes. Neglecting either parameter would result in an incomplete understanding of their characteristics, hindering accurate risk assessment. The measurements of source aerosol concentrations and airflow rates is essential for a comprehensive characterization of the source strength. Moreover, the study emphasized the significance of the occupant breathing zone in terms of air quality control. This specific area, where the highest concentration of potentially infectious aerosol particles may be present, necessitates targeted interventions and measures. Effective air quality control strategies within the occupant breathing zone are crucial for minimizing the risks associated with airborne diseases.

For data-driven thermal comfort identification, the present research study conducted human subject experiments to collect physiological data and thermal sensation/comfort surveys. However, the physiological responses of participants did

not exhibit clear patterns, which may not align with traditional aggregate or personal thermal comfort models. To address this challenge, the present study incorporated heart rate variability (HRV) indices as additional features to enhance the model performance by providing more information of human thermo-regulation system. The HRV-based data-driven models were developed by multiple machine learning methods, such as KNN, RF, and SVM_RBF. Remarkably, the highest achieved test F1 scores for thermal sensation and thermal comfort predictions exceeded 0.9. This method offers a reliable solution for predicting users' thermal sensation and comfort in indoor environmental controls.

For simultaneous air quality, thermal comfort, and building energy controls, the present dissertation developed a wearable micro air cleaner to provide protection for user's breathing zone, at the same time to minimize the thermal comfort impacts. Tracer gas experiments were conducted to assess the protective performance, while human subject experiments evaluated the thermal comfort influence at three different indoor air temperatures. The wearable micro air cleaner demonstrates approximately 60% - 70% protective efficiency for both nasal and mouth breathing. Unlike traditional mitigation methods like face masks, the wearable micro air cleaner offers acceptable thermal comfort for users at indoor air temperatures exceeding 25 °C. Additionally, the individual thermal preference and energy consumption also needed to be balanced in building controls. This study implemented the extremum seeking control to conduct real-time optimization of building temperature set-point. The staggered extremum seeking control, which can be realized with modern building sensor systems that detect occupant presences, saved about 22% of energy compared to the building energy usage

with the constant temperature setpoint (24 °C). Overall, the wearable micro air cleaner and extremum seeking control represented promising occupant-oriented control methods to address occupant requirements related to air quality, thermal comfort, and energy consumption in indoor environments. Their implementation can contribute to healthier and more comfortable built environments while promoting energy-efficient building operation.

7.2 Contributions

The key contributions from the current research are summarized as follows:

1. Air quality characterization in occupant breathing zone:

- The air quality characterization finds the breathing zone is critical for providing effective protection to occupant from getting infected by airborne infectious microorganisms.
- The study finds the characterization of aerosol plumes and associated risk of airborne virus transmission requires both the source aerosol emission rate and plume influence distance.
- Woodwind instruments produce aerosol plumes with approximately 20% higher source aerosol emission rates and 30% greater plume influence distances compared to the average values of the same risk indicators for singing and brass instruments.
- Well-fitted masks are strongly recommended for singing because they can bring source aerosol concentrations to the background level in front of a singer and reduce plume influence distances by 65%.

- Bell covers with filters are strongly recommended for brass and woodwind instruments performances because they can bring source aerosol concentrations to the background level in front of the instrument bells and reduce plume influence distances by up to 57%.
- An individual musician could produce aerosol plumes with five times higher source aerosol concentrations than those of the other musicians who played the same instrument, resulting in enhanced transmission risk.

2. Data-driven thermal comfort identification:

- The data-driven thermal comfort identification provides a reliable method for thermal comfort prediction in actual building control applications.
- The thermal comfort identification considers HRV for comforts in nonuniform microenvironments created by PCD.
- The PCD creates physiological responses incompatible with traditional comfort models.
- SVM with RBF kernel achieves the best performance among machine learning methods.
- Including multiple HRVs in addition to wrist temperatures improves the model performance.
- The highest model performance indices exceed 0.9 for both thermal sensation and comfort.

3. Simultaneous air quality, thermal comfort, and building energy controls:

- The study provides a novel occupant-oriented indoor environmental control framework which simultaneously considers air quality, thermal comfort, and building energy consumption.
- A wearable micro air cleaner is developed to promise the air quality in occupant breathing zone without impacting user's thermal comfort.
- The wearable micro air cleaner achieves about 60% - 70% protective efficiency for both nasal and mouth breathing.
- The wearable micro air cleaner provides acceptable thermal comfort at the indoor temperatures higher than 25 °C.
- The extremum seeking control is able to balance the conflicts between individual thermal preferences and building energy consumption.
- The extremum seeking control saves about 22% of energy compared to the building energy usage with the constant indoor air temperature setpoint (24 °C).

7.3 Summary of publications

The present dissertation resulted in the following publications:

Journal articles:

- L. Wang, T. Lin, H. Da Costa, S. Zhu, T. Stockman, A. Kumar, J. Weaver, M. Spede, D. K. Milton, J. Hertzberg, D. Toohey, M. Vance, S. L. Miller, J. Srebric, "Characterization of aerosol plumes from singing and playing wind instruments associated with the risk of airborne virus transmission," *Indoor Air*, vol. 32, no. 6, p. e13064, Jun. 2022, doi: 10.1111/INA.13064.

- L. Wang, D. A. Dalgo, N. Mattise, S. Zhu, and J. Srebric, “Physiological responses and data-driven thermal comfort models with personal conditioning devices (PCD),” *Building and Environment*, p. 110290, Apr. 2023, doi: 10.1016/J.BUILDENV.2023.110290.
- L. Wang, S. A. Romo, E. Sanico, H. Da Costa, T. Lin, N. Rabchevsky, M. Kern, S. Zhu, J. Srebric, “A Wearable Micro Air Cleaner for Occupant-oriented Indoor Environmental Controls,” *Building and Environment*, (Under Review).

Conference proceedings:

- L. Wang, T. Hensel, P. Chanpiwat, S. Zhu, and J. Srebric, “Occupant-centric Control of Building Systems based on Real-time Optimization by Extremum Seeking,” in *2022 IEEE International Conference on Environment and Electrical Engineering and 2022 IEEE Industrial and Commercial Power Systems Europe (EEEIC / I&CPS Europe)*, 2022, pp. 1–6. doi: 10.1109/EEEIC/ICPSEurope54979.2022.9854615.
- L. Wang, D. A. Dalgo, N. Mattise, S. Zhu, and J. Srebric, “Evaluation of Machine Learning Methods for Thermal Sensation and Comfort Predictions in Microenvironments Created by Personal Conditioning Devices: Poster Abstract,” in *Proceedings of the 9th ACM International Conference on Systems for Energy-Efficient Buildings, Cities, and Transportation*, in BuildSys ’22. New York, NY, USA: Association for Computing Machinery, 2022, pp. 305–306. doi: 10.1145/3563357.3567758.

Patent:

- J. Srebric, A. Layne, N. Mattise, S. Zhu, S. Romo, L. Wang, “Wearable Air Cleaning Device,” US20220040508A1, United States, June 10, 2020.

Technical reports for Centers for Disease Control and Prevention (CDC), USA:

- Budget period 1: Quarterly report 1-4.
- Budget period 2: Quarterly report 5-8.

Bibliography

- [1] L. Morawska and D. K. Milton, “It Is Time to Address Airborne Transmission of Coronavirus Disease 2019 (COVID-19),” *Clinical Infectious Diseases*, vol. 71, no. 9, pp. 2311–2313, Jul. 2020, doi: 10.1093/cid/ciaa939.
- [2] Y. Al Horr, M. Arif, A. Kaushik, A. Mazroei, M. Katafygiotou, and E. Elsarrag, “Occupant productivity and office indoor environment quality: A review of the literature,” *Build Environ*, vol. 105, pp. 369–389, Aug. 2016, doi: 10.1016/J.BUILDENV.2016.06.001.
- [3] Y. Al horr, M. Arif, M. Katafygiotou, A. Mazroei, A. Kaushik, and E. Elsarrag, “Impact of indoor environmental quality on occupant well-being and comfort: A review of the literature,” *International Journal of Sustainable Built Environment*, vol. 5, no. 1, pp. 1–11, Jun. 2016, doi: 10.1016/J.IJSBE.2016.03.006.
- [4] C. Huizenga, S. Abbaszadeh, L. Zagreus, and E. Arens, “Air Quality and Thermal Comfort in Office Buildings: Results of a Large Indoor Environmental Quality Survey,” 2006. Accessed: Aug. 09, 2021. [Online]. Available: <http://cbe.berkeley.edu>
- [5] P. Antoniadou and A. M. Papadopoulos, “Occupants’ thermal comfort: State of the art and the prospects of personalized assessment in office buildings,” *Energy Build*, vol. 153, pp. 136–149, Oct. 2017, doi: 10.1016/J.ENBUILD.2017.08.001.
- [6] S. Aghniaey and T. M. Lawrence, “The impact of increased cooling setpoint temperature during demand response events on occupant thermal comfort in

- commercial buildings: A review,” *Energy Build*, vol. 173, pp. 19–27, Aug. 2018, doi: 10.1016/J.ENBUILD.2018.04.068.
- [7] M. Brøgger and K. B. Wittchen, “Estimating the energy-saving potential in national building stocks – A methodology review,” *Renewable and Sustainable Energy Reviews*, vol. 82, no. July 2017, pp. 1489–1496, 2018, doi: 10.1016/j.rser.2017.05.239.
- [8] D. Mariano-Hernández, L. Hernández-Callejo, A. Zorita-Lamadrid, O. Duque-Pérez, and F. Santos García, “A review of strategies for building energy management system: Model predictive control, demand side management, optimization, and fault detect & diagnosis,” *Journal of Building Engineering*, vol. 33. Elsevier Ltd, p. 101692, Jan. 01, 2021. doi: 10.1016/j.jobbe.2020.101692.
- [9] S. Hu, D. Yan, E. Azar, and F. Guo, “A systematic review of occupant behavior in building energy policy,” *Build Environ*, vol. 175, p. 106807, May 2020, doi: 10.1016/J.BUILDENV.2020.106807.
- [10] Y. Zhang, X. Bai, F. P. Mills, and J. C. V. Pezzey, “Rethinking the role of occupant behavior in building energy performance: A review,” *Energy Build*, vol. 172, pp. 279–294, 2018, doi: 10.1016/j.enbuild.2018.05.017.
- [11] L. Hamner *et al.*, “High SARS-CoV-2 Attack Rate Following Exposure at a Choir Practice — Skagit County, Washington, March 2020,” *MMWR Morb Mortal Wkly Rep*, vol. 69, no. 19, pp. 606–610, May 2020, doi: 10.15585/mmwr.mm6919e6.

- [12] N. Lebrecht, “Concertgebouw chorus is devastated after pre-Covid Bach Passion,” *Slipped Disc*, 2020.
- [13] F. Colborne, “German choirs silenced as singing branded virus risk,” *Yahoo*, 2020.
- [14] N. Charlotte, “High Rate of SARS-CoV-2 Transmission Due to Choir Practice in France at the Beginning of the COVID-19 Pandemic,” *Journal of Voice*, Dec. 2020, doi: 10.1016/j.jvoice.2020.11.029.
- [15] Y. Furuse *et al.*, “Clusters of coronavirus disease in communities, Japan, January-April 2020,” *Emerg Infect Dis*, vol. 26, no. 9, pp. 2176–2179, Sep. 2020, doi: 10.3201/eid2609.202272.
- [16] W. Fautré, “COVID-19: Treatment of Clusters in Protestant Churches and the Shincheonji Church in South Korea. A Comparative Study,” *The journal of CESNUR*, vol. 4, no. 5, 2020.
- [17] M. Alsved *et al.*, “Exhaled respiratory particles during singing and talking,” *Aerosol Science and Technology*, vol. 54, no. 11, pp. 1245–1248, 2020. doi: 10.1080/02786826.2020.1812502.
- [18] D. Mürbe, M. Kriegel, J. Lange, L. Schumann, A. Hartmann, and M. Fleischer, “Aerosol emission of adolescents voices during speaking, singing and shouting,” *PLoS One*, vol. 16, no. 2, p. e0246819, Feb. 2021, doi: 10.1371/journal.pone.0246819.
- [19] L. Bourouiba, “Turbulent Gas Clouds and Respiratory Pathogen Emissions: Potential Implications for Reducing Transmission of COVID-19,” *JAMA - Journal of the American Medical Association*, vol. 323, no. 18. American

- Medical Association, pp. 1837–1838, May 12, 2020. doi:
10.1001/jama.2020.4756.
- [20] L. F. Pease *et al.*, “Investigation of potential aerosol transmission and infectivity of SARS-CoV-2 through central ventilation systems,” *Build Environ*, vol. 197, p. 107633, Jun. 2021, doi:
10.1016/J.BUILDENV.2021.107633.
- [21] C. Sun and Z. Zhai, “The efficacy of social distance and ventilation effectiveness in preventing COVID-19 transmission,” *Sustain Cities Soc*, vol. 62, p. 102390, Nov. 2020, doi: 10.1016/j.scs.2020.102390.
- [22] H. A. Hedworth, M. Karam, J. McConnell, J. C. Sutherland, and T. Saad, “Mitigation strategies for airborne disease transmission in orchestras using computational fluid dynamics,” *Sci Adv*, vol. 7, no. 26, Jun. 2021, doi:
10.1126/sciadv.abg4511.
- [23] M. E. Rosti, S. Olivieri, M. Cavaola, A. Seminara, and A. Mazzino, “Fluid dynamics of COVID-19 airborne infection suggests urgent data for a scientific design of social distancing,” *Sci Rep*, vol. 10, no. 1, pp. 1–9, Dec. 2020, doi:
10.1038/s41598-020-80078-7.
- [24] V. Stadnytskyi, C. E. Bax, A. Bax, and P. Anfinrud, “The airborne lifetime of small speech droplets and their potential importance in SARS-CoV-2 transmission,” *Proc Natl Acad Sci U S A*, vol. 117, no. 22, pp. 11875–11877, Jun. 2020, doi: 10.1073/pnas.2006874117.
- [25] M. Abkarian, S. Mendez, N. Xue, F. Yang, and H. A. Stone, “Speech can produce jet-like transport relevant to asymptomatic spreading of virus,” *Proc*

- Natl Acad Sci U S A*, vol. 117, no. 41, pp. 25237–25245, Oct. 2020, doi:
10.1073/pnas.2012156117.
- [26] F. K. A. Gregson *et al.*, “Comparing Aerosol Concentrations and Particle Size Distributions Generated by Singing, Speaking and Breathing,” *Aerosol Science and Technology*, pp. 1–14, Feb. 2021, doi: 10.1080/02786826.2021.1883544.
- [27] K.-M. Lai, C. Bottomley, and R. McNerney, “Propagation of Respiratory Aerosols by the Vuvuzela,” *PLoS One*, vol. 6, no. 5, p. e20086, May 2011, doi: 10.1371/journal.pone.0020086.
- [28] R. He, L. Gao, M. Trifonov, and J. Hong, “Aerosol generation from different wind instruments,” *J Aerosol Sci*, vol. 151, no. August 2020, p. 105669, 2021, doi: 10.1016/j.jaerosci.2020.105669.
- [29] T. Stockman *et al.*, “Measurements and Simulations of Aerosol Released while Singing and Playing Wind Instruments,” *ACS Environmental Au*, 2021.
- [30] L. P. McCarthy *et al.*, “Aerosol and droplet generation from performing with woodwind and brass instruments,” *Aerosol Science and Technology*, vol. 55, no. 11, pp. 1277–1287, 2021, doi:
10.1080/02786826.2021.1947470/SUPPL_FILE/UAST_A_1947470_SM0680.
DOCX.
- [31] P. Bahl *et al.*, “Droplets and Aerosols Generated by Singing and the Risk of Coronavirus Disease 2019 for Choirs,” *Clin Infect Dis*, vol. 72, no. 10, pp. e639–e641, Aug. 2021, doi: 10.1093/cid/ciaa1241.
- [32] L. Becher, A. W. Gena, H. Alsaad, B. Richter, C. Spahn, and C. Voelker, “The spread of breathing air from wind instruments and singers using schlieren

- techniques,” *medRxiv*, p. 2021.01.06.20240903, Jan. 2021, doi: 10.1101/2021.01.06.20240903.
- [33] A. Abraham *et al.*, “Risk Assessment and Mitigation of Airborne Disease Transmission in Orchestral Wind Instrument Performance,” *medRxiv*, 2020, doi: 10.1101/2020.12.23.20248652.
- [34] S. Gantner *et al.*, “Impulse dispersion of aerosols during playing wind instruments,” *medRxiv*, p. 2021.01.25.20248984, Jan. 2021, doi: 10.1101/2021.01.25.20248984.
- [35] M. Frontczak, S. Schiavon, J. Goins, E. Arens, H. Zhang, and P. Wargocki, “Quantitative relationships between occupant satisfaction and satisfaction aspects of indoor environmental quality and building design,” *Indoor Air*, vol. 22, no. 2, pp. 119–131, Apr. 2012, doi: 10.1111/j.1600-0668.2011.00745.x.
- [36] L. Pérez-Lombard, J. Ortiz, and C. Pout, “A review on buildings energy consumption information,” *Energy Build*, vol. 40, no. 3, pp. 394–398, Jan. 2008, doi: 10.1016/j.enbuild.2007.03.007.
- [37] P. O. Fanger, “Thermal comfort. Analysis and applications in environmental engineering,” *Thermal comfort. Analysis and applications in environmental engineering.*, 1970.
- [38] ASHRAE, *ASHRAE/ANSI standard 55-2017 thermal environmental conditions for human occupancy*. American Society of Heating, Refrigerating, and Air-Conditioning Engineers, Atlanta, GA, 2017.

- [39] J. van Hoof, “Forty years of Fanger’s model of thermal comfort: comfort for all?,” *Indoor Air*, vol. 18, no. 3, pp. 182–201, Jun. 2008, doi: 10.1111/j.1600-0668.2007.00516.x.
- [40] G. Schiller, “A comparison of measured and predicted comfort in office buildings,” *ASHRAE Trans*, vol. 96, no. 1, pp. 609–622, 1990.
- [41] T.-P. Lin, R. de Dear, and R.-L. Hwang, “Effect of thermal adaptation on seasonal outdoor thermal comfort,” *International Journal of Climatology*, vol. 31, no. 2, pp. 302–312, Feb. 2011, doi: 10.1002/joc.2120.
- [42] R. J. de Dear and G. S. Brager, “Developing an adaptive model of thermal comfort and preference,” in *ASHRAE Transactions*, 1998, pp. 145–167.
Accessed: Oct. 20, 2021. [Online]. Available:
<https://escholarship.org/uc/item/4qq2p9c6>
- [43] R. J. de Dear and M. E. Fountain, “Field experiments on occupant comfort and office thermal environments in a hot-humid climate,” in *ASHRAE Transactions*, 1994, pp. 457–474.
- [44] L. Arakawa Martins, V. Soebarto, and T. Williamson, “A systematic review of personal thermal comfort models,” *Building and Environment*, vol. 207. Elsevier Ltd, p. 108502, Jan. 01, 2022. doi: 10.1016/j.buildenv.2021.108502.
- [45] Y. Feng, S. Liu, J. Wang, J. Yang, Y. L. Jao, and N. Wang, “Data-driven personal thermal comfort prediction: A literature review,” *Renewable and Sustainable Energy Reviews*, vol. 161, p. 112357, Jun. 2022, doi: 10.1016/J.RSER.2022.112357.

- [46] A. K. Melikov, “Personalized ventilation,” *Indoor Air*, vol. 14, no. SUPPL. 7, pp. 157–167, 2004, doi: 10.1111/J.1600-0668.2004.00284.X.
- [47] W. Deng *et al.*, “Masks for COVID-19,” *Advanced Science*, vol. 9, no. 3, p. 2102189, Jan. 2022, doi: 10.1002/ADVS.202102189.
- [48] J. M. Mumma *et al.*, “Development and validation of the discomfort of cloth Masks-12 (DCM-12) scale,” *Appl Ergon*, vol. 98, p. 103616, Jan. 2022, doi: 10.1016/J.APERGO.2021.103616.
- [49] A. Melikov, T. Ivanova, and G. Stefanova, “Seat headrest-incorporated personalized ventilation: Thermal comfort and inhaled air quality,” *Build Environ*, vol. 47, no. 1, pp. 100–108, Jan. 2012, doi: 10.1016/J.BUILDENV.2011.07.013.
- [50] S. Zhu, Z. D. Bolashikov, and A. K. Melikov, “Examination of performance of headset incorporated personalized ventilation unit using CFD method,” in *11th International conference on Indoor Air Quality and Climate - Indoor Air 2008*, 2008.
- [51] M. Bivolarova, W. Kierat, E. Zavrl, Z. Popiolek, and A. Melikov, “Effect of airflow interaction in the breathing zone on exposure to bio-effluents,” *Build Environ*, vol. 125, pp. 216–226, Nov. 2017, doi: 10.1016/J.BUILDENV.2017.08.043.
- [52] C. Xu, P. v. Nielsen, L. Liu, R. L. Jensen, and G. Gong, “Impacts of airflow interactions with thermal boundary layer on performance of personalized ventilation,” *Build Environ*, vol. 135, pp. 31–41, May 2018, doi: 10.1016/J.BUILDENV.2018.02.048.

- [53] Z. D. Bolashikov, A. K. , Melikov, C. M. Velte, and K. E. Meyer, “Airflow Characteristics At The Breathing Zone of a Seated Person: Interaction of the Free Convection Flow and an Assisting Locally Supplied Flow From Below for Personalized Ventilation Application,” in *RoomVent*, 2011.
- [54] S. B. Godithi, E. Sachdeva, V. Garg, R. Brown, C. Kohler, and R. Rawal, “A review of advances for thermal and visual comfort controls in personal environmental control (PEC) systems,” *Intelligent Buildings International*, vol. 11, no. 2. Taylor and Francis Ltd., pp. 75–104, Apr. 03, 2019. doi: 10.1080/17508975.2018.1543179.
- [55] A. Wagner, W. O’Brien, and B. Dong, *Exploring occupant behavior in buildings: Methods and challenges*. Springer International Publishing, 2017. doi: 10.1007/978-3-319-61464-9.
- [56] J. Y. Park *et al.*, “A critical review of field implementations of occupant-centric building controls,” *Build Environ*, vol. 165, no. May, p. 106351, 2019, doi: 10.1016/j.buildenv.2019.106351.
- [57] J. Kim *et al.*, “Occupant comfort and behavior: High-resolution data from a 6-month field study of personal comfort systems with 37 real office workers,” *Build Environ*, vol. 148, no. September 2018, pp. 348–360, 2019, doi: 10.1016/j.buildenv.2018.11.012.
- [58] S. C. Bengea, A. D. Kelman, F. Borrelli, R. Taylor, and S. Narayanan, “Implementation of model predictive control for an HVAC system in a mid-size commercial building,” *HVAC and R Research*, vol. 20, no. 1, pp. 121–135, 2014, doi: 10.1080/10789669.2013.834781.

- [59] Z. Wang and T. Hong, "Reinforcement learning for building controls: The opportunities and challenges," *Appl Energy*, vol. 269, p. 115036, Jul. 2020, doi: 10.1016/J.APENERGY.2020.115036.
- [60] R. S. Papineni and F. S. Rosenthal, "The Size Distribution of Droplets in the Exhaled Breath of Healthy Human Subjects," Mary Ann Liebert, Inc, 1997. [Online]. Available: www.liebertpub.com
- [61] S. Asadi, A. S. Wexler, C. D. Cappa, S. Barreda, N. M. Bouvier, and W. D. Ristenpart, "Aerosol emission and superemission during human speech increase with voice loudness," *Sci Rep*, vol. 9, no. 1, Dec. 2019, doi: 10.1038/s41598-019-38808-z.
- [62] S. Asadi, A. S. Wexler, C. D. Cappa, S. Barreda, N. M. Bouvier, and W. D. Ristenpart, "Effect of voicing and articulation manner on aerosol particle emission during human speech," *PLoS One*, vol. 15, no. 1, Jan. 2020, doi: 10.1371/journal.pone.0227699.
- [63] L. Becher, C. Voelker, V. Rodehorst, and M. Kuhne, "Background-oriented schlieren technique for two-dimensional visualization of convective indoor air flows," *Opt Lasers Eng*, vol. 134, Nov. 2020, doi: 10.1016/j.optlaseng.2020.106282.
- [64] M. Raffel, C. E. Willert, S. T. Wereley, and J. Kompenhans, "Particle Image Velocimetry A Practical Guide Second Edition," 2018.
- [65] F. Fox, *Essentials of Brass Playing: An Explicit, Logical Approach to Important Basic Factors that Contribute to Superior Brass Instrument Performance*. Alfred Publishing Company, 1978.

- [66] J. M. Eargle, “Acoustics of Woodwind Instruments,” in *Music, Sound, and Technology*, Boston, MA: Springer US, 1995, pp. 105–124. doi: 10.1007/978-1-4757-5936-5_6.
- [67] B. M. Doscher, *The functional unity of the singing voice*. 1994.
- [68] J. W. Coltman, “Sounding Mechanism of the Flute and Organ Pipe,” *J Acoust Soc Am*, vol. 44, no. 4, pp. 983–992, Oct. 1968, doi: 10.1121/1.1911240.
- [69] J. Wolfe, “Double reed acoustics: oboe, bassoon and others,” *The University of New South Walse*. <https://newt.phys.unsw.edu.au/jw/double-reed-acoustics.html>
- [70] X. Xie, Y. Li, A. T. Y. Chwang, P. L. Ho, and W. H. Seto, “How far droplets can move in indoor environments – revisiting the Wells evaporation–falling curve,” *Indoor Air*, vol. 17, no. 3, pp. 211–225, Jun. 2007, doi: 10.1111/J.1600-0668.2007.00469.X.
- [71] L. Liu, J. Wei, Y. Li, and A. Ooi, “Evaporation and dispersion of respiratory droplets from coughing,” *Indoor Air*, vol. 27, no. 1, pp. 179–190, Jan. 2017, doi: 10.1111/INA.12297.
- [72] G. R. Johnson *et al.*, “Modality of human expired aerosol size distributions,” *J Aerosol Sci*, vol. 42, no. 12, pp. 839–851, Dec. 2011, doi: 10.1016/J.JAEROSCI.2011.07.009.
- [73] L. Morawska *et al.*, “Size distribution and sites of origin of droplets expelled from the human respiratory tract during expiratory activities,” *J Aerosol Sci*, vol. 40, no. 3, pp. 256–269, Mar. 2009, doi: 10.1016/J.JAEROSCI.2008.11.002.

- [74] M. Nicas, W. W. Nazaroff, and A. Hubbard, “Toward Understanding the Risk of Secondary Airborne Infection: Emission of Respirable Pathogens,” *J Occup Environ Hyg*, vol. 2, no. 3, p. 143, Mar. 2005, doi: 10.1080/15459620590918466.
- [75] H. Holmgren, E. Ljungström, A. C. Almstrand, B. Bake, and A. C. Olin, “Size distribution of exhaled particles in the range from 0.01 to 2.0 μm ,” *J Aerosol Sci*, vol. 41, no. 5, pp. 439–446, May 2010, doi: 10.1016/J.JAEROSCI.2010.02.011.
- [76] TSI Incorporated, “AEROTRAK™ Handheld Airborne Particle Counter Operation Manual,” no. February, 2010.
- [77] ASHRAE, “STANDARD 55 - Thermal Environmental Conditions for Human Occupancy,” *American Society of Heating, Refrigerating and Air-Conditioning Engineers*, 2020.
- [78] C. Huizenga, S. Abbaszadeh, L. Zagreus, and E. Arens, “Air quality and thermal comfort in office buildings: Results of a large indoor environmental quality survey,” in *HB 2006 - Healthy Buildings: Creating a Healthy Indoor Environment for People, Proceedings*, 2006, pp. 393–397.
- [79] J. Ling *et al.*, “Energy savings and thermal comfort evaluation of a novel personal conditioning device,” *Energy Build*, vol. 241, p. 110917, 2021, doi: 10.1016/j.enbuild.2021.110917.
- [80] M. Heidarinejad, D. A. Dalgo, N. W. Mattise, and J. Srebric, “Personalized cooling as an energy efficiency technology for city energy footprint reduction,”

- J Clean Prod*, vol. 171, pp. 491–505, Jan. 2018, doi:
10.1016/J.JCLEPRO.2017.10.008.
- [81] C. Cândido, R. J. de Dear, R. Lamberts, and L. Bittencourt, “Air movement acceptability limits and thermal comfort in Brazil’s hot humid climate zone,” *Build Environ*, vol. 45, no. 1, pp. 222–229, Jan. 2010, doi:
10.1016/j.buildenv.2009.06.005.
- [82] “ISO 7330, Ergonomics of the thermal environment – Analytical determination and interpretation of thermal comfort using calculation of the PMV and PPD indices and local thermal comfort criteria,” 2005.
- [83] J. Van Hoof, “Forty years of Fanger’s model of thermal comfort: Comfort for all?,” *Indoor Air*, vol. 18, no. 3, pp. 182–201, 2008, doi: 10.1111/j.1600-0668.2007.00516.x.
- [84] N. Djongyang, R. Tchinda, and D. Njomo, “Thermal comfort: A review paper,” *Renewable and Sustainable Energy Reviews*, vol. 14, no. 9, pp. 2626–2640, 2010, doi: 10.1016/j.rser.2010.07.040.
- [85] Z. Wang *et al.*, “Individual difference in thermal comfort: A literature review,” *Build Environ*, vol. 138, no. April, pp. 181–193, 2018, doi:
10.1016/j.buildenv.2018.04.040.
- [86] J. Xie, H. Li, C. Li, J. Zhang, and M. Luo, “Review on occupant-centric thermal comfort sensing, predicting, and controlling,” *Energy Build*, vol. 226, p. 110392, 2020, doi: 10.1016/j.enbuild.2020.110392.
- [87] D. Li, C. C. Menassa, and V. R. Kamat, “Robust non-intrusive interpretation of occupant thermal comfort in built environments with low-cost networked

- thermal cameras,” *Appl Energy*, vol. 251, p. 113336, Oct. 2019, doi:
10.1016/J.APENERGY.2019.113336.
- [88] Y. Zhou, Y. Su, Z. Xu, X. Wang, J. Wu, and X. Guan, “A hybrid physics-based/data-driven model for personalized dynamic thermal comfort in ordinary office environment,” *Energy Build*, vol. 238, p. 110790, May 2021, doi:
10.1016/J.ENBUILD.2021.110790.
- [89] Z. Qavidel Fard, Z. S. Zomorodian, and S. S. Korsavi, “Application of machine learning in thermal comfort studies: A review of methods, performance and challenges,” *Energy Build*, vol. 256, p. 111771, Feb. 2022, doi:
10.1016/J.ENBUILD.2021.111771.
- [90] W. Zhang, Y. Wu, and J. K. Calautit, “A review on occupancy prediction through machine learning for enhancing energy efficiency, air quality and thermal comfort in the built environment,” *Renewable and Sustainable Energy Reviews*, vol. 167, p. 112704, Oct. 2022, doi: 10.1016/J.RSER.2022.112704.
- [91] J. Kim, S. Schiavon, and G. Brager, “Personal comfort models – A new paradigm in thermal comfort for occupant-centric environmental control,” *Build Environ*, vol. 132, no. January, pp. 114–124, 2018, doi:
10.1016/j.buildenv.2018.01.023.
- [92] L. Xiong and Y. Yao, “Study on an adaptive thermal comfort model with K-nearest-neighbors (KNN) algorithm,” *Build Environ*, vol. 202, p. 108026, Sep. 2021, doi: 10.1016/J.BUILDENV.2021.108026.
- [93] C. Dai, H. Zhang, E. Arens, and Z. Lian, “Machine learning approaches to predict thermal demands using skin temperatures: Steady-state conditions,”

- Build Environ*, vol. 114, pp. 1–10, Mar. 2017, doi:
10.1016/J.BUILDENV.2016.12.005.
- [94] T. Chaudhuri, Y. C. Soh, H. Li, and L. Xie, “A feedforward neural network based indoor-climate control framework for thermal comfort and energy saving in buildings,” *Appl Energy*, vol. 248, pp. 44–53, Aug. 2019, doi:
10.1016/J.APENERGY.2019.04.065.
- [95] S. Liu, S. Schiavon, H. P. Das, M. Jin, and C. J. Spanos, “Personal thermal comfort models with wearable sensors,” *Build Environ*, vol. 162, p. 106281, Sep. 2019, doi: 10.1016/J.BUILDENV.2019.106281.
- [96] M. Luo *et al.*, “Comparing machine learning algorithms in predicting thermal sensation using ASHRAE Comfort Database II,” *Energy Build*, vol. 210, p. 109776, 2020, doi: 10.1016/j.enbuild.2020.109776.
- [97] Y. Peng, Z. Nagy, and A. Schlüter, “Temperature-preference learning with neural networks for occupant-centric building indoor climate controls,” *Build Environ*, vol. 154, no. January, pp. 296–308, 2019, doi:
10.1016/j.buildenv.2019.01.036.
- [98] S. Seyedzadeh, F. P. Rahimian, I. Glesk, and M. Roper, “Machine learning for estimation of building energy consumption and performance: a review,” *Visualization in Engineering 2018 6:1*, vol. 6, no. 1, pp. 1–20, Oct. 2018, doi:
10.1186/S40327-018-0064-7.
- [99] Z. Liu *et al.*, “Accuracy analyses and model comparison of machine learning adopted in building energy consumption prediction,” *Energy Exploration and Exploitation*, vol. 37, no. 4, pp. 1426–1451, Jul. 2019, doi:

10.1177/0144598718822400/ASSET/IMAGES/LARGE/10.1177_0144598718
822400-FIG2.JPEG.

- [100] J. Ngarambe, G. Y. Yun, and M. Santamouris, “The use of artificial intelligence (AI) methods in the prediction of thermal comfort in buildings: energy implications of AI-based thermal comfort controls,” *Energy Build*, vol. 211, p. 109807, 2020, doi: 10.1016/j.enbuild.2020.109807.
- [101] X. Shan and E. H. Yang, “Supervised machine learning of thermal comfort under different indoor temperatures using EEG measurements,” *Energy Build*, vol. 225, p. 110305, Oct. 2020, doi: 10.1016/J.ENBUILD.2020.110305.
- [102] A. Aryal and B. Becerik-Gerber, “Thermal comfort modeling when personalized comfort systems are in use: Comparison of sensing and learning methods,” *Build Environ*, vol. 185, p. 107316, Nov. 2020, doi: 10.1016/j.buildenv.2020.107316.
- [103] D. Al Assaad, C. Habchi, K. Ghali, and N. Ghaddar, “Simplified model for thermal comfort, IAQ and energy savings in rooms conditioned by displacement ventilation aided with transient personalized ventilation,” *Energy Convers Manag*, vol. 162, pp. 203–217, Apr. 2018, doi: 10.1016/j.enconman.2018.02.033.
- [104] E. Z. E. Conceição, C. I. M. Santiago, M. M. J. R. Lúcio, and H. B. Awbi, “Predicting the air quality, thermal comfort and draught risk for a virtual classroom with desk-type personalized ventilation systems,” *Buildings*, vol. 8, no. 2, Feb. 2018, doi: 10.3390/buildings8020035.

- [105] M. Al-Othmani, N. Ghaddar, and K. Ghali, “A multi-segmented human bioheat model for transient and asymmetric radiative environments,” *Int J Heat Mass Transf*, vol. 51, no. 23–24, pp. 5522–5533, Nov. 2008, doi: 10.1016/j.ijheatmasstransfer.2008.04.017.
- [106] M. Veselý and W. Zeiler, “Personalized conditioning and its impact on thermal comfort and energy performance - A review,” *Renewable and Sustainable Energy Reviews*, vol. 34, pp. 401–408, 2014, doi: 10.1016/j.rser.2014.03.024.
- [107] Y. Wu, H. Liu, B. Li, Y. Cheng, D. Tan, and Z. Fang, “Thermal comfort criteria for personal air supply in aircraft cabins in winter,” *Build Environ*, vol. 125, pp. 373–382, Nov. 2017, doi: 10.1016/J.BUILDENV.2017.09.005.
- [108] T. Mashita, T. Kanayama, and P. Ratsamee, “Personal Atmosphere: Estimation of Air Conditioner Parameters for Personalizing Thermal Comfort,” *Applied Sciences 2020, Vol. 10, Page 8067*, vol. 10, no. 22, p. 8067, Nov. 2020, doi: 10.3390/APP10228067.
- [109] M. Luo, B. Cao, W. Ji, Q. Ouyang, B. Lin, and Y. Zhu, “The underlying linkage between personal control and thermal comfort: Psychological or physical effects?,” *Energy Build*, vol. 111, pp. 56–63, Jan. 2016, doi: 10.1016/J.ENBUILD.2015.11.004.
- [110] M. Zhu, Y. Pan, Z. Wu, J. Xie, Z. Huang, and R. Kosonen, “An occupant-centric air-conditioning system for occupant thermal preference recognition control in personal micro-environment,” *Build Environ*, vol. 196, p. 107749, Jun. 2021, doi: 10.1016/J.BUILDENV.2021.107749.

- [111] “The Autonomic Nervous System and Thermoregulation,” in *Handbook of the Autonomic Nervous System in Health and Disease*, CRC Press, 2002, pp. 262–291. doi: 10.1201/9780203908891-10.
- [112] R. McCraty and F. Shaffer, “Heart rate variability: New perspectives on physiological mechanisms, assessment of self-regulatory capacity, and health risk,” *Global Advances In Health and Medicine*, vol. 4, no. 1. GAHM LLC, pp. 46–61, 2015. doi: 10.7453/gahmj.2014.073.
- [113] F. Shaffer and J. P. Ginsberg, “An Overview of Heart Rate Variability Metrics and Norms,” *Front Public Health*, vol. 5, no. September, pp. 1–17, 2017, doi: 10.3389/fpubh.2017.00258.
- [114] Y. Hasebe, M. Iriki, and K. Takahasi, “Usefulness of R-R interval and its variability in evaluation of thermal comfort,” *Int J Biometeorol*, vol. 38, no. 3, pp. 116–121, 1995, doi: 10.1007/BF01208486.
- [115] L. Lan, Z. Lian, W. Liu, and Y. Liu, “Investigation of gender difference in thermal comfort for Chinese people,” *Eur J Appl Physiol*, vol. 102, no. 4, pp. 471–480, 2007, doi: 10.1007/s00421-007-0609-2.
- [116] Y. Yao, Z. Lian, W. Liu, and Q. Shen, “Experimental study on skin temperature and thermal comfort of the human body in a recumbent posture under uniform thermal environments,” *Indoor and Built Environment*, vol. 16, no. 6, pp. 505–518, 2007, doi: 10.1177/1420326X07084291.
- [117] W. Liu, Z. Lian, and Y. Liu, “Heart rate variability at different thermal comfort levels,” *Eur J Appl Physiol*, vol. 103, no. 3, pp. 361–366, 2008, doi: 10.1007/s00421-008-0718-6.

- [118] Y. Yao, Z. Lian, W. Liu, C. Jiang, Y. Liu, and H. Lu, “Heart rate variation and electroencephalograph - The potential physiological factors for thermal comfort study,” *Indoor Air*, vol. 19, no. 2, pp. 93–101, Apr. 2009, doi: 10.1111/j.1600-0668.2008.00565.x.
- [119] J. Xiong, Z. Lian, X. Zhou, J. You, and Y. Lin, “Potential indicators for the effect of temperature steps on human health and thermal comfort,” *Energy Build*, vol. 113, pp. 87–98, 2016, doi: 10.1016/j.enbuild.2015.12.031.
- [120] H. Zhu, H. Wang, Z. Liu, D. Li, G. Kou, and C. Li, “Experimental study on the human thermal comfort based on the heart rate variability (HRV) analysis under different environments,” *Science of the Total Environment*, vol. 616–617, pp. 1124–1133, Mar. 2018, doi: 10.1016/j.scitotenv.2017.10.208.
- [121] Y. Chen, Z. Wang, X. Tian, and W. Liu, “Evaluation of cognitive performance in high temperature with heart rate: A pilot study,” *Build Environ*, vol. 228, p. 109801, Jan. 2023, doi: 10.1016/j.buildenv.2022.109801.
- [122] K. N. Nkurikiyeyezu, Y. Suzuki, and G. F. Lopez, “Heart rate variability as a predictive biomarker of thermal comfort,” *J Ambient Intell Humaniz Comput*, vol. 9, no. 5, pp. 1465–1477, Oct. 2018, doi: 10.1007/s12652-017-0567-4.
- [123] F. Kobiela, R. Shen, M. Schweiker, and R. Dürichen, “Personal thermal perception models using skin temperatures and HR/HRV Features - comparison of smartwatch and professional measurement devices,” *Proceedings - International Symposium on Wearable Computers, ISWC*, pp. 96–105, 2019, doi: 10.1145/3341163.3347737.

- [124] N. Morresi *et al.*, “Sensing physiological and environmental quantities to measure human thermal comfort through machine learning techniques,” *IEEE Sens J*, vol. 21, no. 10, pp. 12322–12337, May 2021, doi: 10.1109/JSEN.2021.3064707.
- [125] Z. Wang, R. Matsushashi, and H. Onodera, “Towards wearable thermal comfort assessment framework by analysis of heart rate variability,” *Build Environ*, vol. 223, p. 109504, Sep. 2022, doi: 10.1016/J.BUILDENV.2022.109504.
- [126] J. Yu, G. Cao, W. Cui, Q. Ouyang, and Y. Zhu, “People who live in a cold climate: Thermal adaptation differences based on availability of heating,” *Indoor Air*, vol. 23, no. 4, pp. 303–310, Aug. 2013, doi: 10.1111/ina.12025.
- [127] H. Shin, “Ambient temperature effect on pulse rate variability as an alternative to heart rate variability in young adult,” *J Clin Monit Comput*, vol. 30, no. 6, pp. 939–948, 2016, doi: 10.1007/s10877-015-9798-0.
- [128] P. van Gent, H. Farah, N. van Nes, and B. van Arem, “HeartPy: A novel heart rate algorithm for the analysis of noisy signals,” *Transp Res Part F Traffic Psychol Behav*, vol. 66, pp. 368–378, Oct. 2019, doi: 10.1016/J.TRF.2019.09.015.
- [129] J. Xiong, Z. Lian, X. Zhou, J. You, and Y. Lin, “Effects of temperature steps on human health and thermal comfort,” *Build Environ*, vol. 94, no. P1, pp. 144–154, Dec. 2015, doi: 10.1016/J.BUILDENV.2015.07.032.
- [130] J. Yu, Q. Ouyang, Y. Zhu, H. Shen, G. Cao, and W. Cui, “A comparison of the thermal adaptability of people accustomed to air-conditioned environments and

- naturally ventilated environments,” *Indoor Air*, vol. 22, no. 2, pp. 110–118, Apr. 2012, doi: 10.1111/J.1600-0668.2011.00746.X.
- [131] S. Schiavon, B. Yang, Y. Donner, V. W. C. Chang, and W. W. Nazaroff, “Thermal comfort, perceived air quality, and cognitive performance when personally controlled air movement is used by tropically acclimatized persons,” *Indoor Air*, vol. 27, no. 3, pp. 690–702, May 2017, doi: 10.1111/INA.12352.
- [132] S. Y. Sim *et al.*, “Estimation of Thermal Sensation Based on Wrist Skin Temperatures,” *Sensors 2016, Vol. 16, Page 420*, vol. 16, no. 4, p. 420, Mar. 2016, doi: 10.3390/S16040420.
- [133] M. Favero, I. Sartori, and S. Carlucci, “Human thermal comfort under dynamic conditions: An experimental study,” *Build Environ*, vol. 204, p. 108144, Oct. 2021, doi: 10.1016/J.BUILDENV.2021.108144.
- [134] S. Takada, S. Matsumoto, and T. Matsushita, “Prediction of whole-body thermal sensation in the non-steady state based on skin temperature,” *Build Environ*, vol. 68, pp. 123–133, Oct. 2013, doi: 10.1016/J.BUILDENV.2013.06.004.
- [135] R. Dhumane, Y. Du, J. Ling, V. Aute, R. Radermacher, and M. H. Bldg, “Transient Modeling of a Thermosiphon based Air Conditioner with Compact Thermal Storage : Modeling and Validation,” *International Compressor Engineering, Refrigeration and Air Conditioning, and High Performance Buildings Conferences*, no. Vcc, pp. 1–10, Jan. 2016.

- [136] Z. Fang, H. Liu, B. Li, M. Tan, and O. M. Olaide, “Experimental investigation on thermal comfort model between local thermal sensation and overall thermal sensation,” *Energy Build*, vol. 158, pp. 1286–1295, Jan. 2018, doi: 10.1016/j.enbuild.2017.10.099.
- [137] S. Zhu, D. Dalgo, J. Srebric, and S. Kato, “Cooling efficiency of a spot-type personalized air-conditioner,” *Build Environ*, vol. 121, pp. 35–48, 2017, doi: 10.1016/j.buildenv.2017.05.007.
- [138] D. Wang, H. Zhang, E. Arens, and C. Huizenga, “Observations of upper-extremity skin temperature and corresponding overall-body thermal sensations and comfort,” *Build Environ*, vol. 42, no. 12, pp. 3933–3943, Dec. 2007, doi: 10.1016/j.buildenv.2006.06.035.
- [139] F. Riganello, S. Garbarino, and W. G. Sannita, “Heart rate variability, homeostasis, and brain Function: A tutorial and review of application,” *J Psychophysiol*, vol. 26, no. 4, pp. 178–203, 2012, doi: 10.1027/0269-8803/a000080.
- [140] A. Geron, *Hands-On Machine Learning with Scikit-Learn, Keras, and TensorFlow: Concepts, Tools, and Techniques to Build Intelligent Systems*, 2nd ed. O’Reilly Media, Inc., 2019.
- [141] T. Chaudhuri, D. Zhai, Y. C. Soh, H. Li, and L. Xie, “Thermal comfort prediction using normalized skin temperature in a uniform built environment,” *Energy Build*, vol. 159, pp. 426–440, 2018, doi: 10.1016/j.enbuild.2017.10.098.

- [142] H. Zhu, H. Wang, Z. Liu, G. Kou, C. Li, and D. Li, “Experimental study on the variations in human skin temperature under simulated weightlessness,” *Build Environ*, vol. 117, pp. 135–145, May 2017, doi: 10.1016/j.buildenv.2017.03.008.
- [143] Yutaka Sasaki, *The truth of the F-measure*. 2007.
- [144] D. J. Hand and R. J. Till, “A Simple Generalisation of the Area Under the ROC Curve for Multiple Class Classification Problems,” *Mach Learn*, vol. 45, no. 2, pp. 171–186, 2001, doi: 10.1023/A:1010920819831/METRICS.
- [145] S. Zhu, S. Kato, and L. Yang, “Examination of thermal adaptive effect of postural and positional adjustment of a seated human body exposed to spot airflow,” *ASHRAE Trans*, vol. 113, no. 2, 2007.
- [146] A. Ghahramani, G. Castro, S. A. Karvigh, and B. Becerik-Gerber, “Towards unsupervised learning of thermal comfort using infrared thermography,” *Appl Energy*, vol. 211, pp. 41–49, Feb. 2018, doi: 10.1016/J.APENERGY.2017.11.021.
- [147] I. Manisalidis, E. Stavropoulou, A. Stavropoulos, and E. Bezirtzoglou, “Environmental and Health Impacts of Air Pollution: A Review,” *Front Public Health*, vol. 8, p. 14, Feb. 2020, doi: 10.3389/FPUBH.2020.00014/BIBTEX.
- [148] D. Kim, Z. Chen, L. Zhou, and S. Huang, “Air pollutants and early origins of respiratory diseases,” *Chronic Dis Transl Med*, vol. 4, no. 2, pp. 75–94, Jun. 2018, doi: 10.1016/J.CDTM.2018.03.003.

- [149] M. Guarnieri and J. R. Balmes, “Outdoor air pollution and asthma,” *The Lancet*, vol. 383, no. 9928, pp. 1581–1592, May 2014, doi: 10.1016/S0140-6736(14)60617-6.
- [150] R. R. Duan, K. Hao, and T. Yang, “Air pollution and chronic obstructive pulmonary disease,” *Chronic Dis Transl Med*, vol. 6, no. 4, pp. 260–269, Dec. 2020, doi: 10.1016/J.CDTM.2020.05.004.
- [151] S. G. Al-Kindi, R. D. Brook, S. Biswal, and S. Rajagopalan, “Environmental determinants of cardiovascular disease: lessons learned from air pollution,” *Nature Reviews Cardiology* 2020 17:10, vol. 17, no. 10, pp. 656–672, May 2020, doi: 10.1038/s41569-020-0371-2.
- [152] L. Fajersztajn, M. Veras, L. V. Barrozo, and P. Saldiva, “Air pollution: a potentially modifiable risk factor for lung cancer,” *Nature Reviews Cancer* 2013 13:9, vol. 13, no. 9, pp. 674–678, Aug. 2013, doi: 10.1038/nrc3572.
- [153] P. Grennfelt, A. Engleryd, M. Forsius, Ø. Hov, H. Rodhe, and E. Cowling, “Acid rain and air pollution: 50 years of progress in environmental science and policy,” *Ambio*, vol. 49, no. 4, pp. 849–864, Apr. 2020, doi: 10.1007/S13280-019-01244-4/FIGURES/8.
- [154] V. Hosseini and H. Shahbazi, “Urban Air Pollution in Iran,” *Iranian Studies*, vol. 49, no. 6, pp. 1029–1046, Nov. 2016, doi: 10.1080/00210862.2016.1241587.
- [155] J. Fiegel, R. Clarke, and D. A. Edwards, “Airborne infectious disease and the suppression of pulmonary bioaerosols,” *Drug Discov Today*, vol. 11, no. 1–2, pp. 51–57, Jan. 2006, doi: 10.1016/S1359-6446(05)03687-1.

- [156] S. Herfst *et al.*, “Drivers of airborne human-to-human pathogen transmission,” *Curr Opin Virol*, vol. 22, pp. 22–29, Feb. 2017, doi: 10.1016/J.COVIRO.2016.11.006.
- [157] N. Fogel, “Tuberculosis: A disease without boundaries,” *Tuberculosis*, vol. 95, no. 5, pp. 527–531, Sep. 2015, doi: 10.1016/J.TUBE.2015.05.017.
- [158] J. Sundell, “On the history of indoor air quality and health,” *Indoor Air*, vol. 14, no. SUPPL. 7, pp. 51–58, 2004, doi: 10.1111/J.1600-0668.2004.00273.X.
- [159] A. Kenarkoohi *et al.*, “Hospital indoor air quality monitoring for the detection of SARS-CoV-2 (COVID-19) virus,” *Science of The Total Environment*, vol. 748, p. 141324, Dec. 2020, doi: 10.1016/J.SCITOTENV.2020.141324.
- [160] S. Zhu *et al.*, “Ventilation and laboratory confirmed acute respiratory infection (ARI) rates in college residence halls in College Park, Maryland,” *Environ Int*, vol. 137, p. 105537, Apr. 2020, doi: 10.1016/J.ENVINT.2020.105537.
- [161] J. Kurnitski *et al.*, “Respiratory infection risk-based ventilation design method,” *Build Environ*, vol. 206, p. 108387, Dec. 2021, doi: 10.1016/J.BUILDENV.2021.108387.
- [162] T. Stockman *et al.*, “Measurements and Simulations of Aerosol Released while Singing and Playing Wind Instruments,” *ACS Environmental Au*, Aug. 2021, doi: 10.1021/acsenvironau.1c00007.
- [163] L. Wang *et al.*, “Characterization of aerosol plumes from singing and playing wind instruments associated with the risk of airborne virus transmission,” *Indoor Air*, vol. 32, no. 6, p. e13064, Jun. 2022, doi: 10.1111/INA.13064.

- [164] I. Eames, J. W. Tang, Y. Li, and P. Wilson, “Airborne transmission of disease in hospitals,” *J R Soc Interface*, vol. 6, no. SUPPL. 6, Dec. 2009, doi: 10.1098/RSIF.2009.0407.FOCUS.
- [165] Y. Li *et al.*, “Role of ventilation in airborne transmission of infectious agents in the built environment – a multidisciplinary systematic review,” *Indoor Air*, vol. 17, no. 1, pp. 2–18, Feb. 2007, doi: 10.1111/J.1600-0668.2006.00445.X.
- [166] S. Zhu, T. Lin, L. Wang, E. A. Nardell, R. L. Vincent, and J. Srebric, “Ceiling impact on air disinfection performance of Upper-Room Germicidal Ultraviolet (UR-GUV),” *Build Environ*, vol. 224, p. 109530, Oct. 2022, doi: 10.1016/J.BUILDENV.2022.109530.
- [167] A. T. Johnson, “Respirator masks protect health but impact performance: A review,” *J Biol Eng*, vol. 10, no. 1, pp. 1–12, Feb. 2016, doi: 10.1186/S13036-016-0025-4/FIGURES/5.
- [168] S. A. Tabatabaeizadeh, “Airborne transmission of COVID-19 and the role of face mask to prevent it: a systematic review and meta-analysis,” *Eur J Med Res*, vol. 26, no. 1, pp. 1–6, Dec. 2021, doi: 10.1186/S40001-020-00475-6/FIGURES/4.
- [169] A. Scarano, F. Inchingolo, and F. Lorusso, “Facial Skin Temperature and Discomfort When Wearing Protective Face Masks: Thermal Infrared Imaging Evaluation and Hands Moving the Mask,” *International Journal of Environmental Research and Public Health 2020, Vol. 17, Page 4624*, vol. 17, no. 13, p. 4624, Jun. 2020, doi: 10.3390/IJERPH17134624.

- [170] J. B. Powell, J. H. Kim, and R. J. Roberge, “Powered air-purifying respirator use in healthcare: Effects on thermal sensations and comfort,” <https://doi.org/10.1080/15459624.2017.1358817>, vol. 14, no. 12, pp. 947–954, Dec. 2017, doi: 10.1080/15459624.2017.1358817.
- [171] A. K. Melikov, “COVID-19: Reduction of airborne transmission needs paradigm shift in ventilation,” *Build Environ*, vol. 186, p. 107336, Dec. 2020, doi: 10.1016/J.BUILDENV.2020.107336.
- [172] C. Xu *et al.*, “Effects of personalized ventilation interventions on airborne infection risk and transmission between occupants,” *Build Environ*, vol. 180, p. 107008, Aug. 2020, doi: 10.1016/J.BUILDENV.2020.107008.
- [173] J. Pantelic, G. N. Sze-To, K. W. Tham, C. Y. H. Chao, and Y. C. M. Khoo, “Personalized ventilation as a control measure for airborne transmissible disease spread,” *J R Soc Interface*, vol. 6, no. SUPPL. 6, Dec. 2009, doi: 10.1098/RSIF.2009.0311.FOCUS.
- [174] J. Pantelic, K. W. Tham, and D. Licina, “Effectiveness of a personalized ventilation system in reducing personal exposure against directly released simulated cough droplets,” *Indoor Air*, vol. 25, no. 6, pp. 683–693, Dec. 2015, doi: 10.1111/INA.12187.
- [175] W. Liu *et al.*, “Exploring the potentials of personalized ventilation in mitigating airborne infection risk for two closely ranged occupants with different risk assessment models,” *Energy Build*, vol. 253, p. 111531, Dec. 2021, doi: 10.1016/J.ENBUILD.2021.111531.

- [176] H. Alsaad and C. Voelker, “Could the ductless personalized ventilation be an alternative to the regular ducted personalized ventilation?,” *Indoor Air*, vol. 31, no. 1, pp. 99–111, Jan. 2021, doi: 10.1111/INA.12720.
- [177] J. Yang, S. C. Sekhar, K. W. D. Cheong, and B. Raphael, “Performance evaluation of a novel personalized ventilation–personalized exhaust system for airborne infection control,” *Indoor Air*, vol. 25, no. 2, pp. 176–187, Apr. 2015, doi: 10.1111/INA.12127.
- [178] G. Cortellessa, C. Canale, L. Stabile, G. Grossi, G. Buonanno, and F. Arpino, “Effectiveness of a portable personal air cleaner in reducing the airborne transmission of respiratory pathogens,” *Build Environ*, vol. 235, p. 110222, May 2023, doi: 10.1016/J.BUILDENV.2023.110222.
- [179] M. J. Jennings, P. K. Reid, and J. M. Nelson, “A wearable air purifier US 2021/0283544 A1,” 2021
- [180] M. S. Alshitawi, S. Suyambazhahan, and A. S. Alaboodi, “Computational fluid dynamics simulation of breathing zone of the human for air quality with a personalized air curtain,” *Advances in Mechanical Engineering*, vol. 11, no. 5, May 2019, doi: 10.1177/1687814019844688/ASSET/IMAGES/LARGE/10.1177_1687814019844688-FIG2.JPEG.
- [181] X. Wei, D. Yi, W. Xie, J. Gao, and L. Lv, “Protection against inhalation of gaseous contaminants in industrial environments by a personalized air curtain,” *Build Environ*, vol. 206, p. 108343, Dec. 2021, doi: 10.1016/J.BUILDENV.2021.108343.

- [182] X. Wei *et al.*, “Effectiveness of head-mounted air supply in reducing pollutant exposure: A static case,” *Build Environ*, vol. 234, p. 110219, Apr. 2023, doi: 10.1016/J.BUILDENV.2023.110219.
- [183] J. Ma, H. Qian, F. Liu, and X. Zheng, “Performance analysis of a novel personalized air curtain for preventing inhalation of particulate matters in industrial environments,” *Journal of Building Engineering*, vol. 58, p. 105014, Oct. 2022, doi: 10.1016/J.JOBE.2022.105014.
- [184] J. Srebric, A. Layne, N. W. Mattise, S. Zhu, S. Romo, and L. Wang, “Wearable air cleaning device US 2022/0040508 A1,” 2022
- [185] J. Cigler, D. Gyalistras, J. Siroky, V.-N. Tiet, and L. Ferkl, “Beyond Theory: the Challenge of Implementing Model Predictive Control in Buildings,” in *11th REHVA world congress and 8th international conference Energy Efficient, Smart and Healthy Buildings*, 2013, pp. 1008–1018.
- [186] B. Hu, Y. Li, B. Mu, S. Wang, J. E. Seem, and F. Cao, “Extremum Seeking Control of Hybrid Ground Source Heat Pump System,” *International Refrigeration and Air Conditioning Conference*, Jan. 2014, Accessed: Aug. 31, 2021. [Online]. Available: <https://docs.lib.purdue.edu/iracc/1504>
- [187] B. Hu, Y. Li, B. Mu, S. Wang, J. E. Seem, and F. Cao, “Extremum seeking control for efficient operation of hybrid ground source heat pump system,” *Renew Energy*, vol. 86, pp. 332–346, Feb. 2016, doi: 10.1016/j.renene.2015.07.092.
- [188] B. Mu, Y. Li, T. I. Salsbury, and J. M. House, “Extremum seeking based control strategy for a chilled-water plant with parallel chillers,” in *ASME 2015*

Dynamic Systems and Control Conference, DSCC 2015, American Society of Mechanical Engineers, Jan. 2015. doi: 10.1115/DSCC2015-9949.

- [189] P. Li, Y. Li, and J. E. Seem, “Efficient operation of air-side economizer using extremum seeking control,” *Journal of Dynamic Systems, Measurement and Control, Transactions of the ASME*, vol. 132, no. 3, pp. 1–10, May 2010, doi: 10.1115/1.4001216.
- [190] B. Mu, Y. Li, J. M. House, and T. I. Salsbury, “Experimental evaluation of anti-windup extremum seeking control for airside economizers,” *Control Eng Pract*, vol. 50, pp. 37–47, May 2016, doi: 10.1016/j.conengprac.2016.02.008.
- [191] C. Yin, S. Dadras, X. Huang, J. Mei, H. Malek, and Y. Cheng, “Energy-saving control strategy for lighting system based on multivariate extremum seeking with Newton algorithm,” *Energy Convers Manag*, vol. 142, pp. 504–522, Jun. 2017, doi: 10.1016/j.enconman.2017.03.072.
- [192] Y. Li and Z. Tong, “Development of real-time adaptive model-free extremum seeking control for CFD-simulated thermal environment,” *Sustain Cities Soc*, vol. 74, p. 103166, Nov. 2021, doi: 10.1016/j.scs.2021.103166.
- [193] A. Konda, A. Prakash, G. A. Moss, M. Schmoldt, G. D. Grant, and S. Guha, “Aerosol Filtration Efficiency of Common Fabrics Used in Respiratory Cloth Masks,” *ACS Nano*, vol. 14, no. 5, pp. 6339–6347, May 2020, doi: 10.1021/ACSNANO.0C03252/ASSET/IMAGES/MEDIUM/NN0C03252_M001.GIF.

- [194] A. K. Melikov, R. Cermak, and M. Majer, “Personalized ventilation: evaluation of different air terminal devices,” *Energy Build*, vol. 34, no. 8, pp. 829–836, Sep. 2002, doi: 10.1016/S0378-7788(02)00102-0.
- [195] J. Russo and H. E. Khalifa, “CFD analysis of personal ventilation with volumetric chemical reactions,” *HVAC and R Research*, vol. 16, no. 6, pp. 799–812, Nov. 2010, doi: 10.1080/10789669.2010.10390935.
- [196] H. Zuo, “Experimental study of personalized air system for the reduction of pollutant exposure,” Hong Kong Polytechnic University, 2004.
- [197] J. S. Russo and E. Khalifa, “Computational study of breathing methods for inhalation exposure,” *HVAC and R Research*, vol. 17, no. 4, pp. 419–431, 2011, doi: 10.1080/10789669.2011.578701.
- [198] J. K. Gupta, C. H. Lin, and Q. Chen, “Characterizing exhaled airflow from breathing and talking,” *Indoor Air*, vol. 20, no. 1, pp. 31–39, Feb. 2010, doi: 10.1111/J.1600-0668.2009.00623.X.
- [199] L. Wang, D. A. Dalgo, N. Mattise, S. Zhu, and J. Srebric, “Physiological responses and data-driven thermal comfort models with personal conditioning devices (PCD),” *Build Environ*, p. 110290, Apr. 2023, doi: 10.1016/J.BUILDENV.2023.110290.
- [200] L. Wang, D. A. Dalgo, N. Mattise, S. Zhu, and J. Srebric, “Evaluation of Machine Learning Methods for Thermal Sensation and Comfort Predictions in Microenvironments Created by Personal Conditioning Devices: Poster Abstract,” in *Proceedings of the 9th ACM International Conference on Systems for Energy-Efficient Buildings, Cities, and Transportation*, in BuildSys ’22.

New York, NY, USA: Association for Computing Machinery, 2022, pp. 305–306. doi: 10.1145/3563357.3567758.

- [201] K. Parsons, *Human thermal environments: The effects of hot, moderate, and cold environments on human health, comfort, and performance, third edition*. CRC Press, 2014. doi: 10.1201/b16750.
- [202] J. Y. Kwon and J. Choi, “Clothing insulation and temperature, layer and mass of clothing under comfortable environmental conditions,” *J Physiol Anthropol*, vol. 32, no. 1, p. 11, Jul. 2013, doi: 10.1186/1880-6805-32-11.
- [203] N. Walikewitz, B. Jänicke, M. Langner, F. Meier, and W. Endlicher, “The difference between the mean radiant temperature and the air temperature within indoor environments: A case study during summer conditions,” *Build Environ*, vol. 84, pp. 151–161, Jan. 2015, doi: 10.1016/j.buildenv.2014.11.004.
- [204] CIBSE guide, *Chartered Institute of Building Services (CIBS)*. 1993.
- [205] D. Dochain, M. Perrier, and M. Guay, “Extremum seeking control and its application to process and reaction systems: A survey,” *Math Comput Simul*, vol. 82, no. 3, pp. 369–380, Nov. 2011, doi: 10.1016/j.matcom.2010.10.022.